John T. Harding

Report No. FRA-ORD & D-74-41

AN EVALUATION OF THE DYNAMICS OF A MAGNETICALLY LEVITATED VEHICLE

By: H. T. COFFEY, J. D. COLTON, J. C. SOLINSKY and J. R. WOODBURY

March 1974

Final Report

Task III

Prepared for:

FEDERAL RAILROAD ADMINISTRATION
OFFICE OF RESEARCH, DEVELOPMENT AND DEMONSTRATION
WASHINGTON, D.C. 20590

The contents of this report reflect the views of Stanford Research Institute which is responsible for the facts and the accuracy of the data presented herein. The contents do not necessarily reflect the official views or policy of the Department of Transportation. This report does not constitute a standard, specification or regulation.

TECHNICAL REPORT STANDARD TITLE PAGE

1. Report No.	2. Government Accession No.	3. Recipient's Catalog No.
FRA-ORD&D-74-41		

4. Title and Subtitle	5. Report Date
An Evaluation of the Dynamics of A Magnetically Levitated Vehicle	March 1974
	6. Performing Organization Code
7. Author(s) H.T. Coffey, J.D. Colton, J.C. Solinsky and J.R. Woodbury	8. Performing Organization Report No. 1080
9. Performing Organization Name and Address Stanford Research Institute 333 Ravenswood Avenue Menlo Park, California 94025	10. Work Unit No. 11. Contract or Grant No. DOT-FR-10001
12. Sponsoring Agency Name and Address Federal Railroad Administration Office of Research Development and Demonstration Washington, D.C. 20590	13. Type of Report and Period Covered Final Report March 1973 - March 1974 14. Sponsoring Agency Code

15. Supplementary Notes

"Related reports include NTIS Report No. PB 221696 - "Study of a Magnetically Levitated Vehicle" and NTIS Report No. PB 210505-"The Feasibility of Magnetically Levitating High Speed Ground Vehicles."

16. Abstract

An analytical and experimental evaluation was made of the stability and dynamic characteristics of a small scale magnetically levitated vehicle. The vehicle was levitated over a variety of guideway perturbations in an attempt at stimulating unstable modes of oscillation. No instabilities developed in the five degrees of freedom measured using either passive or active damping. The analytical model was used to simulate the observed motions of the vehicle using a computer. Reasonable agreement was found although more damping was observed than was simulated using the model.

This work was performed as a part of the Federal Railroad Administration's program of research and development on high speed ground transportation for use in intercity passenger service.

17. Key Words	18. Distribution Statement
Magnetic Levitation (MAGLEV), High Speed Ground Transportation, Dynamics, Damping, Stability, Test vehicle, Experiments	Unlimited

19. Security Classif. (of this report)	20. Security Classif. (of this page)	21. No. of Pages	22. Price
Unclassified	Unclassified	160	

Form DOT F 1700.7 (8-69)

CONTENTS

CONTENTS (concluded)

ILLUSTRATIONS

ILLUSTRATIONS (Continued)

ILLUSTRATIONS (Continued)

ILLUSTRATIONS (Continued)

LIST OF TABLES

PREFACE

The work reported herein is a continuation of a program initiated in February 1971 to determine the feasibility of using magnetic forces for the suspension and guidance of high-speed passenger carrying vehicles. In the first phase of this program, several aspects of magnetic levitation were explored to determine the best type of magnetic levitation system and to determine the technical feasibility of using this system in the vehicle. Suspensions using (1) permanent magnets on the vehicle and an aluminum guideway (diamagnetic levitation), (2) permanent magnets on the vehicle and a permanent magnet guideway (repulsive magnetic levitation), (3) superconducting magnets on the vehicle and an aluminum guideway (diamagnetic levitation), and (4) normal electromagnets on the vehicle and a ferromagnetic guideway (ferromagnetic levitation) were investigated. The system employing superconducting magnets was selected by SRI as the most promising, and subsequent efforts have been concentrated on this system.

We explored several optional systems that employ superconducting magnets. A system using continuous sheets of aluminum in the guideway was selected. The interaction forces resulting in levitation and guidance were calculated as a part of this phase of the program and were checked by experiment, and a computer program was written for calculating the dynamic motions of magnetically levitated vehicles.

Experiments were performed by moving a single superconducting magnet over an aluminum guideway and measuring the forces exerted on the magnet. The magnet was mounted on a wheeled vehicle that permitted the position of the magnet to be varied within the guideway. These experiments indicated that the calculated force was accurate but that a small error--the

source of which is known and estimable but not readily calculable--existed in the drag force. This calculation is not too restrictive for most purposes. However, there was a substantial error in the guidance force. It was assumed that the velocity dependence of the guidance force was the same as that of the lift force. This was only approximately correct. The experiments also showed that electrical continuity was mandatory between the vertical and horizontal plates of the guideway if suitable guidance forces were to be achieved. A full-scale vehicle was conceptually designed based on the formulae derived during this phase of the work. In conjunction with the experiments, and cryogen consumption rates based on a conceptual dewar design, the vehicle was found to be technically feasible for passenger carrying operation at speeds in excess of 300 mph. This work is reported in Reference 1, which provided the basis for References 2 through 5.

The second phase of this program was devoted to designing, constructing, and testing a small vehicle levitated and guided by four superconducting magnets. Rudimentary measurements were made of the dynamic properties of the vehicle in levitated flight. The main purpose of these dynamic measurements was to validate the calculated ability of the copper plates, placed below the superconducting magnets, to dampen the vehicle oscillations. The tests were successful and the calculations were in good agreement with the experiments to the extent that they could be checked by the experiments performed. A part of this phase of work was to reformulate the calculation of the guidance force, which brought the theory and experiments into acceptable, if not perfect, agreement. Surprisingly, the guidance of the vehicle exceeded expectations. An important experimental point observed during this work was that not only is it necessary that all joints be welded in the guideway but the welds must maintain the electrical continuity of the aluminum sheets. This continuity is necessary to avoid unacceptable accelerations

when the vehicle crosses the welds. This work was reported in Reference 6 and provides the basis for Reference 7

The objective of the work reported here was to assess the dynamics of the test vehicle more fully, both experimentally and analytically, placing special emphasis on any features that might cause problems in revenue service. For that reason, the vehicle was subjected to severe perturbations to uncover any instabilities , coupling of modes that might lead to instabilities, severe track alignment requirements , etc. Major portions of the guideway had to be rewelded to achieve a ride quiet enough to evaluate these parameters.

During the same period, similar work was being performed by the Ford Motor Company under contract with the Federal Railroad Administration. The objective of the first phase of Ford's work was similar to the work performed by SRI. It differed mainly in the testing of superconducting magnets over a rotating aluminum wheel -- in essence moving the guideway rather than the vehicle. The agreement in results between these efforts provided confidence in the experiments at each laboratory. Later work at Ford concentrated on dynamics, damping, the design of a full-scale test vehicle, evaluation of the normal magnet-ferromagnetic guideway and other features of these systems as reported in References 8 and 9.

This work, as well as that at Ford, is a part of the overall effort of the Federal Railroad Administration to find the best system for transporting passengers between cities at speeds incompatible with steel wheels on steel rails. The other major system being considered at this time is the tracked air cushion vehicle. A test vehicle of this type is currently being evaluated at the High Speed Ground Test Center in Pueblo, Colorado. The overall problem extends well beyond the construction of a suspension system to such diverse topics as new forms of tunnelling, route planning,

passenger acceptance, and aerodynamic noise studies. Currently, proposals are being evaluated by the FRA for a test sled to be evaluated at speeds up to 300 mph (500 kmph).

The authors would like to acknowledge the assistance in this work provided by Mr. Robert McKee (electronics, data taking and reduction), Mr. Thomas Kittredge (active control construction), Mr. Irwin Sauer and Mr. Walter Johnson (mechanical construction and towing winch operation), Mrs. Betty Bain and Mr. David Stillinger (computer programming), and Dr. Richard Singleton (PSD analyses). The experimental work was often performed in inclement weather and not infrequently continued until after dark. The cooperation and sense of humor provided under these circumstances is greatly appreciated.

We are greatly indebted to Dr. Charles Cook for his supervision of the program and for his many suggestions for improvements in this work. Mr. Clark Henderson has discussed at length the general transportation requirements of such a system and has attempted to focus the authors' attention on the most important problems at this stage of development.

Finally, we would like to acknowledge the many constructive suggestions of Dr. John Harding of the Federal Railroad Administration.

I INTRODUCTION

The phenomenon of magnetic levitation is not original with the vehicle described in this report; a fundamental understanding of the principles has existed for many years. Some of the phenomena observed in the vehicle are common to such items as magnetic toys, watt-hour meters, speedometers, magnetic brakes, and linear induction motors. The uniqueness, therefore, does not lie in the concept but in implementing the concept in a safe, reliable, economical, passenger carrying transportation system.

As with any other system bearing the ultimate responsibility for the lives of people, confidence in the system must be gained at various levels as development progresses. The standards by which the system must be judged become increasingly more stringent. At each stage of development, there will be those who are optimistic and those who have reservations regarding the ultimate utility of such a system. Scientists and engineers can be convinced rapidly that the fundamental principles of this system are sound, which was demonstrated in the first phase of this program in 1971. In the second phase of this program, a visual demonstration of the system convinced nontechnically oriented observers that the system works--whatever the principle might be. The second phase also assured the scientists and engineers involved that the principle of passive damping was sound and provided adequate inherent stability to keep the vehicle on the guideway. Such stability is a necessary, but not a sufficient condition for the damping system to be used on the ultimate vehicle. In a strictly technical sense, there is little room for doubt at this time that a magnetically levitated vehicle can be safely incorporated into a passenger carrying transportation system.

To justify a new system -- entailing the expenditure of several billion dollars -- many technical, economic, social, and political problems must be addressed and solved. These problems should not be left to one interest group, and a solution in one setting will not necessarily be valid in another. Answers to these problems will evolve slowly. Unfortunately, until each of these problems has an obvious, attainable solution, a major effort to solve them will not be mounted-- a common, but trying circle. The purpose of this program is to answer specific technical questions that must be answered in the logical development of the system. These questions relate to the stability and ride quality of the vehicle using passive and active damping and to a demonstration that the analytic model can be used to predict the vehicle's motion.

The vehicle used in these experiments is unique in being the only solid sheet guideway system in operation on a reasonable test scale. The other major system of this type, which is in Japan, employs coils in the guideway. Another unique feature is the guidance of the vehicle by its magnetic forces. It is the only vehicle being evaluated on a test scale that is fully levitated and guided by magnetic forces. The only respect in which the vehicle differs fundamentally in its dynamic characteristics from a full-scale system is in the propulsion mechanism. It is towed by a cable connected to an engine at the end of the guideway, restricting only one of the six degrees of freedom. With this flexibility, the vehicle is ideal for testing dynamic characteristics of magnetically levitated vehicles. Since the investment in this test vehicle is comparatively small, it can and has been subjected to tests entailing significant hazards to the vehicle-- tests not likely to be repeated for some time with larger vehicles. Perhaps the major significance of this work is in the successful completion of these hazardous tests. These results demonstrate a gratifying degree of stability in the system.

The test vehicle was originally designed for the rudimentary dynamic tests of Phase II of this program. As noted in an earlier report,[6] our initial design weight goal was for a vehicle weighing from 400 to 450 pounds (180 to 205 kg.). However, before the first phase of testing was completed, the weight had increased to 650 pounds or 295 kg. On one occasion the vehicle was loaded (with the weight of one of the authors) to approximately 880 pounds or 400 kg. In the current test phase the weight of the vehicle was increased to about 1075 pounds(489 kg) by adding instruments, a recorder, and batteries. This increased weight was of considerable concern, resulting in the necessity of operating the superconducting magnets at currents 50% higher than initially anticipated. On some occasions, the current was still higher, but the magnets performed well, although the safety factor in the magnet design was reduced significantly.

Objectives

As stated previously, the objectives of this program were directed at specific technical problems. These objectives were:

(1) To compare the dynamic performance of the vehicle over the rewelded guideway with the performance observed in the second phase of this program

(2) To assess the performance of the vehicle over the welded guideway using active and passive damping mechanisms and compare the results with results from the computer simulation of the test

(3) To levitate the vehicle over symmetric and asymmetric perturbations in the guideway to produce simultaneous oscillations in several modes and compare the results with a computer simulation using active and passive damping

(4) To produce a quasi-sinusoidal perturbation in the guideway and compare observed and computed motions

(5) To seek evidence of the coupling of modes of oscillation that might lead to instabilities by producing a major oscillation in one mode and seeking evidence of that mode in other modes.

The first objective required only repeating the experiments performed in the second phase of this work, after the guideway was dismantled and rewelded with full-penetration welds. Incidental to this test was the strengthening of the vehicle frame to increase the frequency of the fundamental body flexure mode above the range of interesting rigid body modes. The second and subsequent objectives required a considerable amount of reinstrumentation. The tests that satisfied the second objective were straightforward levitations of the yehicle over the guideway. The third objective required that additional aluminum plates be placed on the guideway and that the vehicle be levitated over them. These plates, when placed on opposite sides of the guideway, produced pitch and heave oscillations, and when placed on only one side of the guideway, produced roll, pitch, heave, yaw, and side slip motions. The fourth objective, the production of a quasi-sinusoidal perturbation in the guideway, was unintentionally achieved in the process of welding the guideway. The contraction of the plates upon cooling resulted in distortions at intervals corresponding to the length of the plates (20 ft = 6.1 m) that were nearly sinusoidal in character. The purpose of this test was to move the vehicle over these distortions at such a velocity that the perturbations would drive the vehicle at its fundamental heave resonance frequency. The fifth objective of producing major oscillations was satisfied during the performance of the tests over the symmetrically located plates and by the introduction of wooden shims on one side of the guideway to produce an analogous motion in the lateral direction.

Implicit in all the objectives are assessments of factors affecting safety and ride quality. Whereas safety can be reasonably extrapolated from the results presented here, ride quality can only be assessed to the extent that various parameters affected the quality of the ride on the test vehicle. An extrapolation to a full-scale, operational vehicle must be made with care and requires a redesign of the levitation magnets and the active and passive damping mechanisms. The substructure of the guideway used in these experiments was constructed in 1970 and was not intended to conform to any particular alignment standards. The warpage caused by welding can also be better controlled in a full-scale system and should not be construed to be a fundamental limitation on the system.

II VEHICLE AND GUIDEWAY

Vehicle Description

The design and construction of the magnetically levitated test vehicle used in these experiments was discussed in an earlier report,[6] but to avoid cross-referencing and to provide a basis for discussing modifications, they are summarized in the following paragraphs.

In the second phase of this program, the vehicle was 4.25 m (13 ft 11 in.) long and approximately 1 m wide, the exact width depending on the placement of the magnets. The vehicle chassis was weighed after construction, and the final weight, after instrumentation, was estimated from the weight of the components to be 650 pounds (295 kg). The vehicle is supported at rest by four pneumatic tires, and in flight by four superconducting magnets. Guidance is provided by the superconducting magnets when in flight and by shock-mounted bumpers, located on the sides of the vehicle, when the vehicle rolls on its wheels.

The frame of the vehicle is constructed of lightweight unistrut aluminum channels covered by a flat platform made of aluminum sheathed honeycomb. The objective was to make the vehicle construction functional at the lowest possible cost--not to achieve aesthetic beauty.

The four superconducting magnets, which are 0.32 m long and 0.27 m wide, each contain approximately 580 turns of superconducting wire composed of Nb-Ti filaments embedded in a copper matrix. The magnets are enclosed in liquid-nitrogen shielded helium dewars that are 24.4 cm high, 43.8 cm long, and 37.8 cm wide. Each dewar has a capacity of 7 liters of nitrogen and 10 liters of liquid helium. The nitrogen dewar and outer shell are made of 3.2-mm-thick aluminum, and the helium dewar of 1.6-mm

stainless steel. Insulation is provided by evacuated fiberglass, which also supports the dewars against atmospheric pressure.

Included in the dewars are passive damping plates consisting of single turn copper coils. These coils are soldered to the liquid-nitrogen-cooled radiation shields to increase their electrical conductivity and damping efficiency, as described in detail in our earlier report.

The frame was reinforced for the experiments reported here by adding 1.6-mm-thick sheet-aluminum skirts to each side of the frame between the magnets. Angular aluminum strips were riveted to the bottom of these sheets for added rigidity. The frame was strengthened to increase the fundamental flexure frequency of the chassis above the frequencies of interest because this frequency interfered with the interpretation of the earlier experiments. A camera mount was provided on the rear of the vehicle.

The instrumented and modified vehicle was weighed at one time during the work reported here and weights added or removed were recorded. The weight varied as more instruments were successively added to the vehicle, but ranged from 440 to 453 kg for most of the passive damping tests with the fully instrumented vehicle, and from 476 to 483 kg for the active damping tests. The weight also varied as the liquid nitrogen and helium evaporated. The approximate moments of inertia were:

$$I_{pitch} = 950 \text{ kg m}^2; \quad I_{roll} = 37 \text{ kg m}^2; \quad I_{yaw} = 1004 \text{ kg m}^2$$

The vehicle was propelled, as in earlier experiments, by an endless cable powered by a glider towing winch. The 3/16-in. steel cable was attached to a wooden towing skid. A vertical steel pin attached to the skid made contact with the vehicle at its approximate center of mass. As discussed in our earlier report, this coupling arrangement did not restrict the vehicle's motion in roll, pitch, yaw, heave, or slip. Only the motion of the center of mass along the length of the guideway was restricted.

The layout of the vehicle, as used in the latest experiments, is shown in Figures 1 and 2.

Instrumentation

For these experiments, each set of related sensors was clustered as close as possible. The physical dimensions of the sensors prevented locating each sensor in its ideal location. The sensors installed, including their locations, are described in the following paragraphs. References to their numbered locations in Figure 1 are included.

Position Sensors

These sensors consisted of linear potentiometers attached to a rod, terminated with an aluminum wheel which made contact with the appropriate surface of the guideway. To avoid damage to the wheels as well as to reduce the noise of the vehicle while in motion, O-rings were placed in grooves in the wheels to soften the contact of the wheel with the surface. Each of the sensors was spring loaded to ensure contact with the guideway. The spring constant was 0.89 newtons/m. For a lateral displacement of 2 cm, the springs provided a restoring force of 71 newtons or provided an acceleration of 0.015 g's to the vehicle. Although undesirable, this force does not appear to be too restrictive on the experiments. The force in the vertical direction was minimized by having the springs almost completely extended at the usual levitation height. Compared with the magnetic forces, these springs constitute a negligible error. Power to the potentiometers was provided by mercury cells (27).

The vertical sensors were spaced 96.5 cm apart laterally, two being located 117 cm forward (9,14) and two (17,22) the same distance behind the towing pin located at the approximate center of mass. Lateral sensors (10,15,16,21) were located 109 cm forward and aft of the towing pin.

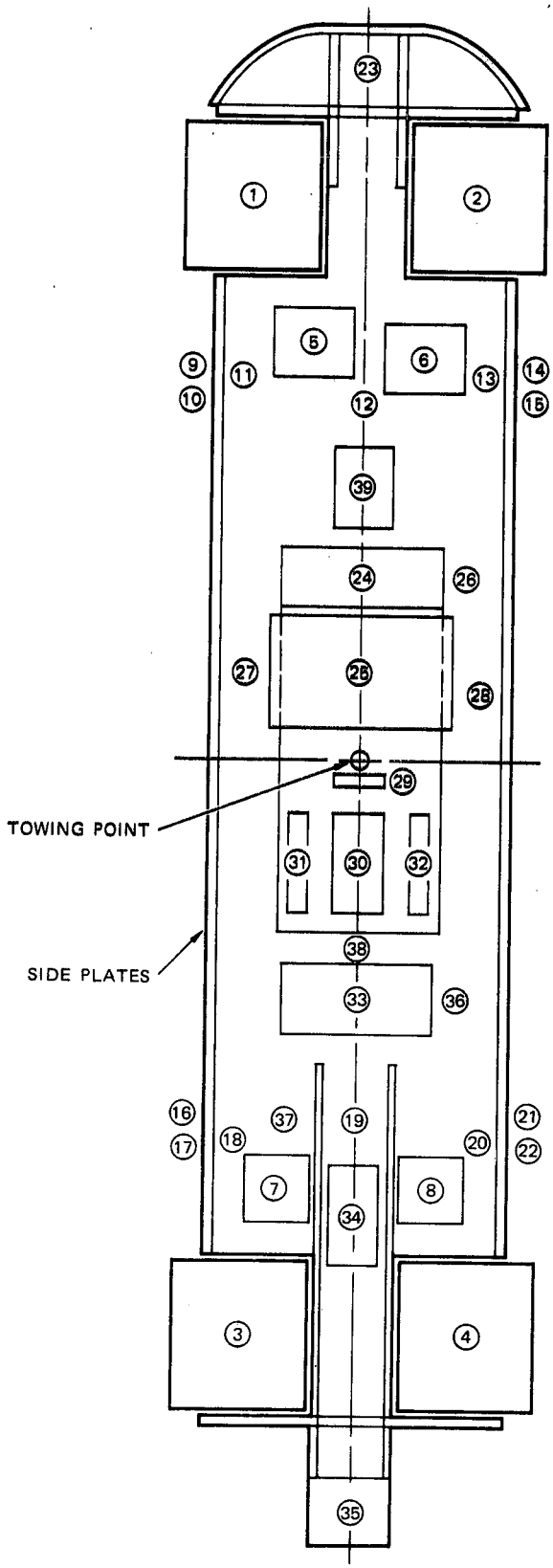

1. FL Magnet + Active Coil
2. FR Magnet + Active Coil
3. BL Magnet + Active Coil
4. BR Magnet + Active Coil
5. FL Active Control
6. FR Active Control
7. BL Active Control
8. BR Active Control
9. FL Vert. Sensor P8
10. FL Lat. Sensor P2
11. FL Vert. Acc. 1
12. Front Lat. Acc. 2
13. FR Vert. Acc. 3
14. FR Vert. Sensor P7
15. FR Lat. Sensor P4
16. BL Lat. Sensor P3
17. BL Vert. Sensor P6
18. BL Vert. Acc. 4
19. Back Lat. Acc. 5
20. BR Vert. Acc. 6
21. BR Lat. Sensor P1
22. BR Vert. Sensor P5
23. Bumper
24. Telem System + Antenna
25. 14 Channel Recorder
26. Volt Bias for Acc. 1, 2, 3
27. Volt Bias for Sensors
28. Active Filters for Accs.
29. Current Shunt
30. Magnet Battery
31. Carbon Rheostat
32. Carbon Rheostat
33. Batt. for Active Coils
34. Curr. SW for Active Coils
35. Camera Mount
36. Volt Bias for Acc. 4, 5, 6
37. Curr. Meter for Magnets
38. Acc. for Motion Down Track
39. Batt. for T. R.

SA-1080-102

FIGURE 1 DIAGRAM OF VEHICLE WITH PLACEMENT OF COMPONENTS

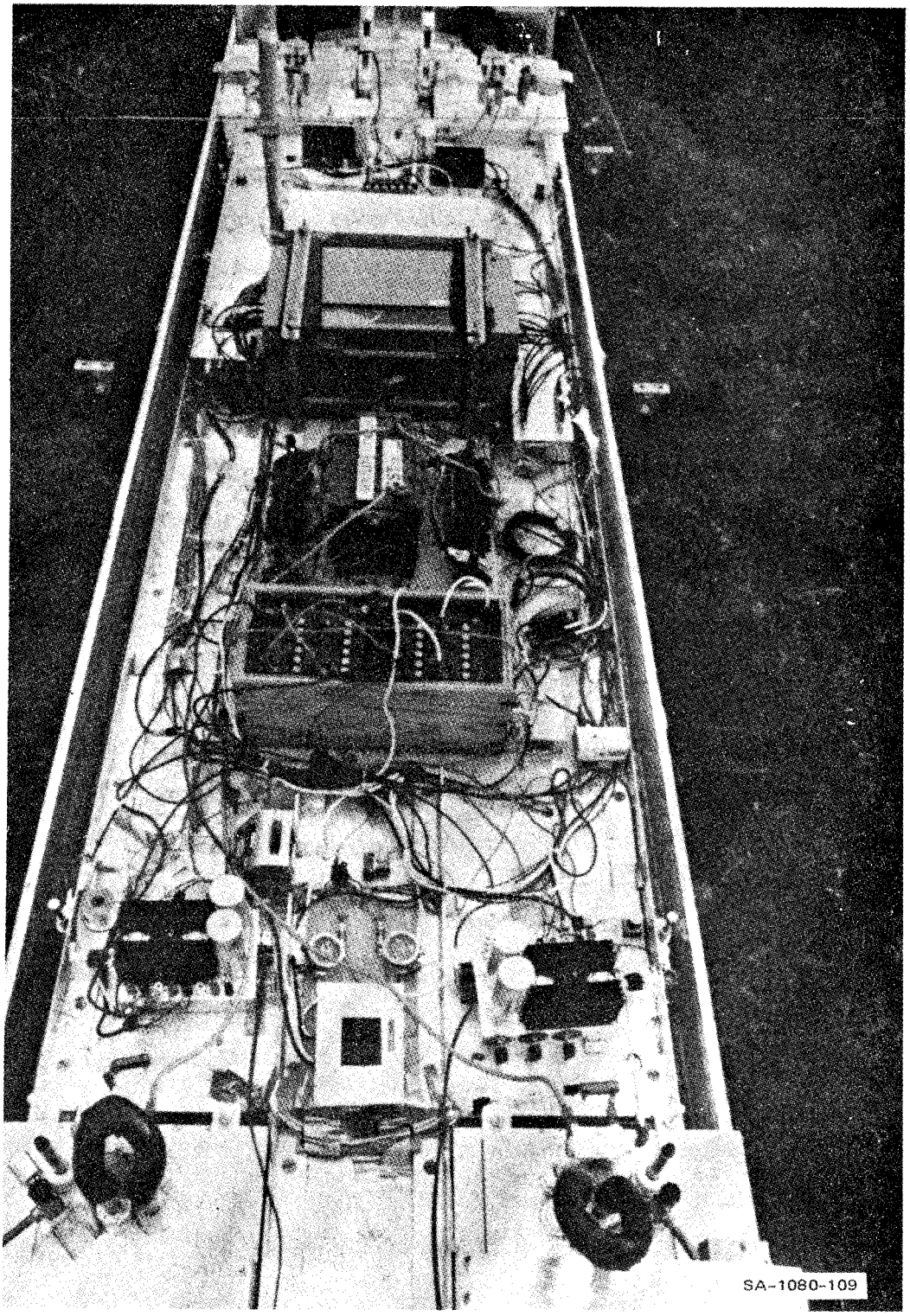

FIGURE 2 MAGNETICALLY LEVITATED VEHICLE AS USED IN ACTIVELY CONTROLLED DAMPING TESTS

Accelerometers

Six Endevco Model QA116-15 accelerometers were used to measure vertical accelerations as close as feasible to each of the suspension magnets, and to measure lateral accelerations at the points at which the lateral positions were measured. The vertical accelerometers (11,13,18,20) were located 117 cm forward and aft of the towing pin and were spaced 86 cm apart laterally. The lateral accelerometers (12,19) were located 109 cm forward and aft and were positioned on the centerline of the vehicle.

The accelerometers were powered by mercury cells (26) to avoid drift, and their outputs were filtered (28) above 150 Hz to avoid unnecessary clutter of the records caused by extraneous noise.

Magnet Current

The current of the levitation magnets connected in series was measured using a high current shunt (29). Power for the magnets was provided by a single 12-volt automobile battery (30) and was controlled by two parallel carbon pile rheostats (31,32). An on-board meter (37) was used for setting the current prior to testing.

Active Damping Coils

The active damping coils were attached to the bottoms of their respective dewars. Each coil was comprised of four 132 turn coils of No.18 copper wire operated in parallel. The current in each coil was independently regulated by control circuits (5,6,7,8) powered by a series of motorcycle batteries (39). A current switch and current meter were located between the rear magnets (34).

Data Recorders

Data from the sensors above were recorded in two ways. A 14-channel Honeywell Model 5600C FM tape recorder (25) was on board and powered

by a second series of motorcycle batteries (33). Early in these experiments these batteries were also used for powering the active damping coil controls, but the current load was too great when crossing the vertical perturbation in the track and a voltage drop occurred that caused the tape recorder to stop. Subsequent experiments were performed with independent power sources. The recorder was used for the six accelerometers and eight position sensors.

Two additional channels of recording were available through a telemetry system (24) transmitting magnet current and longitudinal acceleration (38) to a receiver located beside the guideway. These data and two-position sensing signals were recorded on photosensitive paper. The position signals were obtained from a 10-turn potentiometer connected to an idler wheel on the winch and from three photocells placed in the guideway.

Guideway Description

The guideway configuration was the same as used in our previous experiments and consists of two L-shaped aluminum sheets extending the length of the structure. Two changes were made for this work, however. The welds between successive plates were broken and rewelded through the thickness of the plates to provide better electrical continuity along the guideway. It was suspected from the results of earlier experiments, and confirmed in this work, that perturbations of the vertical motion were being caused not only by the expansion joints in the earlier guideway but also by superficial welds at these joints. Another alteration was a 7.5-cm increase in height of the side wall for a distance of 12.2 m on one side of the guideway. This addition was made to establish the effect of the finite height of the wall on the guidance force.

Each of the L-shaped components of the guideway was 46 cm wide,

15 cm high, and 1.9 cm thick, and was made of either 6101-T6 or 1100-H14 aluminum, both having an electrical resistivity of about 3×10^{-8} Ω m at ambient temperature. Both materials are soft compared with more commonly used aluminum structural alloys. Tensile strengths (yield) are 19.7 and 12.0 kg/mm^2, respectively, compared with a strength of 51.3 for 7075-T6.

The vertical profile of the guideway was surveyed twice during this program--once at 4-foot intervals on one side and later at 1-foot intervals on both sides. The results of this latter survey are shown in Figure 3. The conspicuous rise of approximately 3/4-in. (1.9 cm) between the 40- and 50-foot positions is especially noteworthy in that it was not present in the earlier survey. The only plausible explanation for its occurrence is the amount of rainfall between the two surveys. Only the first 260 feet of the 400-foot guideway were surveyed in the latest survey. This is the region where most experiments were performed--deceleration usually occurred in the farthest sections of the guideway.

The survey starts at the beginning of the aluminum plates, although the wooden substructure extends 54 feet beyond zero in this figure. When vertical offsets were made in the guideway, additional 3/4-in.-thick aluminum plates were placed on the guideway starting at the 48-foot mark. For symmetrical perturbations, two plates, each 20 feet long, were used--one on each side. An asymmetric perturbation was produced by placing both sheets on the same side of the guideway. Any electrical contact with the underlying aluminum was incidental. Plywood sheets were placed over the aluminum sheets preceding the vertical perturbations to avoid an upward step which would damage the vertical sensors.

A lateral perturbation in the form of sheets of wood placed on the inside surface of the vertical plates on one side was begun at the 88- ft. position on the guideway. The lateral profile of the guideway was not

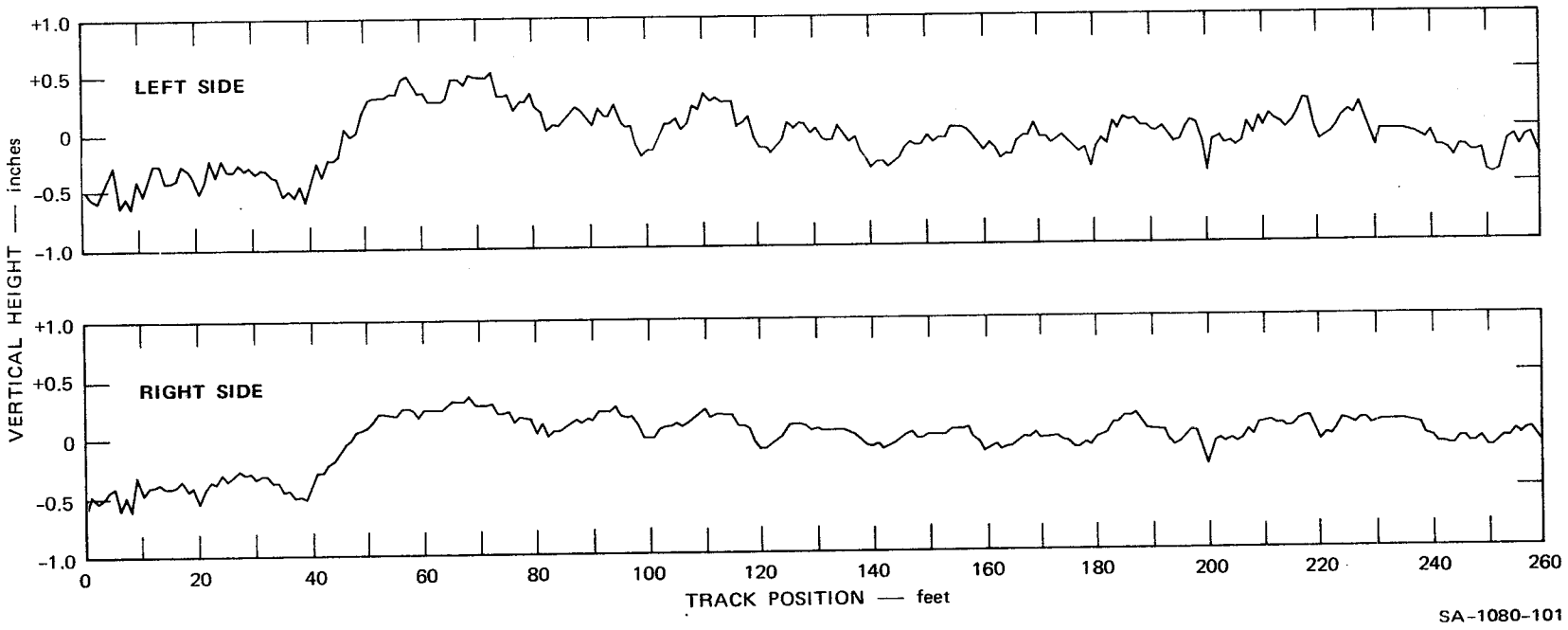

FIGURE 3 GUIDEWAY SURVEY

surveyed, however the gauge was obtained by summing two opposing lateral position sensors. The gauge obtained is shown in Figure 4. In this case, the abcissa is linear in time rather than position. The periodic occurrence of perturbations occurs at 20-foot intervals and provides a measure of the velocity. These perturbations were caused by the contraction of the plates upon cooling after welding the joints.

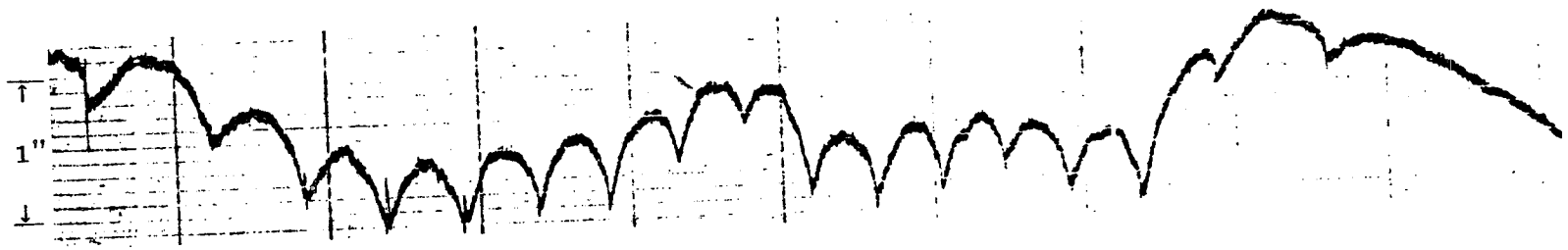

FIGURE 4 TYPICAL VARIATIONS IN GUIDEWAY GAUGE

III DYNAMIC ANALYSIS

In the initial SRI feasibility study of magnetically levitated high-speed-ground vehicles[1] an analysis of the dynamical motion of such a vehicle was undertaken. The ultimate goal of the dynamic analysis was to assess the safety and ride quality of a MAGLEV vehicle when it is subjected to various perturbations, such as wind gusts, centripetal forces in cornering, or guideway irregularities. Because some of these perturbations might lead to sizeable rotations of the vehicle, the analysis was based on the numerical integration of the nonlinear equations of motion, a computer program was written to integrate these equations. The status of this analysis prior to the present program is described below.

In the present program, this analysis was used to determine the extent of agreement between the measured and predicted motions of the vehicle, and as a tool in interpreting the experimental data. For these purposes, several additions to the analysis were required. These additions are described in a later section of this report.

Prior Status of the Analysis

A detailed description of the analysis is given in a previous report[1]. A summary is presented here. The analysis of the dynamical motion of a MAGLEV vehicle is embodied in a computer program. The program solves the governing equations for a general rigid body undergoing large displacements in six degrees of freedom. The six nonlinear equations of motion and six auxiliary equations are numerically integrated

using the Runge-Kutta method.

Coordinate Systems

It is convenient to express the required mathematical relationships in different coordinate systems. Three right-hand Cartesian coordinate systems are used here.

Track Coordinate System--The track coordinate system is fixed in an inertial reference frame with its origin at a fixed point in the track. The track coordinates x_T, y_T, z_T are used to specify the position of the vehicle center of mass relative to a fixed reference frame as shown in Figure 5. All the forces on the vehicle are calculated in the track coordinate system.

Space Coordinate System--The space coordinate system has its origin at the vehicle center of mass. The space coordinates x_S, y_S, z_S are parallel to the track coordinates x_T, y_T, z_T, and are used in describing the orientation of the vehicle with respect to the body coordinate system discussed below. Note that in both the track and space coordinate systems z_S and z_T are positive when oriented downward.

Body Coordinate System--The body coordinate system is fixed in the vehicle with the origin located at the vehicle center of mass and with the x_B-, y_B-, and z_B-axes fixed in the vehicle and parallel to its axes of principal moments of inertia. The equations of motion of the vehicle are written in the body coordinate system.

Euler Angles--To transform from the body coordinate system to the space coordinate system the Euler angles ψ (yaw), θ (pitch) and ϕ (roll) are introduced (Figure 5). The orientation of the space coordinate system can be reached from the body coordinate system by successive rotations as follows: (1) a positive rotation ψ about the z_B-axis resulting in the intermediate coordinate system (x', y', z');

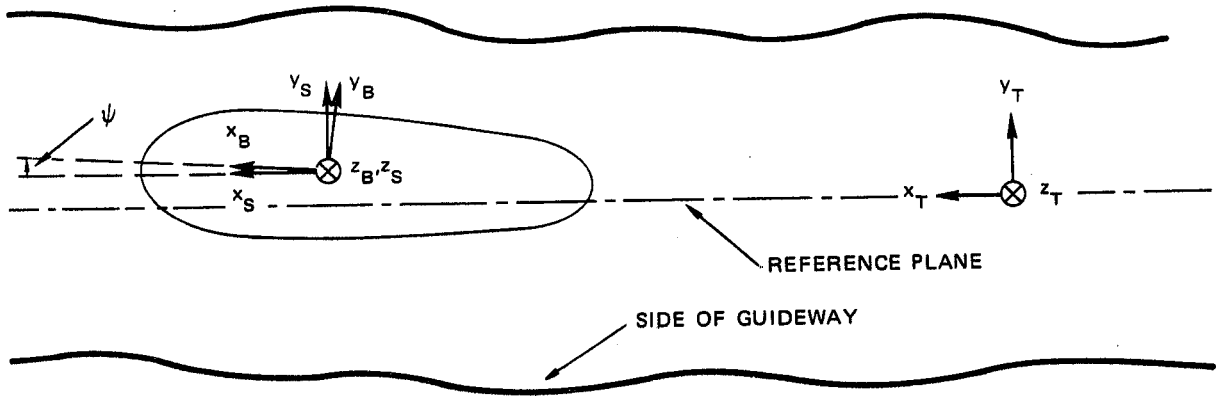

(a) TOP VIEW, SHOWING THE HEADING ANGLE, ψ

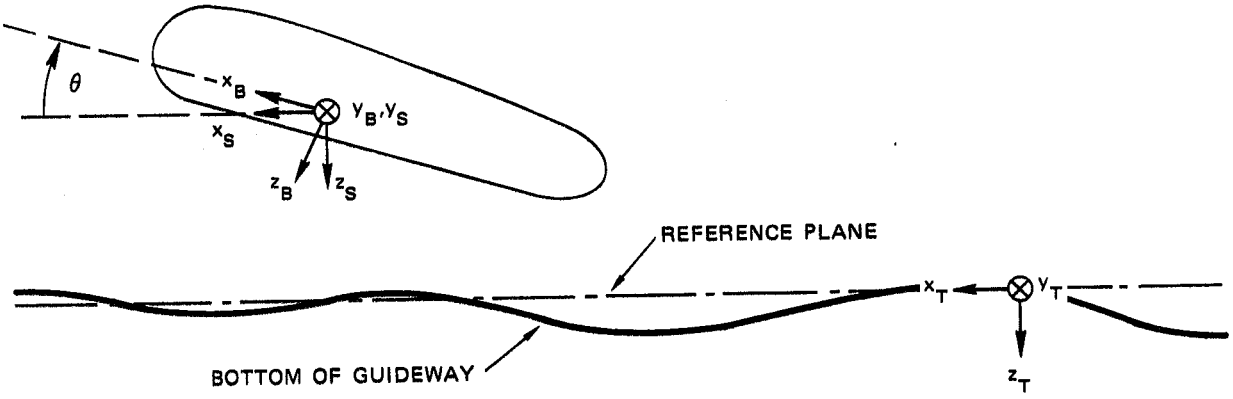

(b) SIDE VIEW, SHOWING THE ANGLE OF ATTACK, θ

SA-1080-51

FIGURE 5 GEOMETRY USED IN THE DYNAMIC ANALYSIS, SHOWING THE TRACK, BODY, AND SPACE COORDINATE SYSTEMS AND THE EULER ANGLES

(2) a positive rotation θ about the y' axis resulting in the intermediate coordinate system (x', y', z'); and (3) a positive rotation ϕ about the x' axis resulting in the space coordinate system (x_S, y_S, z_S).

The resulting matrix of direction cosines between the body coordinate system is

$$[\ell] = \begin{bmatrix} \cos\psi\cos\theta & (-\sin\psi\cos\phi + \cos\psi\sin\theta\sin\phi) & (\sin\psi\sin\phi + \cos\psi\sin\theta\cos\phi) \\ \sin\psi\cos\theta & (\cos\psi\cos\phi + \sin\psi\sin\theta\sin\phi) & (-\cos\psi\sin\phi + \sin\psi\sin\theta\cos\phi) \\ -\sin\theta & \cos\theta\sin\phi & \cos\theta\cos\phi \end{bmatrix}$$

A vector $\vec{R}$ in space coordinates transforms from a vector $\vec{r}$ in body coordinates as follows:

$$\vec{R} = [\ell]\,\vec{r}$$

Since this is an orthogonal transformation, $[\ell]^{-1} = [\ell]^{t}$ and the inverse transformation is

$$\vec{r} = [\ell]^{-1}\vec{R} \text{ or } \vec{r} = [\ell]^{t}\vec{R}$$

where $[1]^{-1}$ and $[\ell]^{t}$ represent the inverse and transpose of matrix $[\ell]$.

Governing Motion Equations

There are six equations of motion: Three governing translation (Newton's second law) and three governing rotation (Euler's dynamical equations). They are expressed in the body coordinate system:

$$\dot{u}_x = -g\sin\theta - u_z\Omega_y + u_y\Omega_z + \frac{A_x + P_x + F_x - F_{Dx} - WF_x}{m} \quad (1)$$

$$\dot{u}_y = g\cos\theta\sin\phi - u_x\Omega_z + u_z\Omega_x + \frac{A_y + P_y + F_y - F_{Dy} - WF_y}{m} \quad (2)$$

$$\dot{u}_z = g\cos\theta\cos\phi - u_y\Omega_x + u_x\Omega_y + \frac{A_z + P_z + F_z - F_{Dz} - WF_z}{m} \quad (3)$$

$$\dot{\Omega}_x = \frac{I_{yy} - I_{zz}}{I_{xx}} \Omega_y \Omega_z + \frac{M_x + \tau_x + G_x}{I_{xx}} \tag{4}$$

$$\dot{\Omega}_y = \frac{I_{zz} - I_{xx}}{I_{yy}} \Omega_z \Omega_x + \frac{M_y + \tau_y + G_y}{I_{yy}} \tag{5}$$

$$\dot{\Omega}_z = \frac{I_{xx} - I_{yy}}{I_{zz}} \Omega_x \Omega_y + \frac{M_z + \tau_z + G_z}{I_{zz}} \tag{6}$$

where

u_i = component of translational velocity

Ω_i = component of rotational velocity

A_i = aerodynamic forces

P_i = propulsive forces

F_i = magnetic forces

F_{Di} = damping forces

W_{Fi} = wheel forces

I_{ii} = moments of inertia

m_i = aerodynamic moments

τ_i = propulsive moments

G_i = magnetic moments

m = vehicle mass

Six auxiliary equations are required to relate the Euler angles and the components of displacement of the vehicle's center of mass in track coordinates to those in body coordinates. These equations are:

$$\dot{\psi} = \sec\theta(\Omega_y \sin\phi + \Omega_z \cos\phi) \tag{7}$$

$$\dot{\theta} = \Omega_y \cos\phi - \Omega_z \sin\phi \tag{8}$$

$$\dot{\phi} = \Omega_x + \tan\theta(\Omega_z \cos\phi + \Omega_y \sin\phi) \tag{9}$$

$$\dot{\bar{S}}_x^* = u_x(\cos\theta\cos\psi) + u_y(-\cos\phi\sin\psi + \sin\phi\sin\theta\cos\psi) + u_z(\sin\phi\sin\psi + \cos\phi\sin\theta\cos\psi) \tag{10}$$

$$\dot{\bar{S}}_y^* = u_x(\cos\theta\sin\psi) + u_y(\cos\phi\cos\psi + \sin\phi\sin\theta\sin\psi) + u_z(-\sin\phi\cos\psi + \cos\phi\sin\theta\sin\psi) \tag{11}$$

$$\dot{\bar{S}}_z^* = u_x(-\sin\theta) + u_y(\sin\phi\cos\theta) + u_z(\cos\theta\cos\phi) \tag{12}$$

where $\dot{\psi}$, $\dot{\theta}$, and $\dot{\phi}$ are the Euler angular velocities and $\dot{\bar{S}}_{x_T}$, $\dot{\bar{S}}_{y_T}$ and $\dot{\bar{S}}_{z_T}$ are the three velocity components of the vehicle's center of mass in track coordinates.

The analysis accounted for three types of forces (and the corresponding moments): velocity-dependent lift forces, perfect-image guidance forces, and damping forces from passive coils with negligible inductance. Several refinements and additions to the representation of the forces and moments acting on the vehicle have been made in the present program as described below.

Modifications to the Analysis

Passive Damping

The subroutine which calculates the damping forces generated by the passive damping coils has been refined to include the inductance of these coils.[6] With this refinement the current in each damping coil is a dependent variable governed by the circuit equation for the coil:

$$Ri_d + i_d \frac{d}{d(2z)}\left(L_d - M_{23}\right)\frac{d(2z)}{dt} + \left(L_d - M_{23}\right)\frac{di_d}{dt} - I_v \frac{dM_{13}}{d(2z)}\frac{d(2z)}{dt} = 0 \tag{13}$$

where

R = coil resistance

i_d = coil current

L_d = coil inductance

M_{23} = mutual inductance between the damping coil and its image

M_{13} = mutual inductance between the vehicle magnet coil and damping coil image

I_v = magnet coil current (assumed constant)

The damping force is then related to the damping current by the equation

$$F_{damp} = 2I_v i_d \frac{dM_{13}}{dz} \tag{14}$$

Thus, four new dependent variables, the damping currents, i_d, or, equivalently, the damping forces, F_{damp}, are introduced. The governing equations for this system now number 16: six equations of motion, six auxiliary equations, and four circuit equations. As before, this system of simultaneous differential equations is numerically integrated by the Runge-Kutta method to obtain the 12 dependent variables which define the motion of the vehicle and the four dependent variables which define the forces generated by the passive damping coils.

Active Damping

A new subroutine has been created to account for the forces generated by the active damping coils. The active damping force is given by

$$F_{\text{active damp}} = F_{\infty} \cdot f_L(v) \tag{15}$$

where $F_\infty = \frac{\mu_o (NI)(N_c I_c)}{\pi(z_o + z_c)} \left[(L^2 + 4z_o z_c)^{1/2} + (W^2 + 4z_o z_c)^{1/2} \right.$

$$- 2(z_o + z_c) + \frac{(L^2 + 4z_o z_c)^{1/2} - (L^2 + W^2 + 4z_o z_c)^{1/2}}{L^2 + 4z_o z_c} \cdot 4z_o z_c$$

$$\left. + \frac{(W^2 + 4z_o z_c)^{1/2} - (L^2 + W^2 + 4z_o z_c)^{1/2}}{W^2 + 4z_o z_c} \cdot 4z_o z_c \right] \quad (16)$$

μ_o = permeability of the magnet

NI = amp turns in lift magnet

$N_c I_c$ = amp turns in active coil

z_o = height of lift magnet above guideway at equilibrium

z_c = height of active coil above guideway at equilibrium

L = length of lift magnet (equal to length of control coil)

W = width of lift magnet (equal to width of control coil)

$f_L(v)$ = a function which accounts for the dependence of the lift force on the velocity down the guideway.

The control current is determined by the absolute vertical position, velocity, and acceleration of a sensor located near the control coil according to the equation $I_c = \alpha z + \beta \dot{z} + \gamma \ddot{z}$ where the feedback quantities lead the active damping current by 0.01 sec. For the active damping coils on the SRI vehicle the maximum values of the feedback coefficients are

α_{max} = 11,650 A m^{-1}

β_{max} = 770 A m^{-1} sec

γ_{max} = 51 A m^{-1} sec^{+2}

Guidance Force

The calculation of guidance force was modified to include its dependence on the vehicle velocity down the guideway. The guidance force is now calculated according to

$$F_G = F_G(\infty) \cdot f_G(v) \qquad (17)$$

where $F_G(\infty)$ is the perfect-image guidance force (at infinite velocity) and $f_G(v)$ is a function which accounts for the dependence of the guidance force on the velocity down the guideway as shown in our earlier report.[6]

Guideway Profile

Two deviations from a perfectly flat guideway were present in the vehicle experiments: relatively small inherent irregularities arising from plate warping, ground settling, etc., and larger, well defined purturbations designed to give the vehicle large oscillations. In an effort to simulate the experimental data analytically and to determine the effect of inherent track perturbations on vehicle motion, both types of guideway perturbations were modeled in the analysis.

The inherent irregularities were first determined in a survey of the guideway. In the survey the vertical deviation of the guideway from a horizontal flat plane was measured at a discreet number of points at 1-foot intervals. Both sides of the guideway were surveyed. At each time step in the programmed solution the vertical deviation of the guideway was then calculated by linear interpolation between two adjacent surveyed points.

The explicit perturbations produced by a 3/4-inch thick aluminum plate placed on the surface of the guideway were also modeled. Physically the vertical deviation in the guideway at each end of such a plate spans an infinitesimal length of the guideway (i.e., a discontinuity). However, the lift magnet has a finite length; therefore the resulting perturbation in lift force is a continuous function of time and has a

duration equal to the time it takes the magnet to traverse the edge of the plate.

In the analysis the lift magnet is modeled as a point, i.e., it has an infinitesimal length. Therefore, to produce a perturbation in lift force which is a continuous function of time and has the correct duration, each edge of the plate was modeled as a vertical deviation in the guideway over a length equal to that of the actual magnet. More specifically, each was modeled as a ramp with a maximum vertical deviation of 3/4 inch. Hence, the overall shape of the plate is that of a trapezoid.

Longitudinal Acceleration Input

In most experiments the velocity of the vehicle down the track is not constant. Since the frequency of track perturbations, the magnetic force, and other parameters are determined by the instantaneous value of the vehicle velocity, some information about how the velocity is changing is required to model the vehicle motion. In the present analysis this information was input through the measured longitudinal acceleration $\dot{u}_x$. (In the analysis this quantity was most conveniently interpreted as a net propulsive force $P_x = m\dot{u}_x$ shown on the right-hand side of Equation (1).) After the initial vehicle velocity u_{xo} is specified, the velocity at later times is then obtained in the integration of the equations of motion.

Sensor Output

In the experiments the vehicle motion was monitored by measuring the position and acceleration in the vertical and lateral directions at several points on the vehicle. So that a direct comparison could be made between the experiments and the analysis, the twelve dependent variables which describe the motion of the vehicle were interpreted in terms of the quantities measured by the sensors.

To interpret the calculated vehicle motion in terms of the quantity measured by a vertical position sensor two modifications to the analysis

were required. First, the vertical position of the vehicle at the location of the sensor, r_s, was calculated according to the relation

$$r_s = \bar{S}_{z*} - r_x \sin\theta + r_y \sin\varphi \qquad (18)$$

where $r_i = \vec{r} \cdot \vec{e}_i$

$\vec{r}$ = the position vector from the vehicle center of mass to the sensor in body coordinates,

$\vec{e}_i$ = a unit vector in body coordinates, and $\bar{S}_{z*}$ is the vertical c.m. position.

Second, the discontinuities in the guideway (e.g., the edge of a plate) which cause a discontinuity in the output of a vertical sensor were also included in the analytical output.

To interpret the calculated vehicle motion in terms of the vertical acceleration measured by an accelerometer, the acceleration at a point other than the center of mass was calculated. This acceleration, a_z, is related to the dependent variables by the relation

$$a_z = \dot{u}_z + (r_x\Omega_z - r_z\Omega_x)\Omega_x - (r_z\Omega_y - r_y\Omega_z)\Omega_y + r_y\dot{\Omega}_x - r_x\dot{\Omega}_y \qquad (19)$$

Drag Force Calculation

The capability to calculate the magnetic drag according to the analysis given in a previous report[1] has been added to the computer program. This force, like the lift force, is introduced as a function fitted to the results from a seperate program that performs the exact analysis. This capability requires that the propulsion force (provided by the winch cable in the experiments) also be inputted.

Lift Current Input

The capability to calculate the magnetic forces from a variable magnet current has also been added to the computer program. This current can be inputted from that measured in experiments.

IV ACTIVE DAMPING SYSTEMS ANALYSES

One of the advantages of a MAGLEV (superconducting magnetic repulsion) system for high-speed ground transportation is that large suspension heights ($\sim$ 0.3 m for 300 mph) of the vehicle above the track can be obtained. Consequently, the ride quality of the vehicle is less sensitive to track irregularities than magnetic levitation schemes operating with considerably smaller clearances (e.g., magnetic attraction clearance $\sim$ 1 cm). Since the construction and maintenance of an accurate guideway can be expensive, and constitute a substantial percentage of the total cost of such a system, there is a great advantage to being able to tolerate initial guideway inaccuracies and guideway changes over time.

The ride quality specifications established by the FRA determine the maximum permissible vehicle accelerations as a function of frequency. These specifications are flat from 0 to 1 Hz and require a slight decrease in the accelerations from 1 to 3 Hz, with a substantial drop above 4.5 Hz. The natural heave frequency of a full-scale MAGLEV vehicle is expected to be in the 1 to 2 Hz range. Consequently, the vertical heave acceleration will also be peaked in this range, and may exceed the FRA specification. Thus, some form of damping is desirable to improve the ride quality by lowering the frequency and amplitude of the peak to the less stringent 0 to 1 Hz region of the FRA specification. Damping is basically necessary to avoid instabilities in the vehicle's motions. Passive electromagnetic damping was employed for the above purposes in earlier tests and was tested more extensively in this work.

It is not known at this time whether sufficient damping is available from passive techniques, to provide the ride quality required for a

revenue vehicle. The use of passive damping is highly desirable even if other types of damping are also employed, since it provides a reliable back-up system to ensure safety in the event an active damping system fails.

Active damping can be used to achieve a desired ride quality over a guideway too rough to be used with passive damping alone. Consequently, there may be a considerable economic advantage to using an active system in conjunction with a passive damping system.

Active damping uses a conventional electromagnet placed between the superconducting magnet used for suspension and the conducting guideway. By servo-controlling the current in the electromagnet to respond to changes in vertical acceleration, velocity, or position, active damping of the vehicle's vertical motions can be accomplished. Two characteristics are of primary concern in active damping. First, the natural heave frequency can be shifted to a lower frequency, if position or acceleration feedback is used. Second, the proper combination of feedback parameters will result in the required ride quality for the least amount of active control power.

This active damping problem has been examined by Ford[9] and is discussed by Wilkie.[10] Wilkie examines an active damping system which incorporates a small ($\sim$ 5%) additional current in the main suspension magnet to control the ride quality. A similar approach was taken in the current program, but in this program the control current drives a second magnet close to the main magnet. The analysis of this system can be shown to be identical to that of Wilkie, with slight modifications.

When there is no perturbation in the guideway, the control current, I_c, should be zero. The interaction of the actively controlled magnet with its image drops out of the calculation because $I_c = 0$ at equilibrium. (The problem is defined in Figure 6.) The interaction of the magnets with their images produces four lift forces: two are identical,

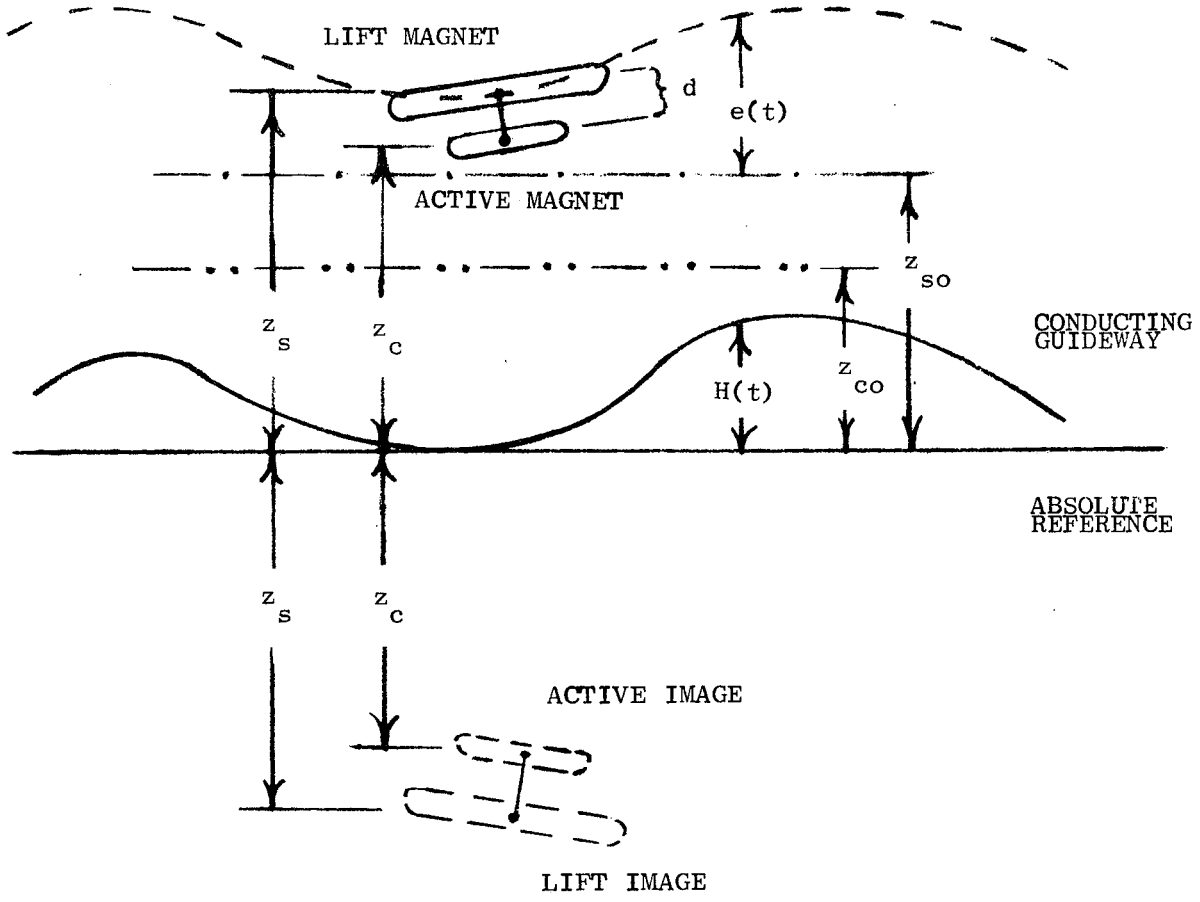

LIFT MAGNET:

Absolute Position $z_s = z_{so} + e(t)$

Relative Position $r_s = z_{so} + e(t) - H(t)$

ACTIVE MAGNET:

Absolute Position $z_c = z_{co} + e(t)$

Relative Position $r_c = z_{co} + e(t) - H(t)$

Note: Magnets are structurally bound such that $z_s = z_c + d$

FIGURE 6 DIAGRAM OF GEOMETRY USED IN ACTIVE CONTROL ANALYSIS

one drops out, and a fourth is the main lift force on the superconducting magnet.

The dependence of the lift force on the magnet current, and the vehicle's velocity and suspension height, were given in an earlier report.[1] The damping force is similar to the lift force in these respects. The earlier formulae, however, must be modified to correct for the suspension height of the control coil (which is a distance, d, lower than the suspension magnets) and the magnet currents. This suspension height correction is introduced through a parameter K. The suspension force is proportional to the square of the current in the suspension magnet, but the damping force is proportional to the product of the currents in the suspension and control magnets. This correction is introduced through a parameter α, and modifies Wilkie's Equation (9) to give the following equation of motion:

$$\ddot{e}(t) + \omega_n^2[e(t) - H(t)] - 2K\alpha I_c = 0, \qquad (20)$$

where e(t) is the vertical deviation of the suspension magnet from a straight line in the inertial frame, H(t) is the vertical deviation of the guideway in the same reference frame, and I_c is the active control current. The natural frequency of vertical oscillation is given by:

$$\omega_n^2 = \frac{-2I_{so}^2 N_s^2}{m} f'(2z_{so}) \qquad (21)$$

where I_{so} is the constant current in the suspension magnet, N_s and N_c are the numbers of turns in the suspension and control magnets, respectively, and

$$\alpha = N_c g / N_s I_{so}. \qquad (22)$$

The vertical position correction parameter K is given by

$$K = \frac{I_{so}^2 N_s^2}{mg} f(2z_{so} - d) \tag{23}$$

and equals

$$\frac{f(2z_o - d)}{f(2z_o)} \tag{24}$$

for the initial conditions $e(t) = 0$, $H(t) = 0$, and $I_c = 0$. K is unity when the control and suspension magnets are coincident ($d = 0$). The function, f, is the normalized constant velocity lift force given in our earlier reports.[1,6]

The control current, I_c, can be made to depend on absolute values of the vertical acceleration or velocity and either absolute or relative positions or combinations of any of these. This can be accomplished by assuming the following form for I_c:

$$I_c = q_o \ddot{e}(t) + q_1 \dot{e}(t) + q_2 e(t) - q_2' H(t). \tag{25}$$

For absolute position feedback, $q_2' = 0$, and for relative position feedback $q_2' = q_2$. This form of active control current yields the following general equation of motion:

$$\ddot{e}(t)[1 - 2K\alpha q_o] - \dot{e}(t)2K\alpha q_1 + e(t)[\omega_n^2 - 2K\alpha q_2]$$

$$= [\omega_n^2 - 2K\alpha q_2']H(t). \tag{26}$$

The oscillatory, steady-state form of this equation can be found by taking its Fourier transform to obtain:

$$E(j\omega) = \frac{[\omega_n^2 - 2K\alpha q'_2]\tilde{H}(j\omega)}{[\omega_n^2 - 2K\alpha q_2] - \omega^2[1 - 2K\alpha q_o] - j\omega\, 2K\alpha q_1} \tag{27}$$

where $E(j\omega)$ and $\tilde{H}(j\omega)$ are the transformed functions e(t) and H(t). This expression is similar to Equation (13) of Reference[10] if $q_o = 0$ and $q_2' = q_2$.

The corresponding acceleration is shown below using the earlier initial conditions.

$$\ddot{E}(j\omega) = \frac{-\omega^2[\omega_n^2 - 2K\alpha q_2']\tilde{H}(j\omega)}{[\omega_n^2 - 2K\alpha q_2] - \omega^2[1 - 2K\alpha q_o] - j\omega\, 2K\alpha q_1} \quad (28)$$

It should be noted from Equation (28) that velocity feedback alone (q_o, $q_2 = 0$) does not shift the resonances of the vertical accelerations. However, position (q_2), or acceleration, (q_o), feedback will shift the resonant frequency. It also should be noted that the transformation from relative position feedback ($q_2' = q_2$) to absolute position feedback ($q_2' = 0$) increases the frequency independent coefficient on the right side of Equation (28) ($[\omega_n^2 - 2K\alpha q_2']$), since $2K\alpha q_2'$ is positive definite. This means that more control power is used in correcting the motion from a given track perturbation, when absolute rather than relative position feedback is used. Ford[8] did a parametric study of the feedback for this problem and concluded that the best ride quality was obtained with the least control power when absolute velocity and relative position feedback were used.

The above analysis does not include relative velocity and acceleration feedback. In the tests performed only absolute velocity feedback was used for controlling the active damping currents.

It is advantageous to use a separate magnet for active damping because the active control is not required to handle the large dc currents associated with the main lift magnets. When the lift magnets are in a persistent mode of operation, there is an added safety feature resulting from a sustained lift force during a vehicle power failure. It is also

possible with a separate actively controlled magnet to position it closer to the guideway to increase the correction force for a given control current ($K \gg 1$) and to reduce ac losses in the superconducting magnet by a reduced mutual inductance. In conclusion, it is generally possible to incorporate an active damping system with a superconducting magnet MAGLEV vehicle by the use of a separate, active magnet and improve the ride quality with reduced tolerances in the guideway.

Circuit Analysis

An active damping system of this type was incorporated in the SRI MAGLEV vehicle. All three parameters, referenced to the inertial frame, were available for active control of the currents. The control current in each of the magnets was given by the following equation.

$$I_c = q_o \ddot{e}(t) + q_1 \dot{e}(t) + q_2 e(t) \tag{29}$$

On-board sensing of $\ddot{e}(t)$ was obtained from vertical accelerometers placed near each magnet. Equation (29) can be rewritten as

$$I_c = q_o \ddot{e}(t) + \frac{q_1}{\omega_c}\left(\omega_c \int_o^t dt\right)\ddot{e}(t) + \frac{q_2}{\omega_c^2}\left(\omega_c^2 \int_o^t \int_o^t dt^2\right)\ddot{e}(t) \tag{30}$$

where the latter two terms have the same form as single and double analog integrators with unity gain at frequency ω_c, operating on the acceleration $\ddot{e}(t)$. Then, if the acceleration is in the form of a voltage, Equation (30) is also in the form of an actual circuit equation. Using the following substitutions

$$q_o = Gmq_o'', \quad q_1 = Gm\omega_c q_1'', \quad q_2 = Gm\omega_c^2 q_2'' \tag{31}$$

where Gm is the overall gain conversion for the analog circuit and has a value of 500 A per g, Equation (30) becomes

$$I_c = Gm\left[q_o''\ddot{e}(t) + q_1''\left(\omega_c \int_o^t dt\right)\ddot{e}(t) + q_2''\left(\omega_c \int_o^t \int_o^t dt^2\right)\ddot{e}(t)\right] \quad (32)$$

where q_o'', q_1'', q_2'' refer to the percentage of full-scale setting of potentiometers Nos. 1, 2, and 3 in the circuit of Figure B-1 in the Appendix. For a vehicle velocity of 10 m/sec, a weight of 1000 lb, and a current, I_{so}, of 100 A in the superconducting magnets, a suspension height of z_{so} = 8.5 cm, and a value of d = 5.0 cm, f(z) can be found from the earlier report and gives the value K = 1.72. The nominal values of the magnetic windings used were N_s = 580 and N_c = 132, respectively. The integration frequency was set at $\omega_c = 2\pi(2.4\ \text{Hz})$. The slope of the f(z) curve in the earlier report for a value of z = 8.5 cm at a velocity of 10 m/sec is -4.3×10^{-6} N $(\text{At})^{-2}\,\text{m}^{-1}$. The vehicle weight per magnet is 1.1×10^3 N. Thus, from the definition of ω_n^2 given earlier and using the values of the parameters listed above, ω_n has the value of $2\pi(2.34\ \text{Hz})$, which simplifies the calculations, because the ratio ω_n/ω_c is then unity. The integrators will operate above a frequency of 0.2 Hz, which is well below the resonant peak. From Equation 28, for the case of velocity feedback, only ($q_2 = q_o = 0$), and using absolute position feedback ($q_2' = 0$), we see that critical damping is obtained for $q_1 = \frac{\omega_n}{K\alpha}$. This requires q_1'' to be set at

$$q_1'' = \frac{1}{Gm}\,\frac{1}{K\alpha}\,\frac{\omega_n}{\omega_c} = \frac{N_s I_{so(1)}}{gN_c GmK} = \frac{(5.8 \times 10^4)}{(6.60 \times 10^4)(1.72)} \approx 1/2 \quad (33)$$

Thus, for the particular case mentioned for velocity feedback only, 1/2 F.S. setting of potentiometer No. 2 would yield critically active damping. The other possible combinations can be examined in a similar manner, but were not used in the experiments.

This circuit is assumed to be operating in an ideal fashion. Since the active controls are limited by the current source used (e.g., a battery),

the active control current response for a particularly large acceleration will degrade above a maximum permissible acceleration, and no longer operate in an ideally damped mode. A recovery time from a large perturbation also exists that will also degrade the circuit's performance. These effects were experimentally observed. Consequently, any passenger vehicle traveling at 300 mph would most likely incorporate forward-looking acceleration sensors to anticipate the active current needs before they are encountered. These sensors would change the vehicle ride quality by having the effect of reducing the size and lengthening the interval for a particular set of guideway perturbations. The circuit described here was primarily used to investigate the improvement in ride quality from acting damping, rather than to necessarily optimize the overall system. Even with only 75% of the actively controlled magnets operating correctly, the experiments clearly demonstrated an improvement in ride quality.

V EXPERIMENTAL RESULTS AND ANALYSES

Introduction

The experiments of Task 3 were performed for two reasons: first, to provide more definitive data on the behavior of the vehicle when using passive and active damping than could be obtained in the previous experiments with a poorly welded guideway and insufficient instruments, and second, to investigate the stability of the vehicle. The emphasis in this program was on obtaining experimental data; it was recognized that detailed analyses could be made in the future.

These experiments can be grouped into four broad categories: Those experiments that were performed (1) to measure the effects of improving the guideway electrical conductivity and vehicle rigidity, (2) to measure the vertical motions of the system, (3) to measure the lateral motion of the vehicle, and (4) to measure the simultaneous vertical and lateral motions of the system as well as all the angular modes of oscillation. These tests were also used to search for evidence of the coupling of different modes of oscillation.

The experimental parameters were restricted by the apparatus used. The maximum suspension height was limited by the height of the sidewalls of the guideway (15 cm) in earlier experiments; however, as the weight of the vehicle increased, the suspension height was limited by the current-carrying capability of the superconducting magnets. As originally designed, the magnets were to conduct approximately 75A while levitating the vehicle. The calculated critical current of the magnets was 160A. Each magnet has conducted 140A without normalizing; however, they have not been tested to their limits. Calculations indicate that above 100A

the magnets should be cryogenically unstable, meaning that any normally conducting zone ocourring in the windings should propagate through the windings, causing a loss of the magnetic field. The current was intentionally set above 100A only once--the last test of the program, when the current was set to 110A to emphasize lateral motions. The ability of the magnets to conduct this large a current was not recognized early in the program and the vehicle was not levitated as high as it could have been in some of the tests.

The earlier test were plagued by normalization problems with the magnets. This problem stemmed from an inadequate liquid helium level in the dewars and from intermittent shorts between the electrical leads and ground. The dewars were filled until the vent gas indicated they were full. This method was inaccurate and occasionally led to partially filled dewars. The counter-flow current leads to the rear magnets sometimes shorted to ground on one side. This grounding was normally not a problem. It was observed, however, that if any other magnet lead also shorted, the momentary alternate current path caused the magnets to normalize.

The vehicle's performance was also limited by the towing and braking mechanism, which constrained the test velocities to approximately 15 m/s (54 kmph). This limit was not too severe, since levitation typically occurred between 4 and 5 m/s. This is also the approximate speed at which the drag peak occurs, so the important regions of the characteristic curves of magnetic levitation were readily encompassed in the tests.

In the original design of the experiments, the drag force experienced by the vehicle was to be measured. This force was to be measured by determining the difference in force between strain gauges or load cells located between the towing skid and the towing cable at the front and rear of the skid. If we had made this measurement, however,

the frictional force on the skid itself would have been included as an apparent drag force on the vehicle. The only way to avoid this problem was to instrument the bearings in the chassis to which the towing pin applied the force. Such a modification would have required a substantial amount of work and a delay in the experiments, since the bearing was mounted in a reinforced section of the honeycomb platform. To enlarge this reinforced section would have required extra plates external to the honeycomb structure. Since the drag force calculations from earlier work were in reasonable agreement with the experimental results, this modification was not made.

The linear sensors used for both vertical and lateral position sensing consisted of a 9 kΩ linear wire wound potentiometer, mechanically linked to a spring-loaded, rubber-tired aluminum wheel. The overall linearity of this measurement system over its entire 2.5 inch range was only about 90%. But, over the range between 1.5 and 2.5 inches extension--the range over which most of the data was obtained--this linearity was increased to greater than 97%. The accelerometer outputs were prefiltered during the tests with an active 150-Hz low-pass filter having a roll-off of 18 db/decade. When played back, the accelerometer outputs were further filtered with the same active filter, set for a cut-off frequency of 30 Hz. The 150 Hz filtering was necessary to remove the saturation of the recorder heads caused by the sensitivity of the accelerometers to the prevalent high frequencies (up to 1 kHz). Since the frequencies of interest extend only to 25 Hz, this filtering has no effect on the data of interest.

During preliminary testing, there was no discernible cross talk between data channels and all sensors were insensitive to the magnetic field where they were located.

Finally, the mass of the vehicle and the distribution are accurate to about 7%. This distribution can result in the center of mass being located slightly away from the assumed center of mass at the towing pin.

The quantities describing the vehicle's motion that were measured directly were the following:

a. Vertical position at four points

b. Vertical acceleration at four points

c. Lateral position at four points

d. Lateral acceleration at two points

e. Longitudinal acceleration

f. Longitudinal position

g. Magnet current

h. Control coil currents (sampled only-lateral position sensors sacrificed for this purpose)

By analog processing of the original data, the following quantities were found for most of the tests. The definitions of these quantities are in inches of displacement as shown in the figures. The sensors are labelled in Figure 1. The following are defined at the approximate center of mass.

$$\text{Heave} = \frac{P5 + P6 + P7 + P8}{4}$$

$$\text{Slip} = \frac{(P2 + P3) - (P4 + P1)}{4} \qquad \text{Motion to Right Positive}$$

$$\text{Pitch} = \frac{(P7 + P8) - (P5 + P6)}{2} \qquad \text{Front Up Positive}$$

$$\text{Yaw} = \frac{(P3 + P4) - (P1 + P2)}{2} \qquad \text{Front to Left Positive}$$

$$\text{Roll} = \frac{(P5 + P7) - (P6 + P8)}{2} \qquad \text{Left Down Positive}$$

The roll, pitch and yaw measurements can be converted to angular measurements by dividing the above quantities by the distance between sensors. For the pitch and yaw measurements, the angular rotation in radians is given by the above equation divided by 92 inches and 86 inches, respectively. The roll angle in radians is obtained by dividing by 38 inches.

Vertical acceleration was obtained by averaging the accelerations measured by the four vertical accelerometers; lateral (slip) acceleration was obtained by averaging the accelerations measured by the two lateral accelerometers.

The data were sufficient to determine angular accelerations in each of these modes, but were not processed to determine these parameters. By integrating the accelerations or differentiating the positions, the velocities in each coordinate could be obtained from the data. (All the data are retained on magnetic tapes for future reference.)

The suspension height, z_o, is measured from the center of the magnet windings to the top surface of the guideway. This height is used in calculating the magnetic forces, but is not the actual height of the wheels above the guideway. The latter height is given by the position sensors. To correlate the two heights, the height of the magnets above the guideway when the vehicle rests on its wheels must be known. This distance varied from experiment to experiment as the magnets' positions were changed. For typical tests with passive damping, this distance was about 6 cm. The dewars had to be raised to accommodate the active coils in the active damping experiments, and was typically 8.2 cm. Therefore, tests having the highest suspension heights did not necessarily have the largest clearances.

Vertical Motion Tests

All experiments performed entailed vertical motions, but in some of these tests, other features of the vehicle's motion were emphasized. The tests described in this section were made specifically to evaluate the vertical motions of the vehicle. The data presented do not include all the data acquired, but are data that most directly, accurately or clearly illustrate the phenomena discussed. Other data pertinent to vertical motions are in Appendix A.

The tests discussed in this section are:

(1) Those made to evaluate the effect of rewelding of the guideway and strengthening the vehicle chassis.

(2) Those made over the standard guideway, without specific perturbations using active and passive damping, and

(3) Those made over the symmetric step perturbation in the guideway.

Guideway Evaluation Tests

The vehicle was levitated six times to obtain data for comparison with earlier tests over the unwelded guideway. Data were recorded in five of these tests. Vehicle speeds varied from 9.4 to 14.1 m/s and levitation heights varied from 7.4 to 10.1 cm. The instrumentation was the same as that used in earlier work--one vertical and one horizontal accelerometer and a vertical position sensor.

The data from test 14-4 of our earlier report and test 5 of the current series of tests are shown in Figure 7. There are several conspicuous differences in the results of these tests. The vertical motion is clearly less pronounced in the later test, as indicated by both the vertical position sensor and the vertical accelerometer. The noisy acceleration spikes in the earlier test were caused by single expansion joints in the guideway, positioned 100 feet from each end of the guideway, and three unwelded joints, located in the center of the guideway to permit the aluminum plates to be repositioned. There are no noteworthy differences in the lateral motion.

In the earlier experiment, the welds in the guideway had been superficial, penetrating only about 1/8 inch into the aluminum. These welds were broken at the joints between successive plates on the guideway and rewelded by tapering the joints and filling to achieve full penetration.

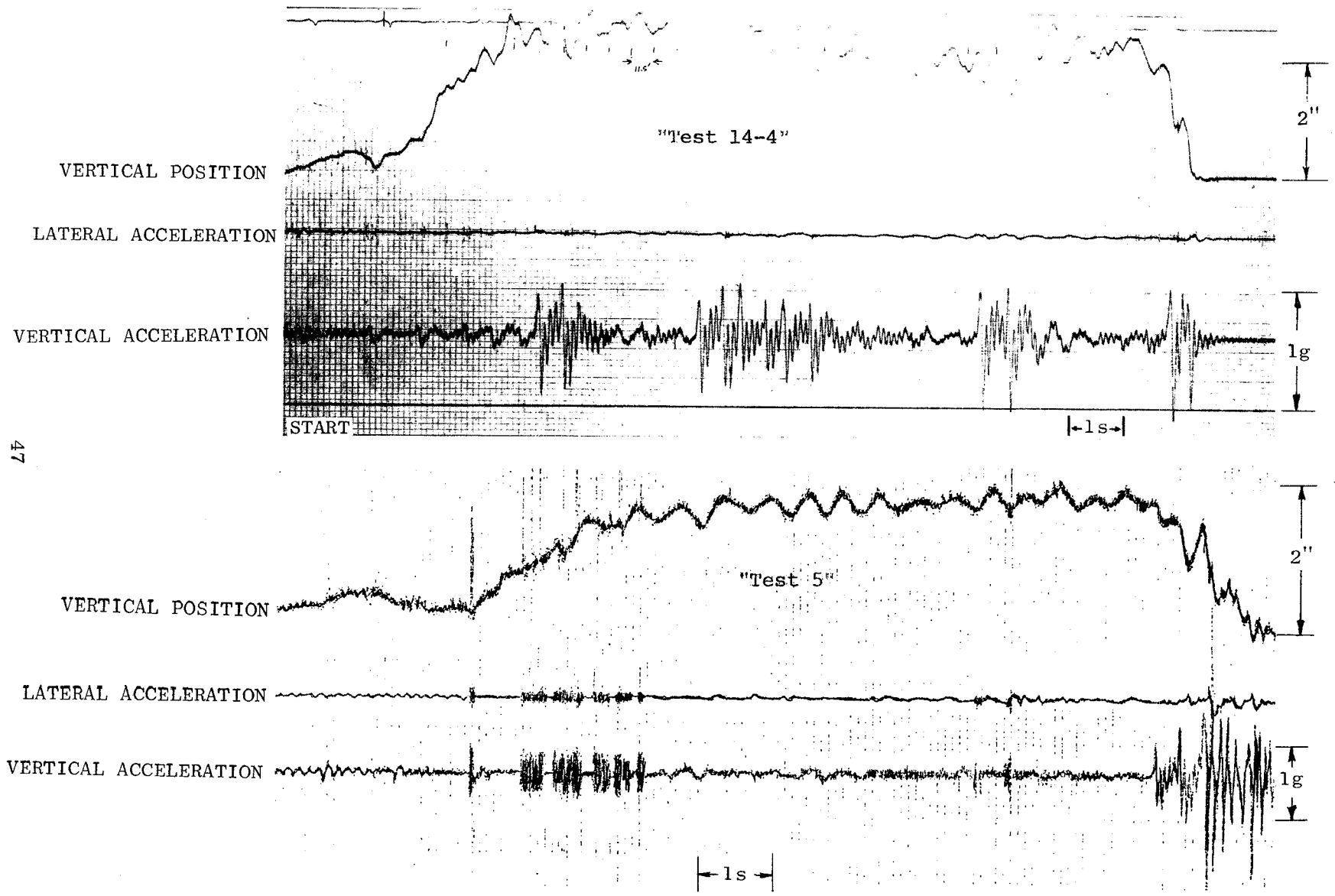

FIGURE 7 COMPARISON OF DATA FROM TESTS 14-4 (UNWELDED GUIDEWAY) AND 5 (WELDED GUIDEWAY)

Close inspection of the data from earlier test shows that lift was reduced at these joints, causing vertical accelerations. A similar periodicity is found in test #5, but is caused by the guideway being warped by the heat of welding rather than by discontinuities in the electrical properties. The acceleration on the far right of the recording from the earlier experiment was caused by the wheels on landing.

Power spectral densities (PSD's) of the vertical accelerations were determined for each of these tests, as shown in Figure 8. The peaks in the two tests between 2 and 3 Hz are the fundamental frequencies of the vertical heave motion. The peak in the earlier test between 9 and 10 Hz was the fundamental frequency of the body flexure mode. In the current program, the vehicle was strengthened, as discussed earlier, to increase this fundamental frequency. Obviously, the 9 to 10 Hz peak was not present in test #5 and new peaks are found at 15 and 30 Hz. The first of these new peaks is presumed to be the fundamental frequency of the body flexure mode of the strengthened vehicle. The identity of this frequency is not positive, since other modes, such as pitch, could not be observed with the instruments used in these experiments. However, although the identity of this frequency is of interest, it is of no importance to the experiments since these frequencies are absent or insignificant in later, more important PSD's.

These tests indicate that although the guideway is not ideal, it has been improved sufficiently to conduct meaningful experiments on the dynamic motions of the test vehicle.

Standard Guideway Tests

The term "standard guideway", as used here, refers to the guideway when no specific perturbations have been introduced. The vehicle was levitated over the standard guideway to determine how effective the damping systems were in providing good ride quality as measured by the

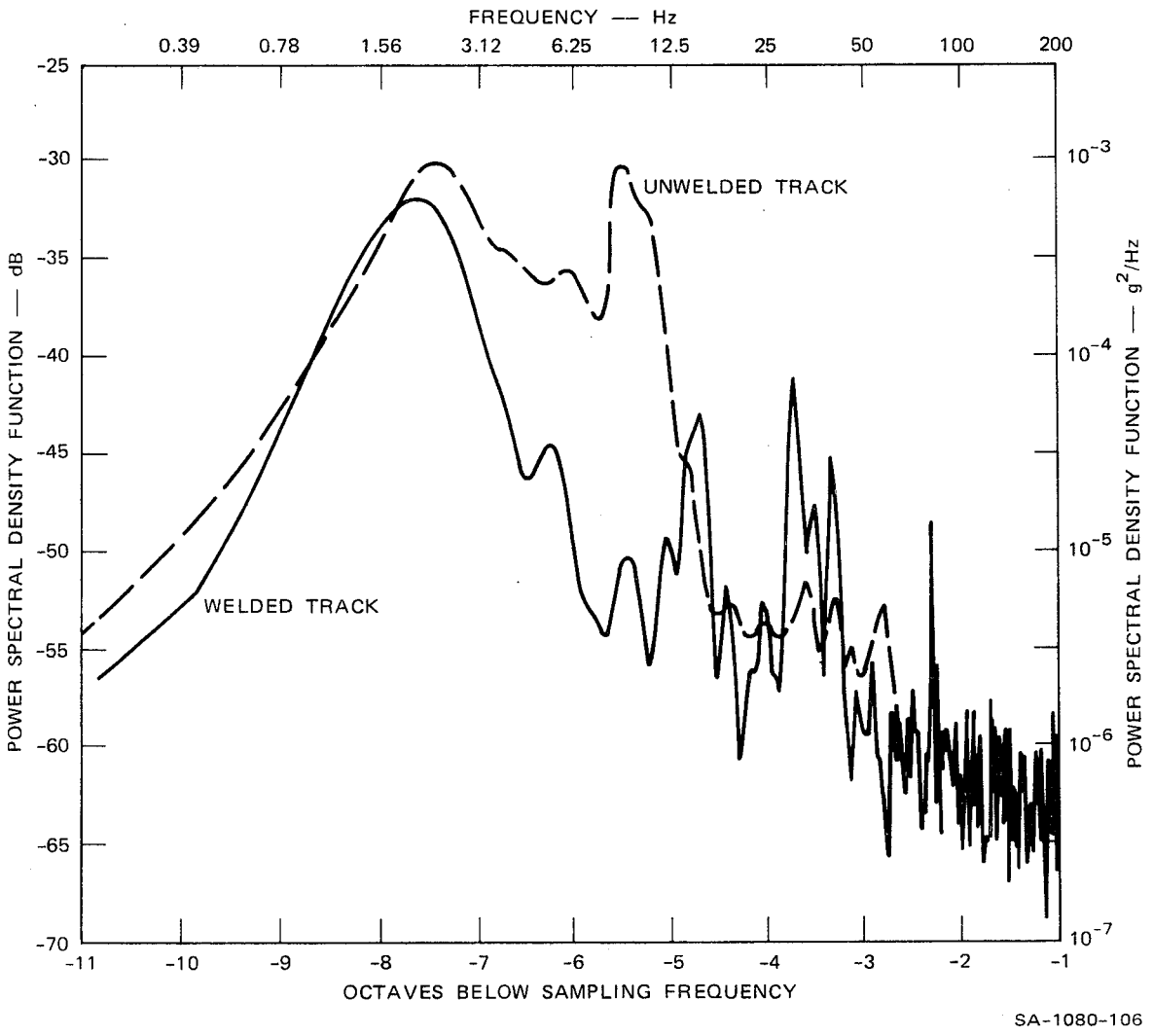

FIGURE 8 PSD OF HEAVE ACCELERATIONS OVER WELDED AND UNWELDED GUIDEWAY

power spectral density of the accelerations. The emphasis on power spectral densities arises from the specification of both the vertical and lateral ride qualities in these terms. In order to avoid misinterpretation, it is important to note that acceleration PSDs determined with this vehicle on this guideway are not those to be expected with a full-scale vehicle.

PSD characteristics depend on the frequency of oscillation of the vehicle in the heave mode, which in turn depends on the stiffness of the magnetic suspension, i.e., the spring constant, and the damping coefficient. In addition, they depend on the roughness of the guideway, usually characterized by the power spectral density of the irregularities in the guideway. Since the spring constant and damping characteristics are determined by the magnet and damping plate designs, the suspension height, the guideway electrical characteristics, and the vehicle speed, extrapolations to other vehicles and guideways must be made carefully. The parameters and analysis relevant to the SRI vehicle and guideway were given in our previous report.[6]

The PSD of the guideway irregularities was approximated by a function of the form A/Ω^2, where Ω is the spatial frequency 2π/wavelength. The guideway was surveyed and the data analyzed by a standard PSD program. The value of A was determined by best fit of an A/Ω^2 function to the plotted data. The results of this fit for the vertical irregularity PSD are shown in Figure 9 and A is approximately 10^{-5} ft-rad.

The experimentally determined parameters relating to the passive damping tests are summarized in Table 1. The currents indicated are approximate since the current increases after the vehicle levitates.

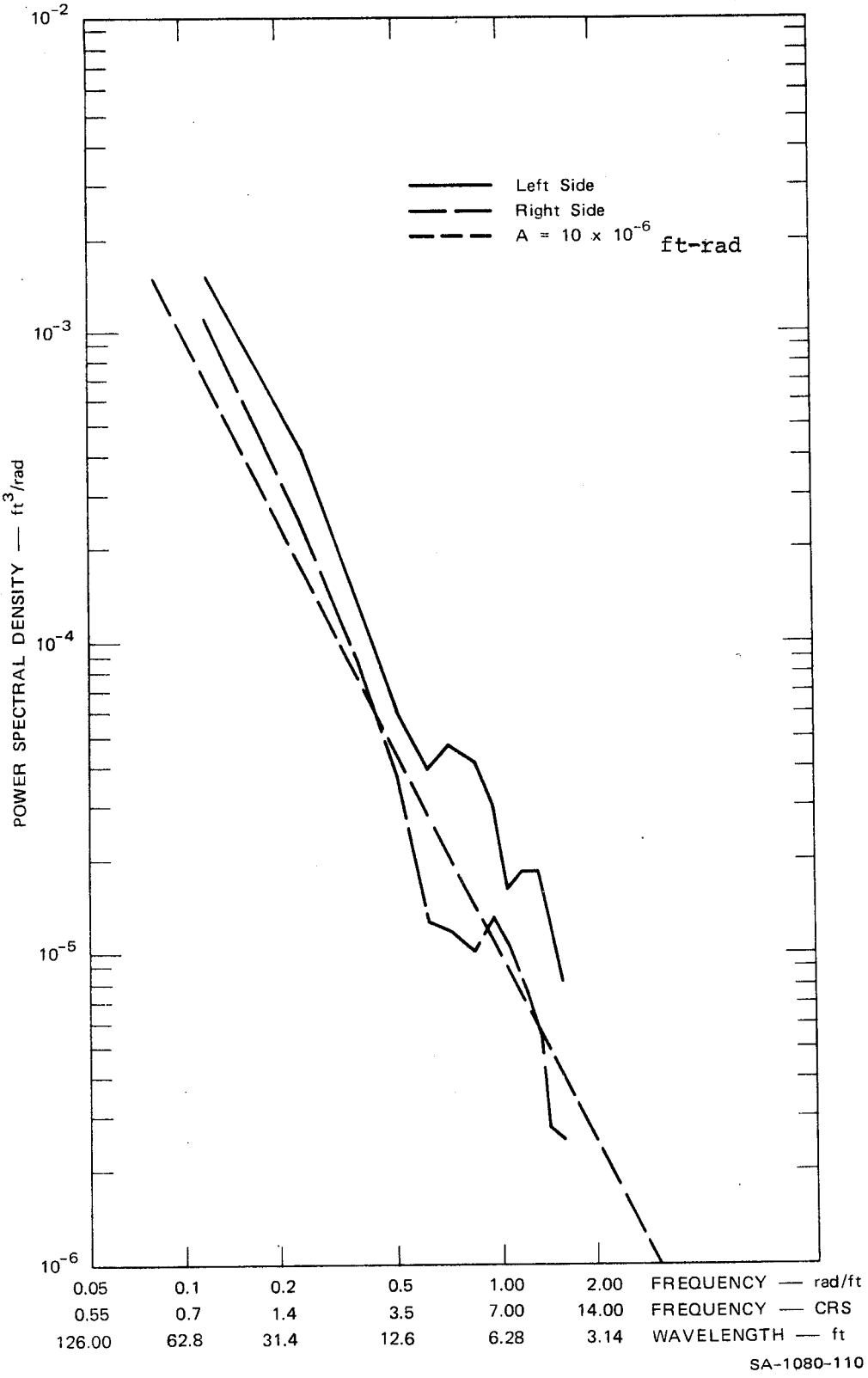

FIGURE 9 PSD OF RIGHT AND LEFT SIDES OF GUIDEWAY (CALCULATED BY MITRE CORPORATION)

Table 1

PASSIVE DAMPING TESTS OF VEHICLE OVER STANDARD GUIDEWAY

Test No.	v m/sec	I A	z_o cm	Peak of PSD rel. to $1g^2/Hz$	Peak Frequency Hz
8	5.5	87-91	6.9	-28dB	6.41
9	5.2	78-79	7.0	NA	NA
13	4.6	87-90	6.9	-33dB	5.96
13	8.9	87-90	8.3	-35dB	2.73
14	6.8	75-79	6.9	-33dB	5.3 and 6.4
15	9.9	89	8.4	NA	NA
16	9.5	87-91	8.7	-35.3dB	2.79
19	9.4	90	7.2	NA	NA
21	8.8	85	8.7	-37dB	2.57

One parameter of interest for vertical motion tests is the suspension height, z_o. The suspension height of each of the magnets can be different, depending on the roll and pitch attitude of the vehicle. For this reason, the suspension height generally referred to is that of the center of mass which, by definition, is unaffected by roll or pitch. Displacement of the center of mass in the vertical direction is called heave. The heave characteristic for test #21 using only passive damping is shown in Figure 10. This test, which was one of the better tests conducted with passive damping, was performed at an average speed of 8.8 m/s during levitation. The suspension height was 8.2 cm, and the clearance of the wheels was 2.3 cm. Time increases in the direction of the arrow. A downward displacement on the record corresponds to an increase in levitation height over the guideway. Perturbations in the suspension height are primarily the result of variations in the height of the guideway. By comparing this record to the lateral track profile as measured by the lateral sensors, ten of the peaks can be correlated with the location of welds and their corresponding perturbations

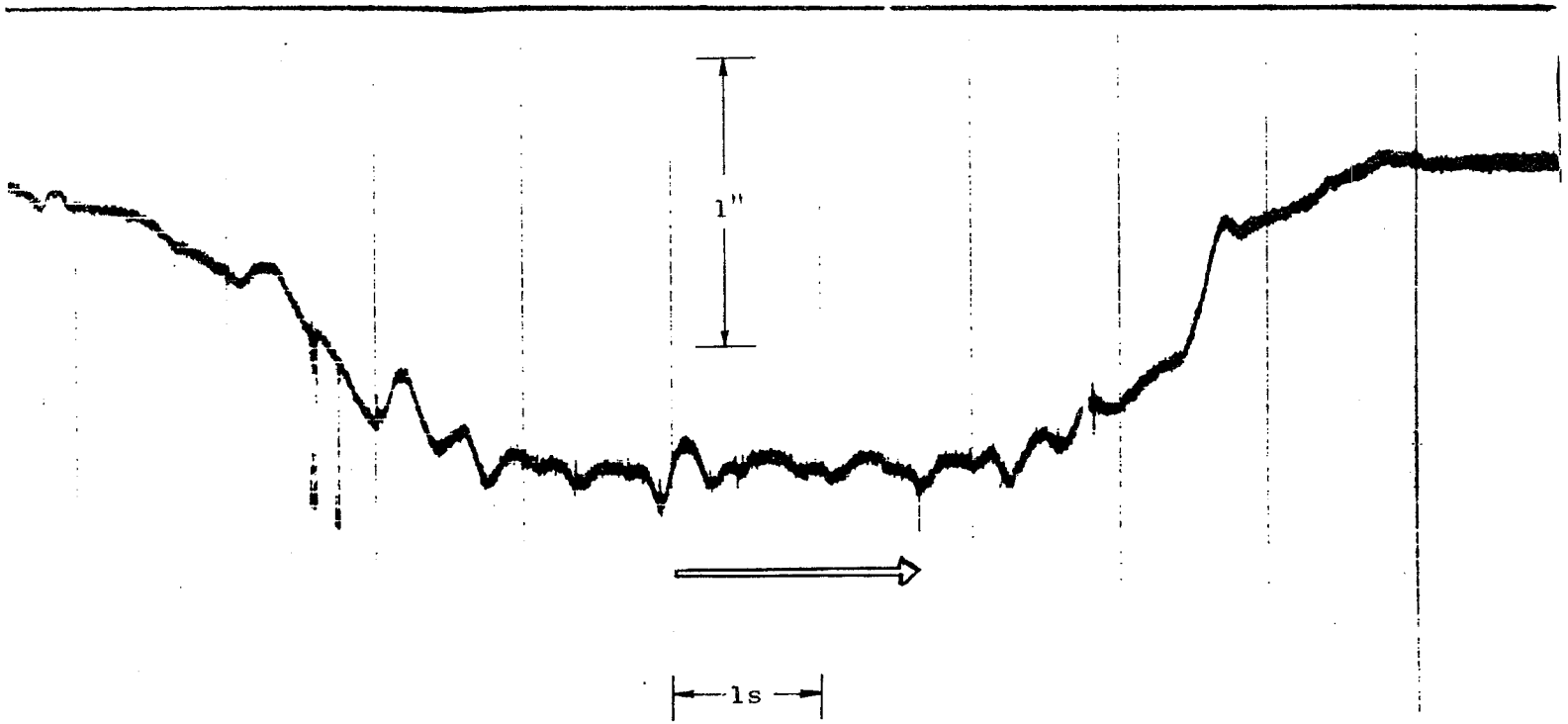

FIGURE 10 HEAVE POSITION VERSUS TIME-TEST 21

in the guideway, Although the vehicle is repeatedly perturbed, the resulting oscillations were rapidly damped. No growth of oscillations occurred. This is more clearly seen in the heave acceleration shown in Figure 11.

Accelerations and positions are not expected to exactly correspond, since the vehicle does not necessarily follow the guideway profile, although the position sensors do. If the vehicle followed a straight line, the vertical position sensors would map the guideway vertical profile while the accelerometers would register no motion at all.

The criterion of performance of the vehicle is the PSD of the vertical acceleration, which is shown in Figure 12. The peak in the PSD occurs at 2.57 Hz. In our earlier report[6], we calculated frequencies of damped oscillation for the heave mode in the range of 2.3 to 2.6 Hz, depending on the speed and suspension height. This calculation was based on a single degree of freedom model but the results were substantially the same as obtained in the experiments with five degrees of freedom. The frequency of heave oscillation of the vehicle after passing over a step perturbation is shown to be of approximately this frequency in the next section.

Irregularities in the guideway affect the motion of the vehicle, and it is therefore necessary to assess the effect of these irregularities on the PSD's. The frequency of the periodic driving force resulting from these periodic irregularities is determined by the distance between the vehicle magnets, the spacing between the irregularities, and the vehicle velocity (V). Since the distance between the centers of the front and rear magnets is 3.51 m, a periodic driving force occurs with a frequency $f_1 = V/3.51$ when the vehicle traverses a single perturbation. A second periodic force is determined by the reciprocal of the time required for the front magnets to pass over one weld induced irregularity after the rear magnets have passed over the preceding weld. This interval defines a frequency $f_2 = V/2.59$. Finally, a third periodic driving force has a frequency defined by the 6.1m(20-feet) distance between guideway welds,

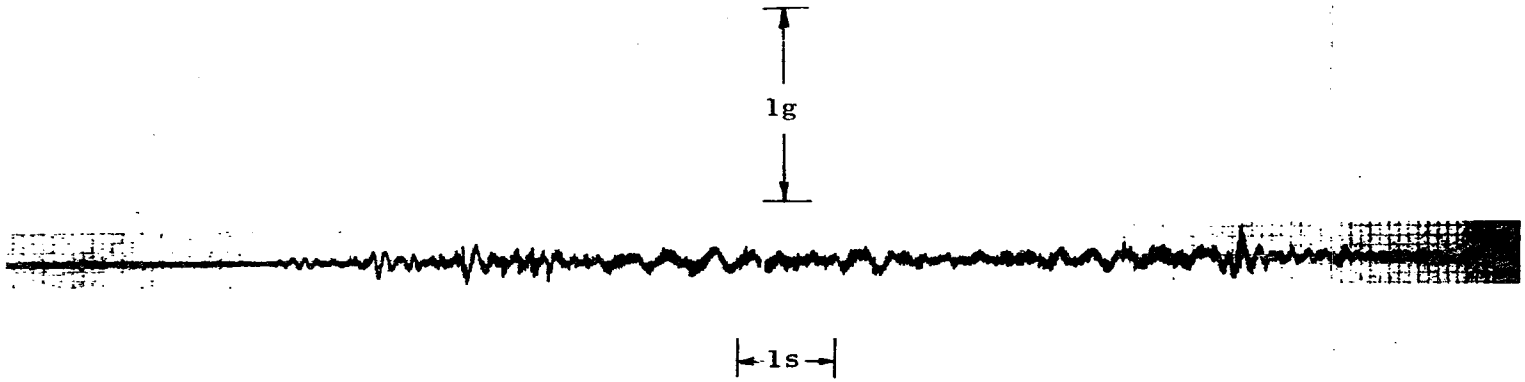

FIGURE 11 HEAVE ACCELERATION VERSUS TIME-TEST 21

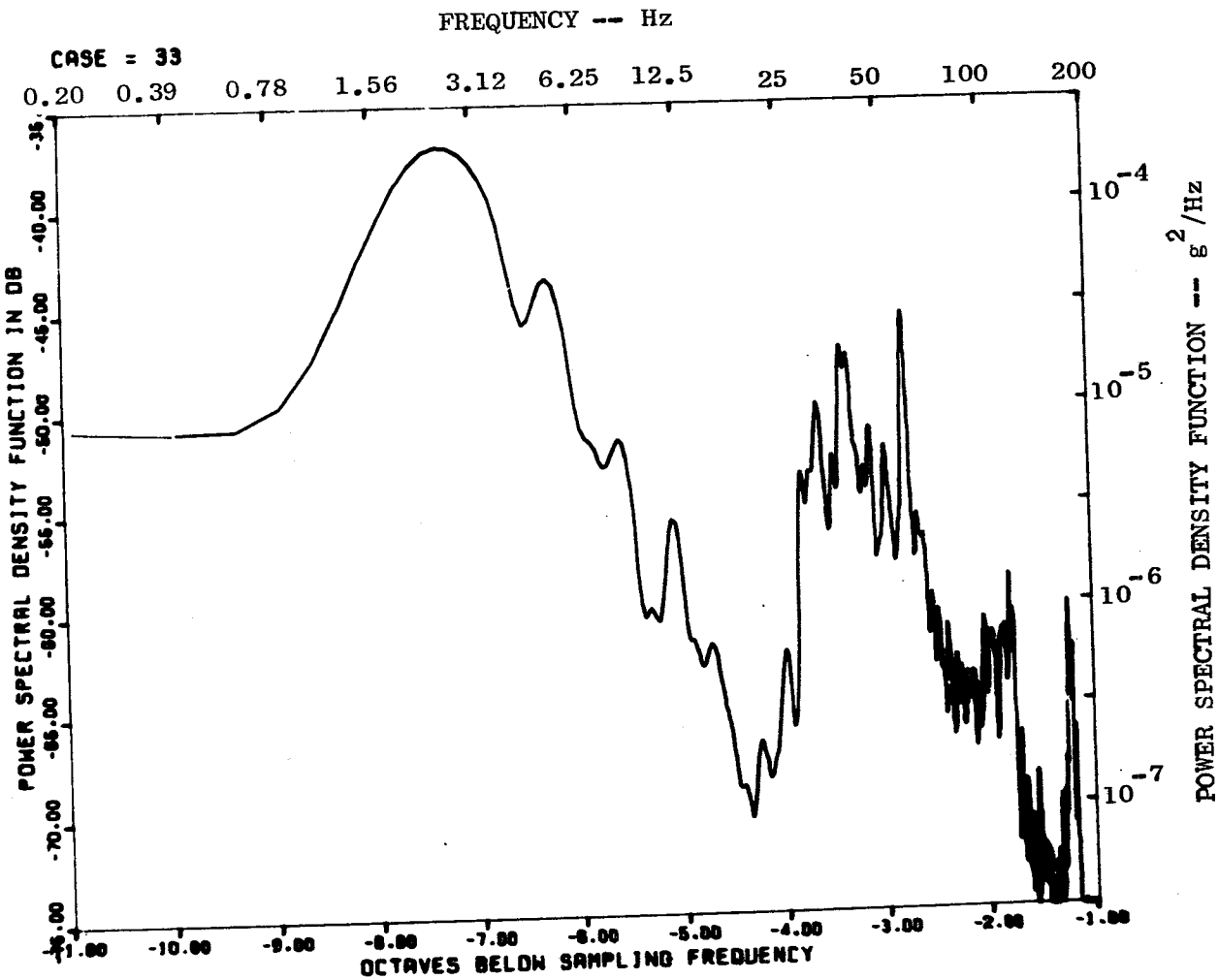

FIGURE 12 HEAVE ACCELERATION PSD-TEST 21

leading to $f_3 = V/6.1$. At a velocity of 8.8 m , as in Test 21, f_1 = 2.51 Hz, f_2 = 3.4 Hz and f_3 = 1.44 Hz.

Of these three frequencies, only f_3 is associated with the guideway alone and is most likely to affect the heave motion. All three frequencies can affect the pitch motion, but in the absence of a strong coupling, between the pitch and heave modes of oscillation, and for small perturbations, f_1 and f_2 will not have an appreciable effect on the heave motion. Neither the f_2 nor f_3 frequencies appear in the PSD in Figure 12. f_1 is near the peak in the PSD and cannot be separately identified. Since the periodic force is not expected to contribute significantly to the heave mode, the peak can safely be identified as the natural frequency of heave oscillation.

Test #16, performed at 9.45 m/s and a suspension height of 8.7 cm, was very similar to test #21, having a peak in the PSD of the vertical acceleration at 2.79 Hz and f_1 = 2.69 Hz, as shown in Figure 13. Test #13 was performed at two nearly constant speeds at different places on the guideway during the same run. The higher speed test with V = 8.93 and a suspension height of 8.3 cm resulted in a peak at 2.73 Hz whereas f_1 = 2.54 Hz.

No attempt has been made to establish the sources of the high frequency peaks in these PSD's. It is suspected that much of this noise arises from vibrations associated with the many components on the vehicle. It will be recalled that the acceleration data are attenuated above 30 Hz.

The low-speed portion of test #13 is markedly different than the high-speed portion in that the frequency of the peak in the PSD occurs at 5.96 Hz in Figure 14. This behavior was also found in tests #8 and #14. In each of these tests the velocity and suspension height were comparatively low (4.6 - 6.8 m/s). The reason for this behavior is unexplained, but might have been caused by one or more wheels remaining

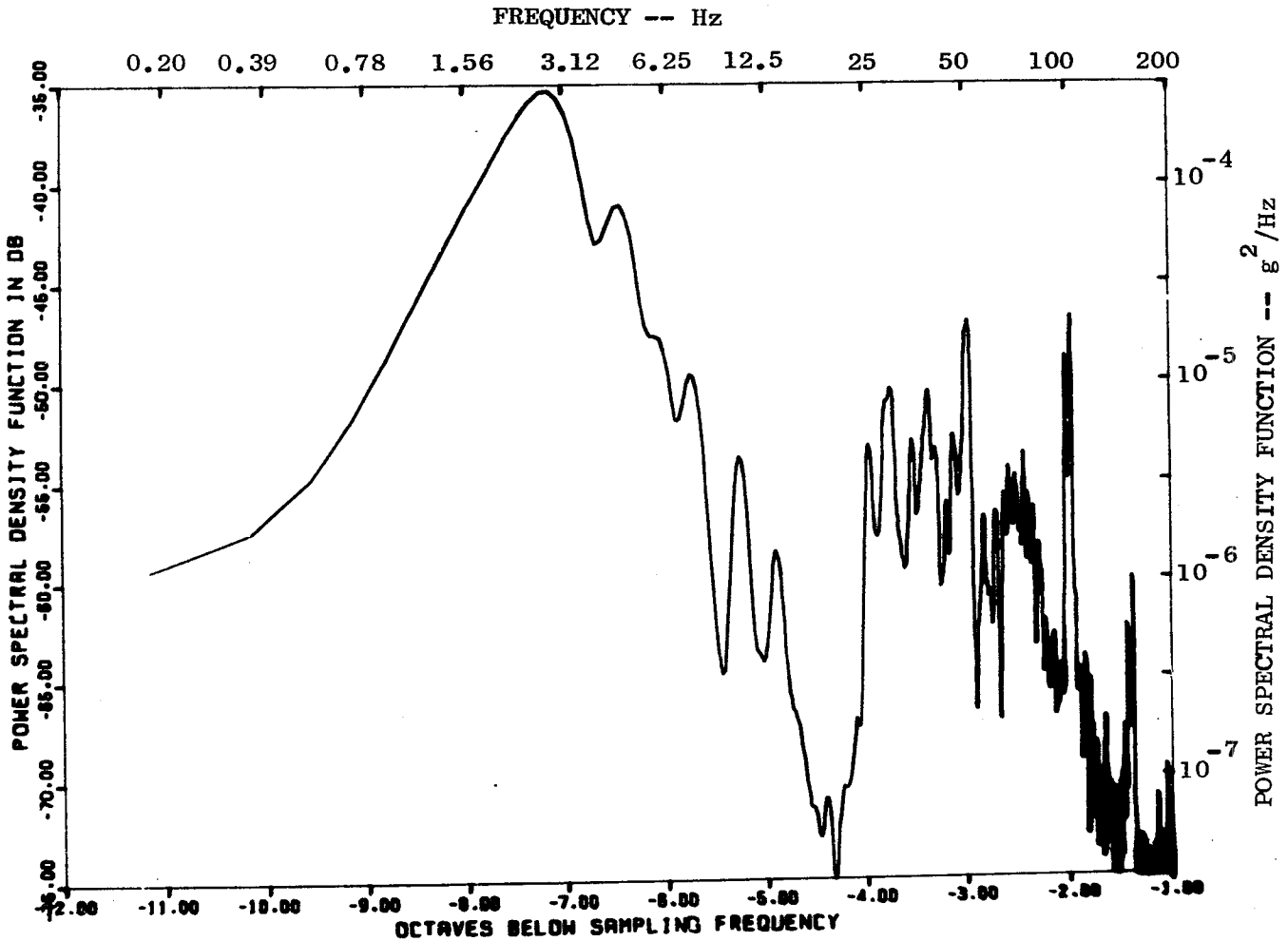

FIGURE 13 HEAVE ACCELERATION PSD-TEST 16

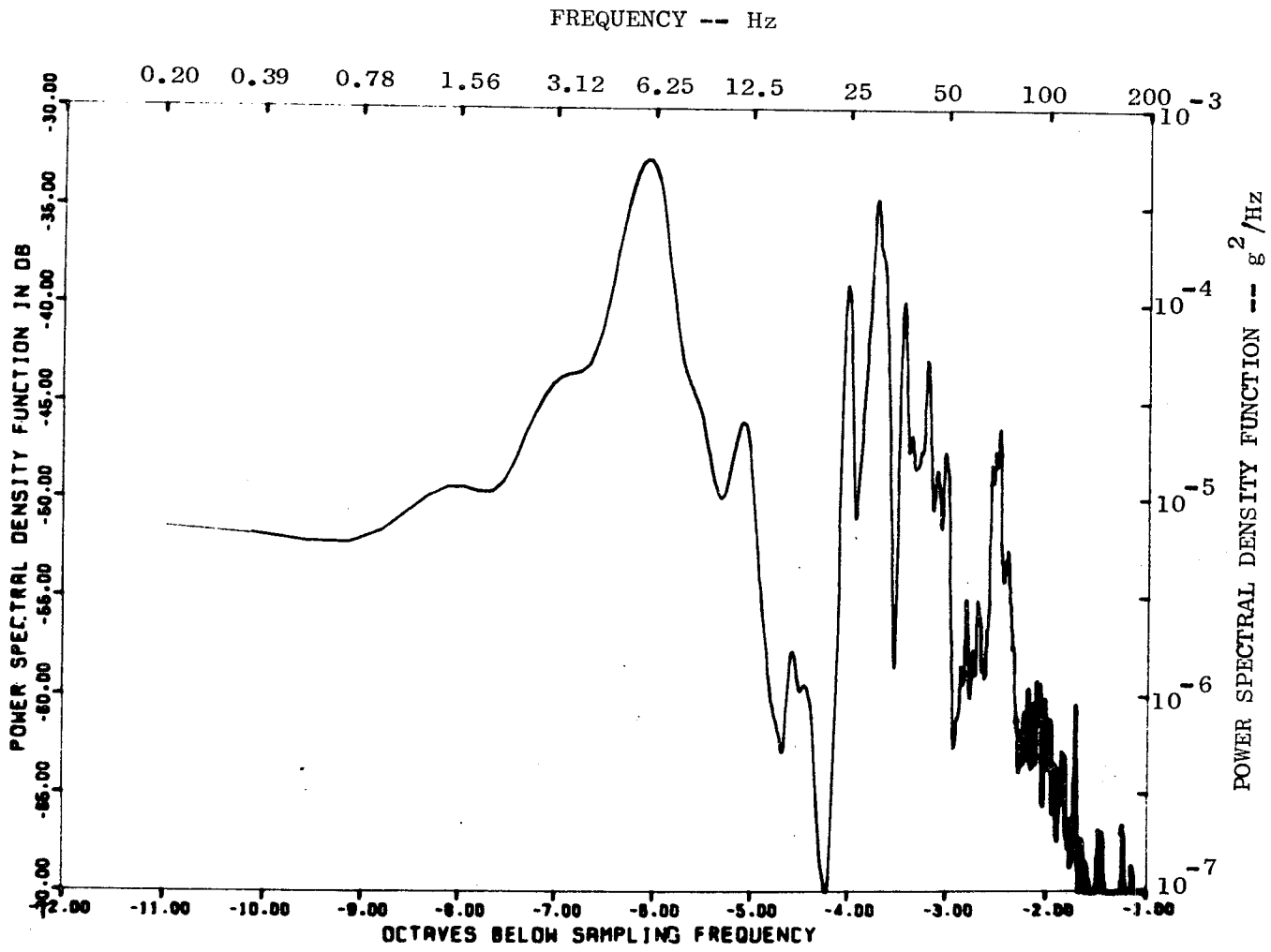

FIGURE 14 HEAVE ACCELERATION PSD-LOW SPEED PORTION-TEST 13

in contact with the guideway due to an imbalance in the vehicle. Figure 11 shows that an oscillation of about this frequency also occurred at the onset of levitation in test #21.

Pitch and roll were also evaluated for these tests and are shown in Figures 15 and 16 for test #21. (Yaw and lateral slip are discussed together with other lateral tests below.) The major spikes in the pitch record can again be identified with the perturbations at the welded joints, but the oscillation between these spikes are characteristic of the suspension system's natural pitch frequency. This is most clearly illustrated by the almost sinusoidal oscillation just to the left of the center of Figure 15. The two lowest points correspond to welds in the guideway. The first peak and following minimum are due to the vehicle oscillations at its natural frequency. The following peak is distorted as the rear magnets traverse the same perturbation ~ 0.44 seconds later. (The velocity at this point was 7.9 m/s.) The approximate frequency of this pitch oscillation is 3 Hz. Having identified this frequency, one can move a scale along the recording in Figure 15 and identify other, less clearly defined, peaks with the same periodicity although the frequency of guideway perturbations changes as the velocity increases to 10.5 m/s. This was the only oscillation of any appreciable magnitude that occurred, and it damped away after little more than one cycle. The ratio of the magnitude of the second minimum to that of the minimum occurring at the weld is approximately 0.46, leading to a damping time of 0.43 seconds, based on admittedly sparse data. Better and more accurate results are presented later.

The results for the roll angle are similar to those of heave and pitch as shown in Figure 16. No clear damping time is evident in this data, although it is obvious that roll oscillations are not growing with time. In these data as in other data obtained by the position sensors, the vehicle may not move as much as the sensors indicate because the

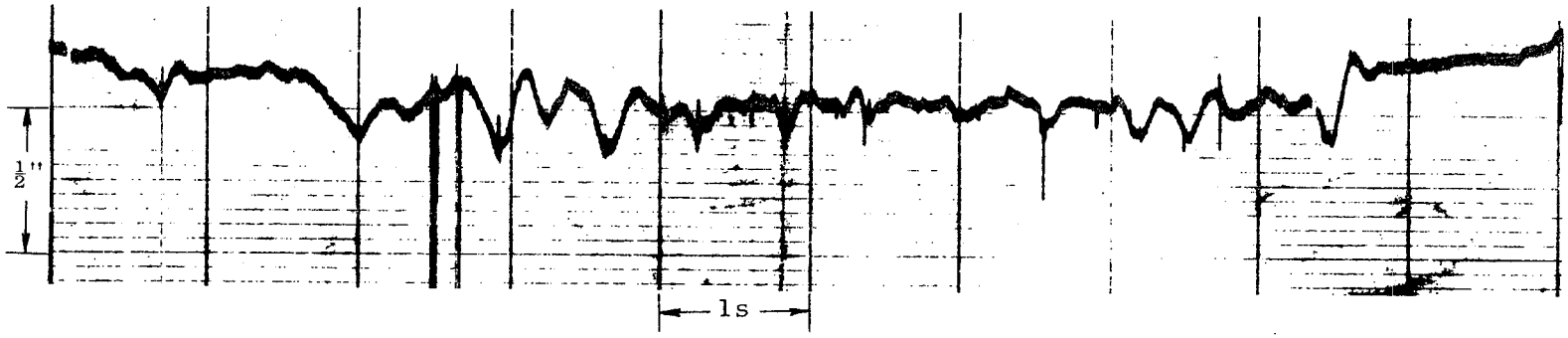

FIGURE 15 PITCH ANGLE VERSUS TIME-TEST 21

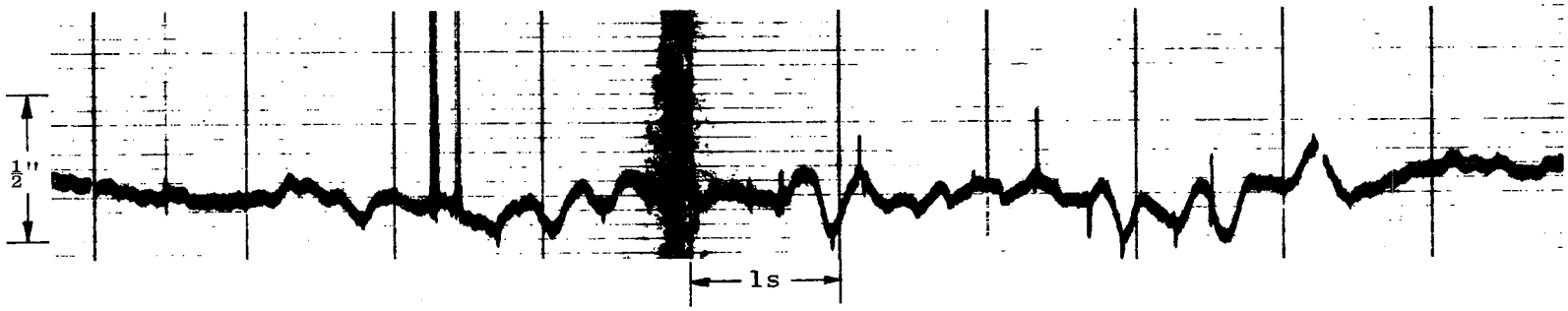

FIGURE 16 ROLL ANGLE VERSUS TIME-TEST 21

sensors also indicate the vertical perturbations in the guideway. To obtain more accurate motions, the accelerometers should be integrated twice to obtain motions relative to an inertial frame rather than with reference to the guideway. This type of analysis was not done, but can be done in the future using the data on magnetic tape.

Three tests (29, 30, 31) were made with the vehicle using actively controlled damping coils and currents proportional to the absolute vertical velocity of the vehicle. The vertical velocity was obtained by integrating the output from the vertical accelerometers.

The heave position measurements from tests #29, #30, and #31 are shown in Figure 17 where the feedback controls were set for approximately 3/8, 5/8 and 1 times critical damping, respectively. By comparing Figure 17 with Figure 10, it can be seen that the actively controlled feedback damping removed many of the minor perturbations occurring in the suspension height, which can also be seen in the vertical (heave) accelerations from these three runs as shown in Figure 18.

The PSD's of these vertical accelerations, shown in Figures 19 through 21 confirm that the peak accelerations were lower by approximately 10 dB (a factor of 10) when the active controls were used in conjunction with the passive coils.

In experiments using a roll perturbation, it is seen that a distinctive roll occurs near the end of the run--the same behavior was noted in each of the other active tests (Figure 22). This feature has now been traced to the defective operation of the left rear active control circuit, leading to a roll when a large vertical perturbation occurred. This electronic failure in one of the four controls also prevented the attenuation of the pitch to the extent expected as seen in Figure 23.

In the direction of roll, all four damping coils act together to inhibit roll in the inertial frame--two react against an upward acceleration

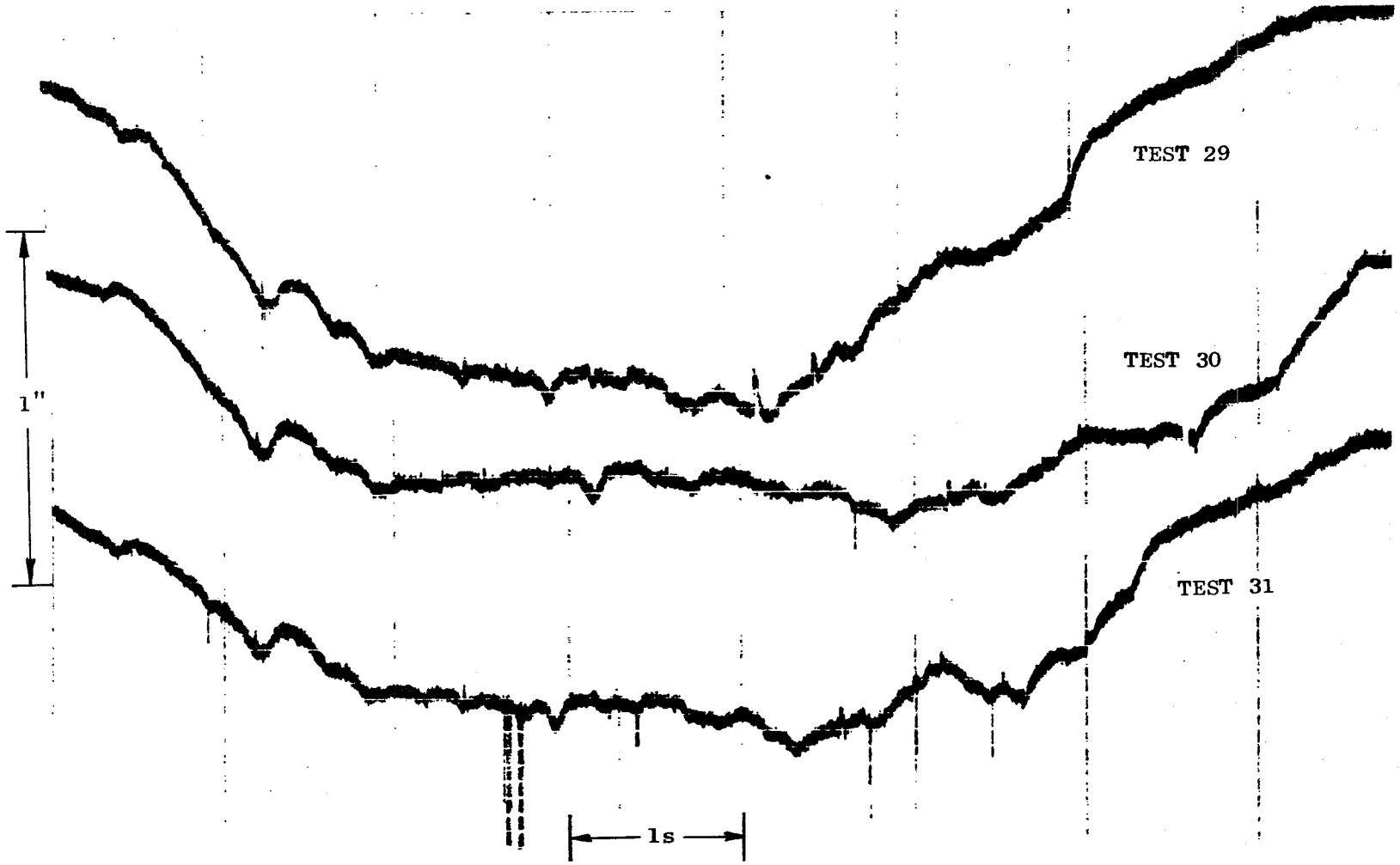

FIGURE 17 HEAVE POSITIONS VERSUS TIME-ACTIVE TESTS 29, 30 AND 31-3/8, 5/8 AND 1 TIMES CRITICAL DAMPING RESPECTIVELY

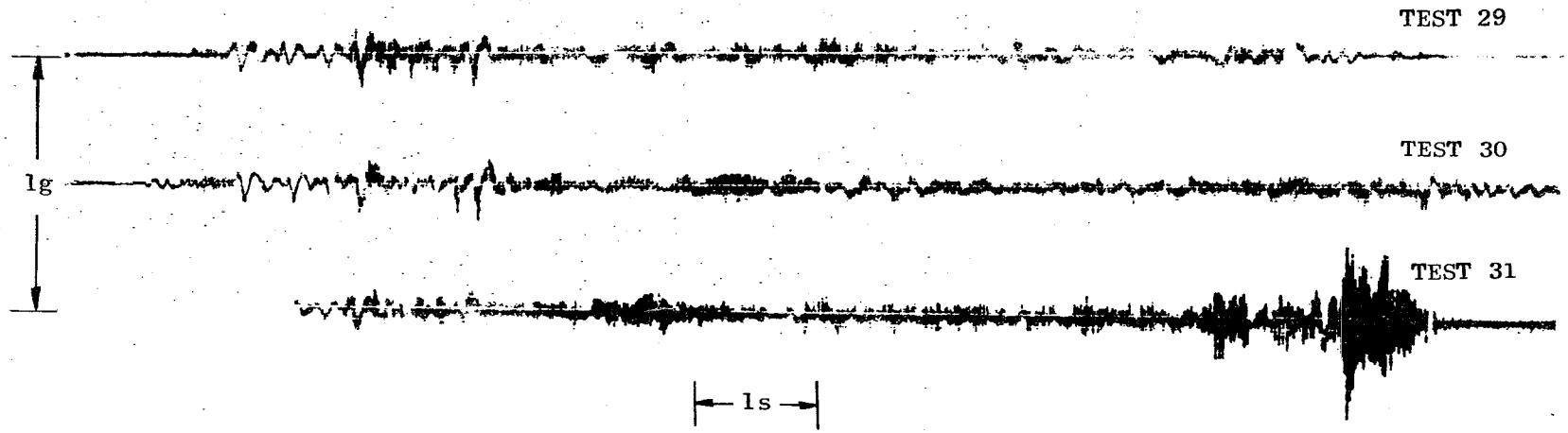

FIGURE 18 HEAVE ACCELERATIONS VERSUS TIME-ACTIVE TESTS 29, 30 AND 31

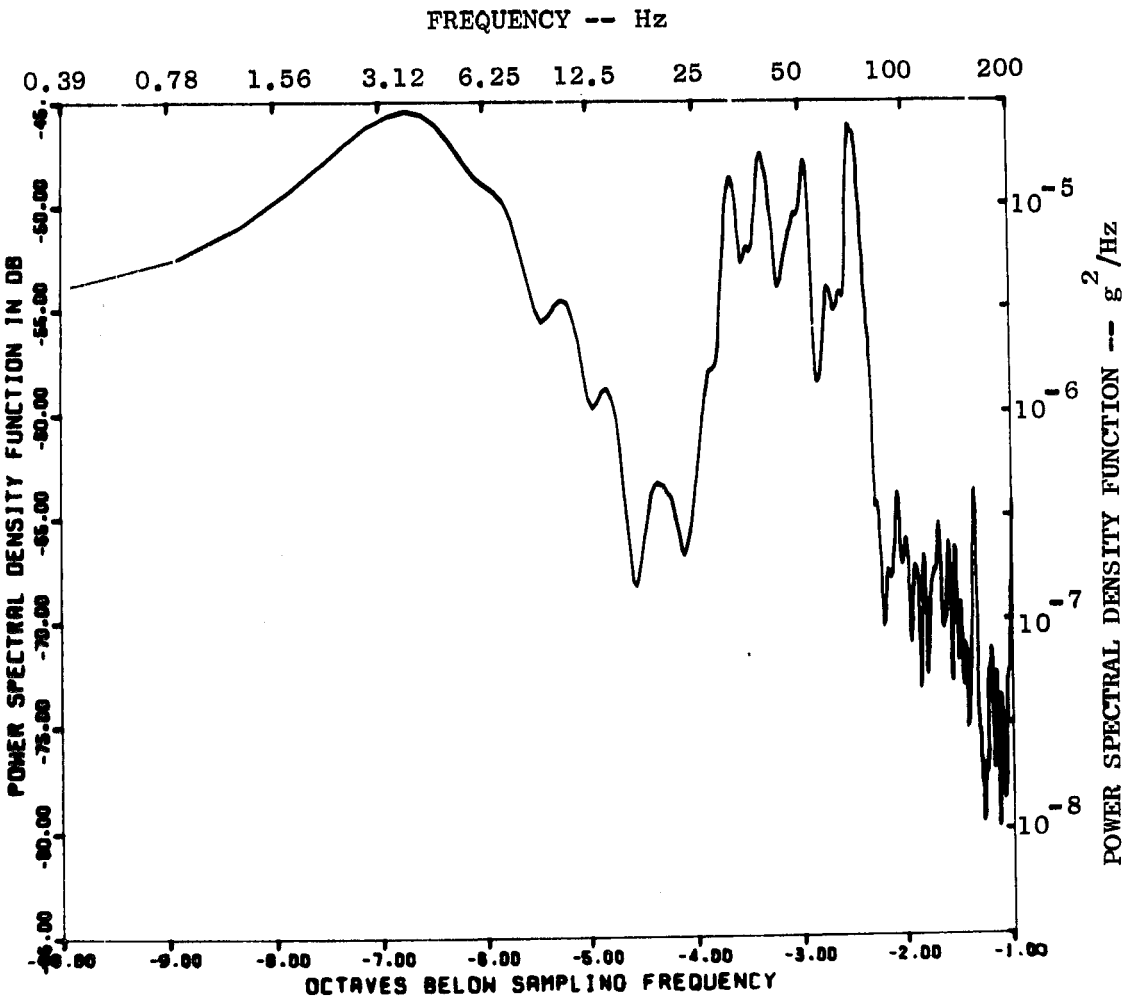

FIGURE 19 HEAVE ACCELERATION PSD-TEST 29

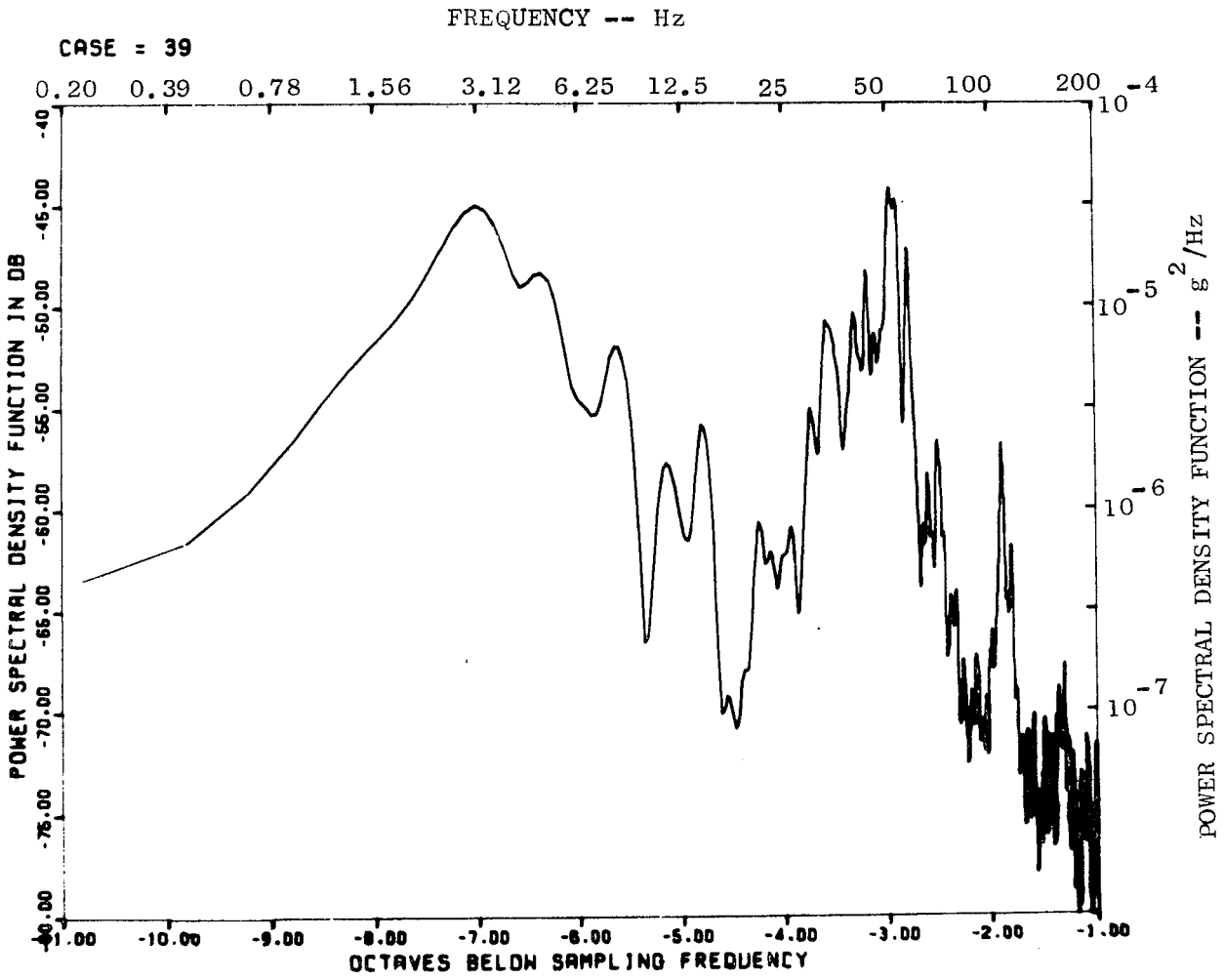

FIGURE 20 HEAVE ACCELERATION PSD-TEST 30

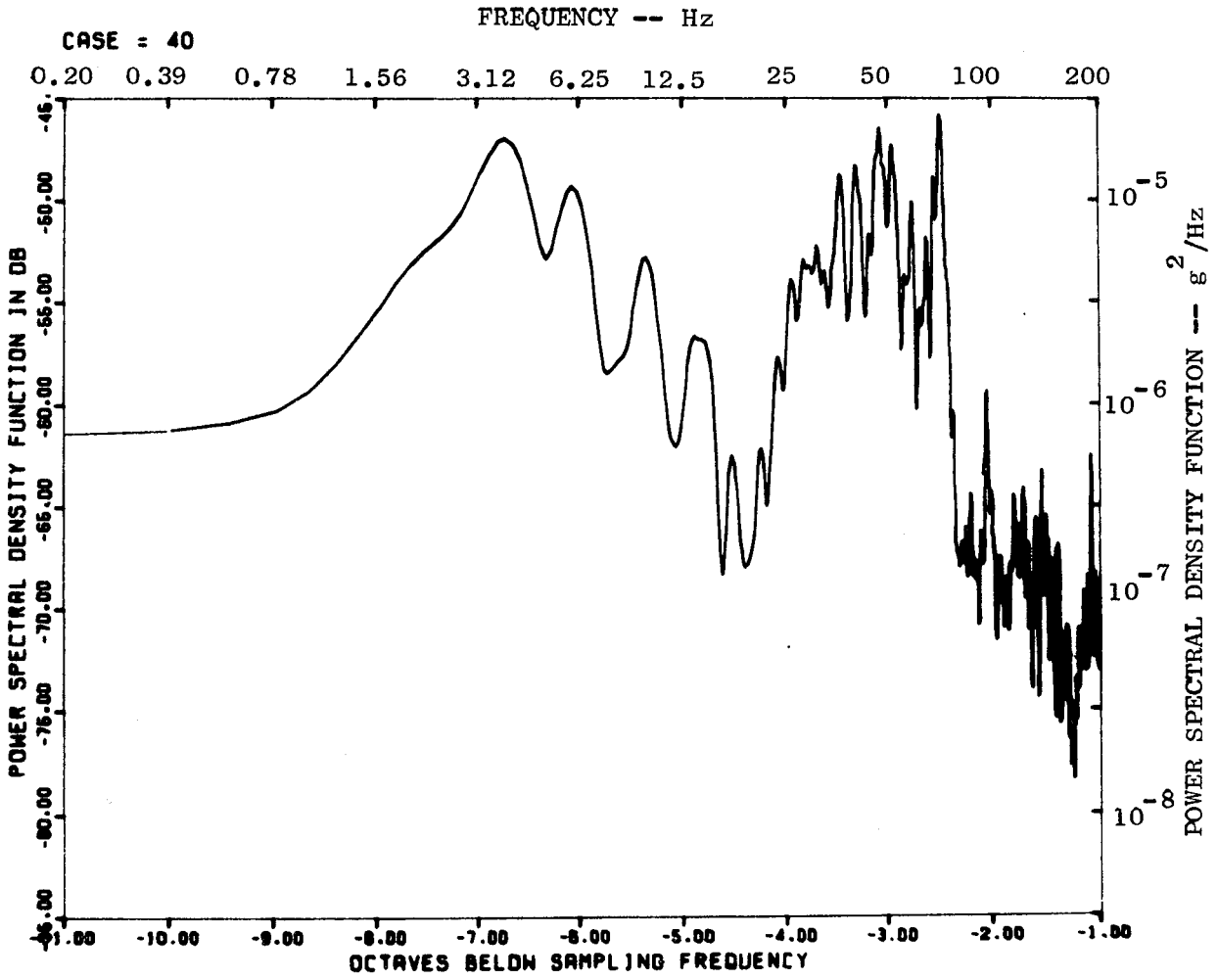

FIGURE 21 HEAVE ACCELERATION PSD-TEST 31

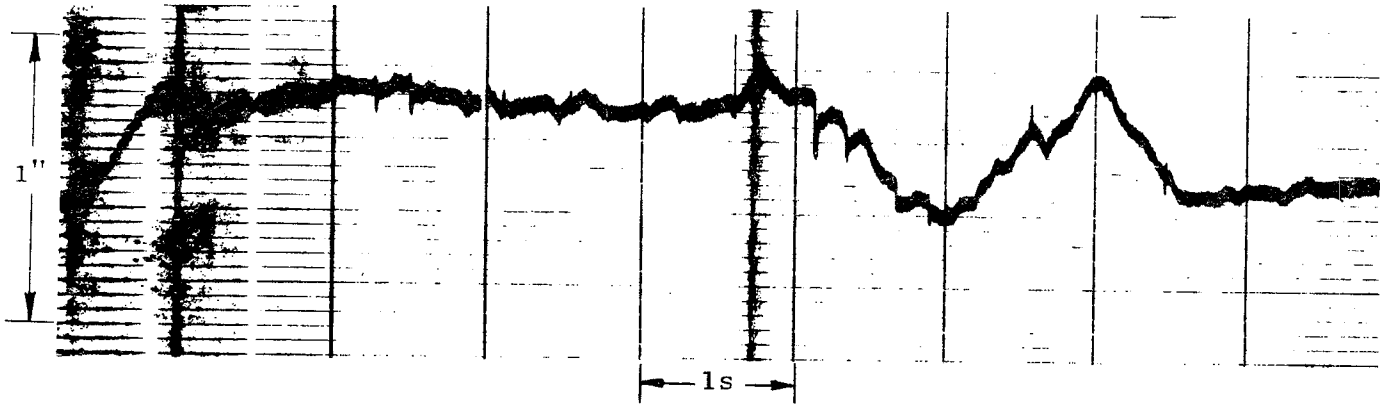

FIGURE 22 ROLL ANGLE VERSUS TIME-TEST 30

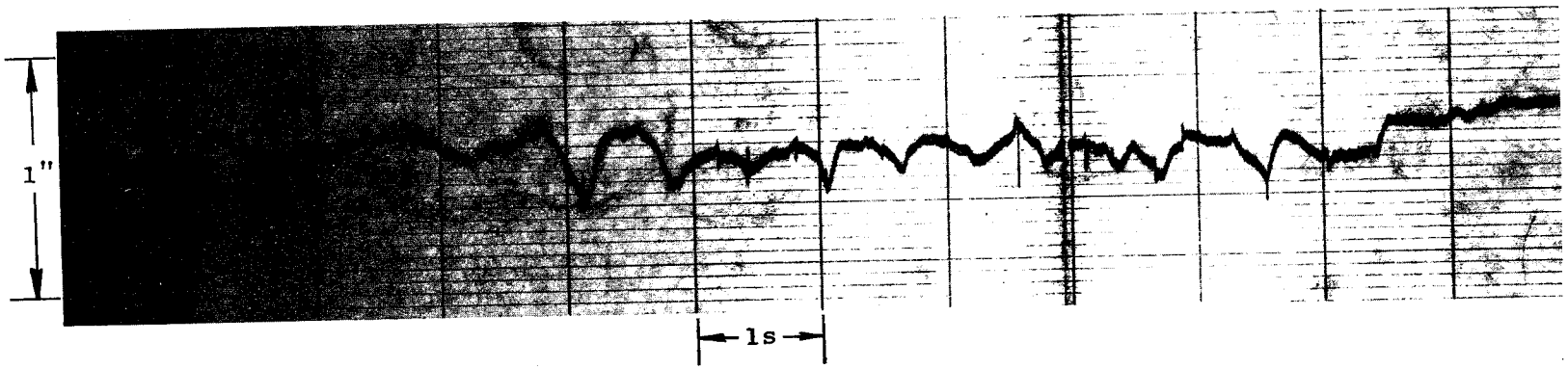

FIGURE 23 PITCH ANGLE VERSUS TIME-TEST 30

and two react against a downward accleration. For this type of motion, three of the four active coils are effective. The same degree of effectiveness applies to the pitch mode when the vehicle is over an unperturbed guideway. If the guideway has an explicit perturbation causing a pitch motion, however, only two coils are subjected to the perturbation at one time, leading to a 50% performance of the controls when one fails. This accounts for the relatively smooth behavior in roll while the pitch motion resulting from explicit perturbations is comparable to that of the passively damped system.

We have seen that the vertical PSD's were about a factor of 10 lower than they were with the passively damped system. This reduction in the PSD's was achieved with only 75% of the controls operating. If the fourth control had operated, one might expect another 3 dB lowering of the PSD.

The data presented so far are referenced to or around the center of mass of the vehicle. At this point, vertical accelerations caused by pitching or rolling are cancelled, and the best ride quality is attained. Power spectral densities were obtained in several cases for the left front vertical accelerometer to measure any characteristic differences between this position and the center of mass. One example is shown in Figure 24 and can be compared with the same, passive test at the center of mass in Figure 12. An obvious difference is observed in the PSD at intermediate frequencies of 10 to 25 Hz. At the center of the mass, the PSD is greatly reduced in this frequency range, whereas at the corner of the vehicle the PSD is as much as a factor of 10 greater. Since, presumably, the vehicle must be designed to meet certain ride quality criteria at any point in the vehicle, the corners provide a more stringent test of the system's quality.

This additional power arises from the pitch and roll motion of the test vehicle. The same type of behavior was observed in the active tests,

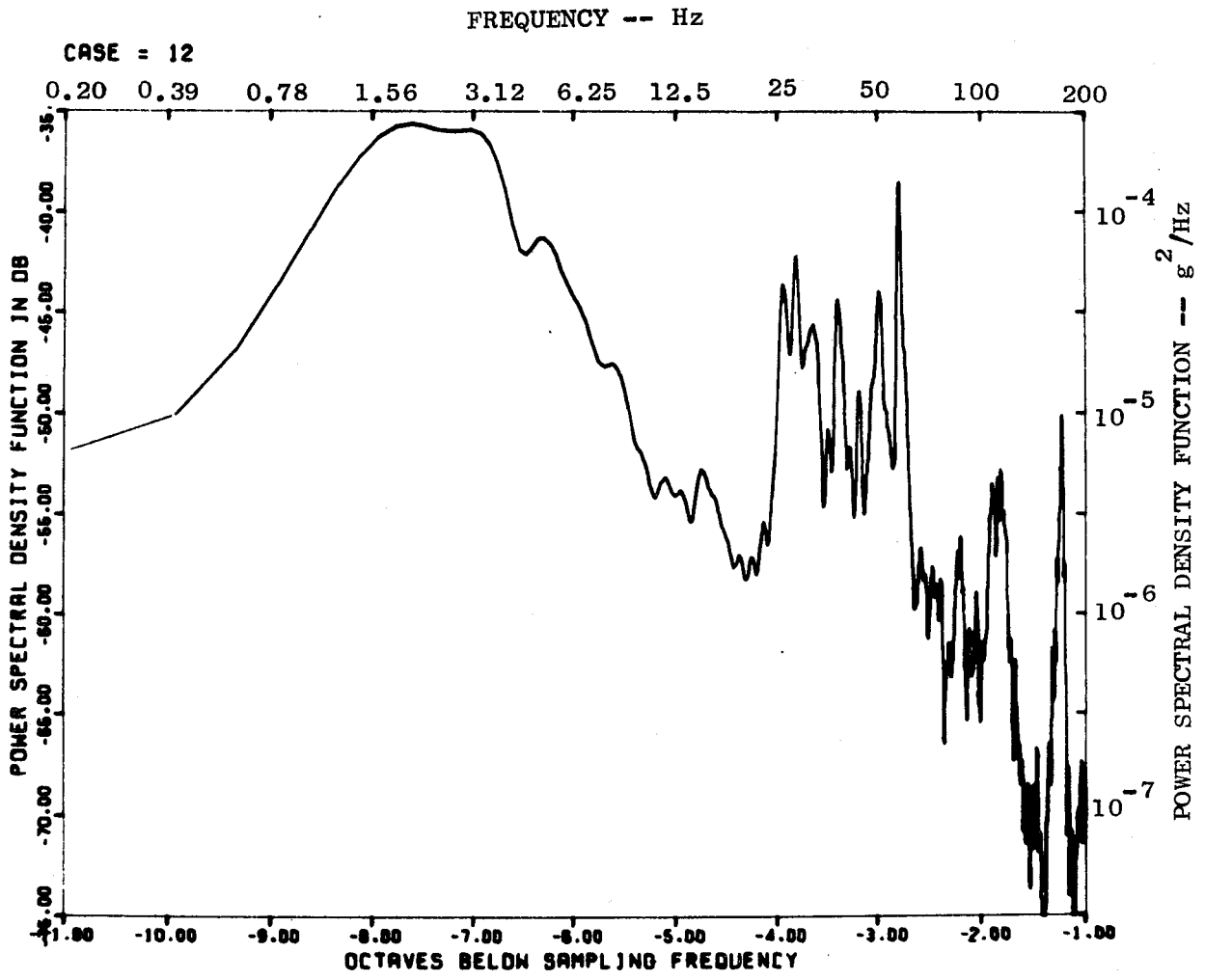

FIGURE 24 LEFT FRONT HEAVE ACCELERATION PSD-TEST 21

but was less pronounced in this frequency range, Figure 25 through 27. Researchers at Ford previously modeled the PSD of the vertical motion at the center of mass, including only the pitch and heave modes of oscillation. They found a minimum in the PSD when $\text{Cos}^2(\omega T_d/2) = 0$, or $\omega T_d = \pi$, where T_d is the time required for successive magnets to traverse a guideway irregularity. $T_d = L/v = 3.506/v(m/s)$ in our case, leading to $\omega/v = \pi/3.506$ as the condition for the first minimum in the PSD. The frequency of the minimum occurred at approximately 20.3 Hz in one experiment with V = 8.8 m/s, leading to $\omega/v = 14.1$, rather than $\pi/3.506 = 0.896$. This substantial difference is not currently explained. It is possible that the peaks above 25 Hz are all due to miscellaneous oscillations of component parts of the vehicle and do not relate to the characteristic rigid body vehicle PSD.

Symmetric Vertical Step Tests

The primary objectives of these tests were to establish the stability of the vehicle under severe perturbations, to provide a stringent test of the analytic model when the force-displacement characteristic of the magnet is clearly nonlinear and to establish the frequencies and damping times of heave and pitch oscillations. The tests were performed with both active and passive damping systems.

These experiments were performed by levitating the vehicle over two symmetrically located 3/4-inch (1.9 cm)-thick aluminum plates placed on top of the standard aluminum guideway. Plywood sheets of the same thickness were placed on the aluminum guideway preceding the supplementary aluminum plates to avoid the possibility of damaging the vertical position sensors which cannot ascend a vertical step. Ideally, the experiments would have been performed by also replacing the plywood with aluminum, providing a single rather than a double step. The nonideal situation led to some complications in interpretation, but generally duplicated by the analytic model.

The parameters appropriate to each test are listed in Table 2. The damping time constants were determined from the amplitudes A_1 and A_2

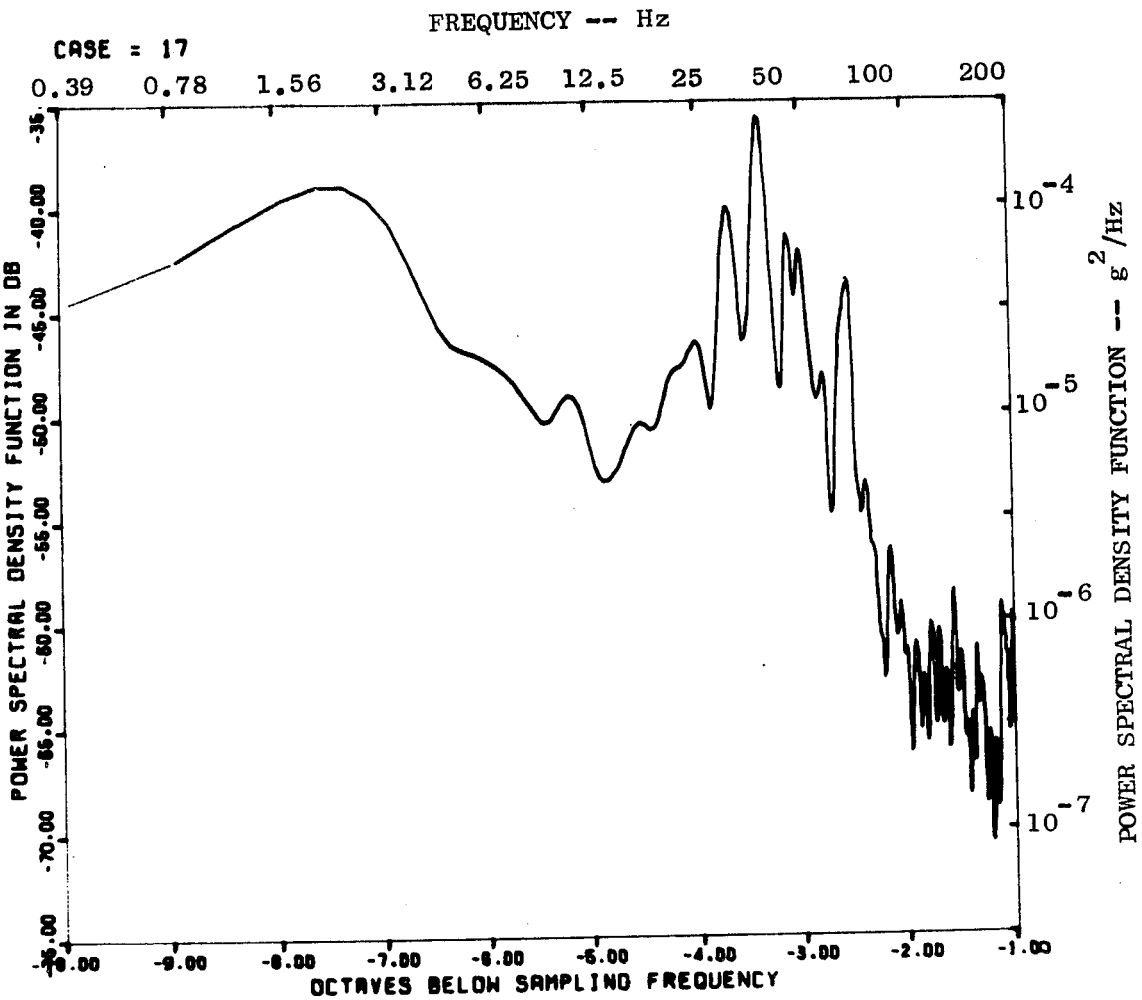

FIGURE 25 LEFT FRONT VERTICAL ACCELERATION PSD-TEST 29

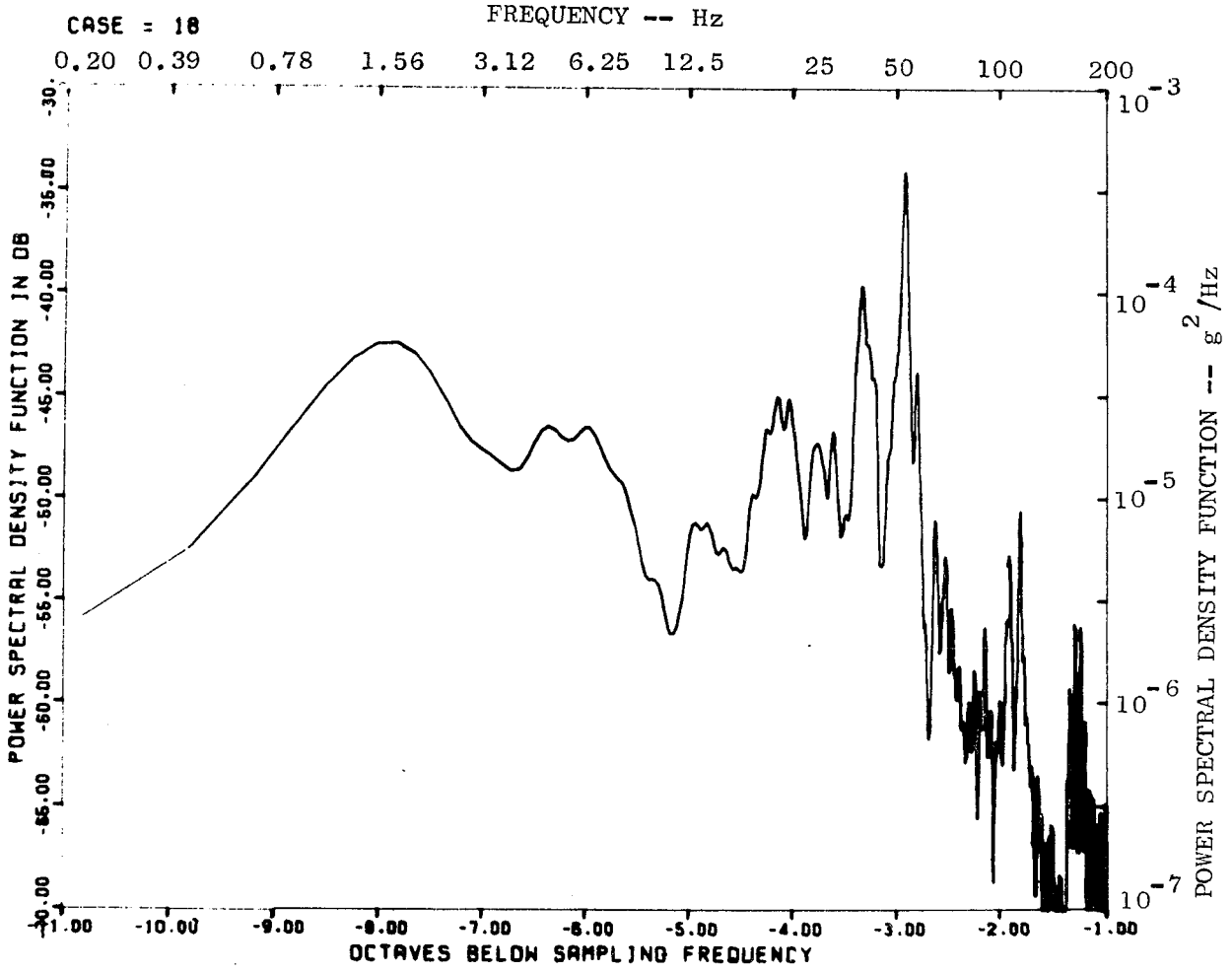

FIGURE 26 LEFT FRONT VERTICAL ACCELERATION PSD-TEST 30

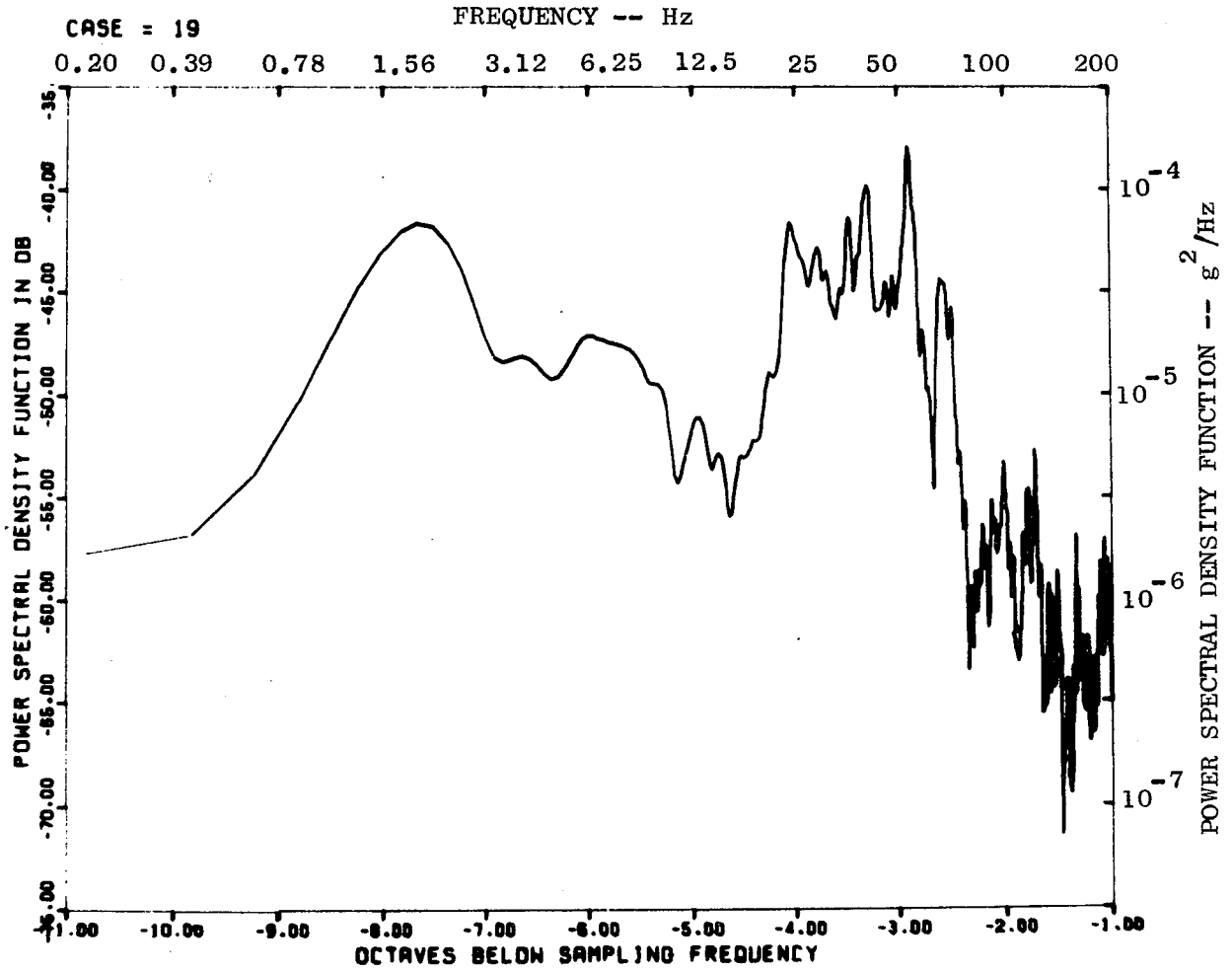

FIGURE 27 LEFT FRONT VERTICAL ACCELERATION PSD-TEST 31

Table 2

PARAMETERS ASSOCIATED WITH VERTICAL SYMMETRIC STEP TESTS

Run #	Active Damp. Set.	z_o (cm)	v_o (m/sec)	I (A)	f_{pitch} (Hz)	τ_{pitch} (sec)	f_{heave} (Hz)	τ_{heave} (sec)	$\frac{f_{pitch}}{f_{heave}}$	$\frac{\tau_{pitch}}{\tau_{heave}}$
22	None-passive	8.1	11.3	86	3.28	0.33	2.4	0.75	1.35	0.44
23	None-passive	7.9	8.8	86	3.38	0.30	2.3	0.65	1.45	0.46
24	None-passive	9.0	8.3	95	3.08	0.30	2.3	0.75	1.35	0.40
34	100% C.D.	9.6	11.7	105	1.91††	No oscillation	2.9**	< 0.48	NA	NA
35	70.7% C.D.	10.6	12.8	107	2.10††	No oscillation	2.7**	< 0.57	NA	NA
36	70.7% C.D.	9.5	7.8	106	1.25††	No oscillation	2.3**	< 0.76	NA	NA

* Measured in region immediately after point D of Figures 28 and 29.

† $z_o = \Delta z_o + \begin{cases} 5.9 \text{ cm for Runs 22-24} \\ 8.2 \text{ cm for Runs 34-36} \end{cases}$ where Δz_o is the actual levitation height of the vehicle.

** Measured over very short region in time with no apparent exponential decay.

†† Frequency actual is coming from 20-foot track perturbations driving active controls. Run 34 active control current "pitch" had a frequency of 1.94 Hz (compared to a vehicle pitch frequency of 1.91 Hz). Since it was a driven frequency, one would not expect a decay time constant.

indicated on Figures 28 and 29, and the expression

$$\tau = t_o \, (\ln A_1/A_2)^{-1} \, ,$$

where t_o is the time between peaks. The amplitude of the first peak was not used since, as was shown in our earlier report, the curve is not purely a damped oscillation but includes an additional exponentially decaying term. By using the later oscillations, we assumed that the additive term had decayed to an insignificant fraction of the usual damped oscillatory term. Both the damping time and the frequency of oscillation are functions of the velocity and suspension height of the vehicle and are therefore time-consuming to calculate from first principle in each case. The computer program used to simulate the vehicle motions includes the corrections and provides the best test of the validity of the model.

The frequency of oscillation, f, was determined from the peak-to-peak time of the data, and z_o is the average suspension height of the center of mass. The velocity, v_o, was determined from the time required to traverse one 20-ft-long aluminum plate as indicated by the lateral position sensors. The calculated damping coefficients, expressed as percentages of critical damping, using absolute velocity feedback, are given in the table for the actively controlled tests.

The heave and pitch motions of the vehicle during test #24 are shown in Figures 28 and 29. In these figures, the vehicle levitated at approximately point A, with the rear of the vehicle levitating first, due to the front magnets being set slightly higher than those in the rear, and possibly a nonuniform distribution of weight. The front wheels might not have left the guideway in this region. At point B, the front magnets encounter the upward step onto the additional plates, causing an oscillatory increase in suspension height and a pitch upward of the front of the vehicle. The front and rear magnets drop off the step at points C and D, respectively. Since the vertical position sensors are

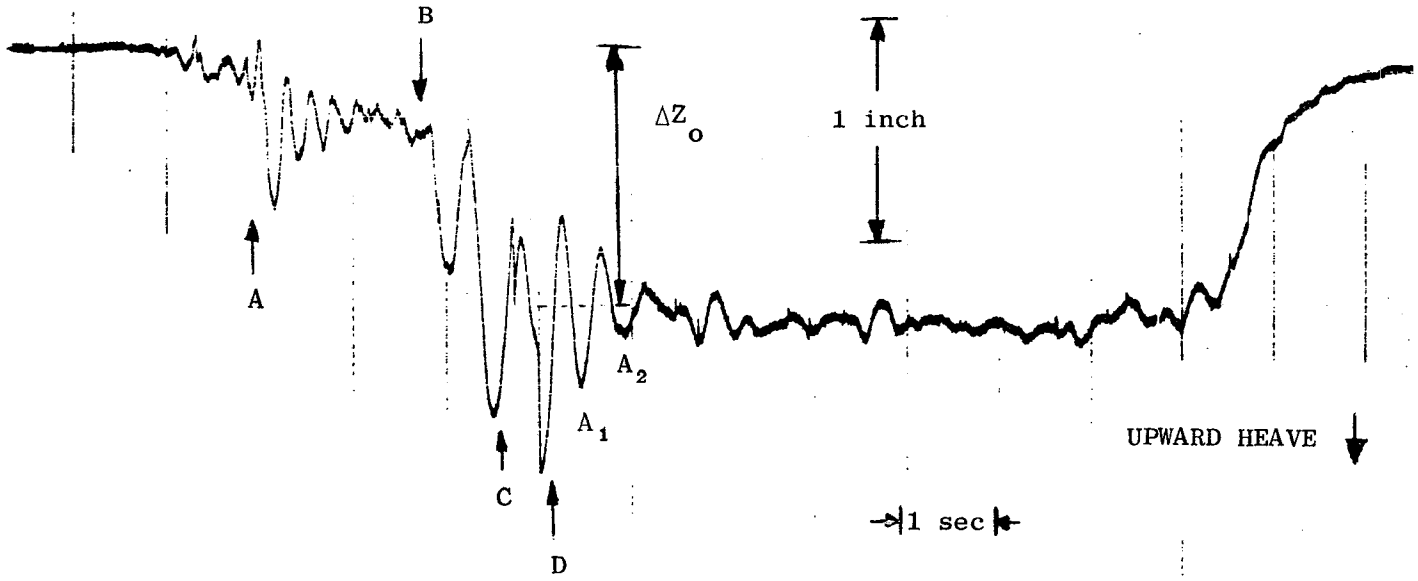

FIGURE 28 HEAVE MOTION-TEST 24

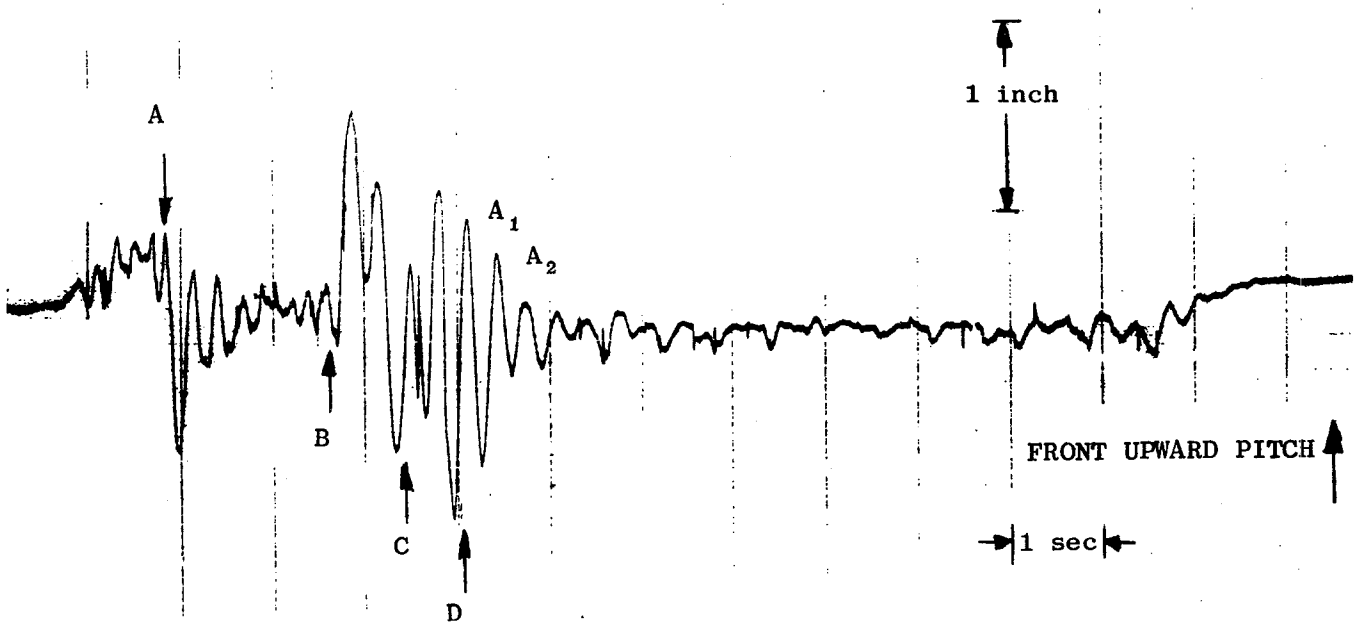

FIGURE 29 PITCH ANGLE VERSUS TIME-TEST 24

between the magnets, the front sensor drops after the front magnets and the rear sensors drop before the rear magnets. The sensors dropping off resulted in the two nearly vertical portions of the trace. After the rear magnets drop off the vertical step, the vehicle oscillates in both heave and pitch with the indicated amplitudes--damping to a level ride marked only by track perturbations. The vehicle was pitched slightly forward, due, as mentioned earlier, to the front magnets being about 0.1 inch higher than those in the rear, and possibly to an uneven weight distribution.

A total of four passive (Nos. 22, 23, 24, 32) and four active (Nos. 33, 35, 35, 36) damping tests were performed over the step perturbation. Only six of these yielded useful data due to the normalization of a magnet in one run (No. 33) and the failure of the data recording system after the step in another (No. 32). The active tests were marred by the failure of one of the active damping controls to produce the required current. The current was only about 10% of that necessary. This failure was not detected in the earlier tests since the current in only one of the controls was measured at that time. The current demanded by the controls was slightly in excess of that which could be supplied by the batteries in some cases when the vehicle traversed the vertical step. This was not always the case, and even when it did occur, the ride quality was markedly improved over that provided by passive damping alone. The pitch motion, however, was not attenuated as occurred in the actively controlled experiments over the standard guideway discussed in the previous section.

The heave oscillations decayed very rapidly in the active control tests, and only an upper limit to the decay time constant could be estimated. The heave frequency was similarly estimated. The fundamental pitch oscillation also decayed rapidly, but had a distinct periodic nature that did not decay and can be identified with track irregularities.

This was caused by one defective active control circuit, as discussed previously. The same pitch frequency was apparent in the heave and roll motions of the test vehicle. The difference in active damping for heave motion for different active control setting was observed in the heave motions of runs Nos. 34 and 35. The damping of Run No. 35 had an overshoot relative to run No. 34 (100% C.D.) which indicated an underdamped control setting (70.7% C.D.).

Direct comparison between the active and passive tests is shown in Figures 30, 31, and 32. In general, the active damping system damped oscillations in both pitch and heave soon after passing the step perturbation, but subsequent minor irregularities continued to perturb the vehicle at 20-ft intervals, as explained earlier. The vertical accelerations of actively controlled test No. 36 in Figure 32 is very quiet, suggesting that the perturbations in the vertical position (Figure 30) are caused by the sensors following the track while the vehicle travelled a considerably smoother course. Note that the heave acceleration frequency (2.35 Hz) of run No. 24 is close to the heave motion frequency. The reduction in vertical acceleration when using active controls is clearly evident in this figure.

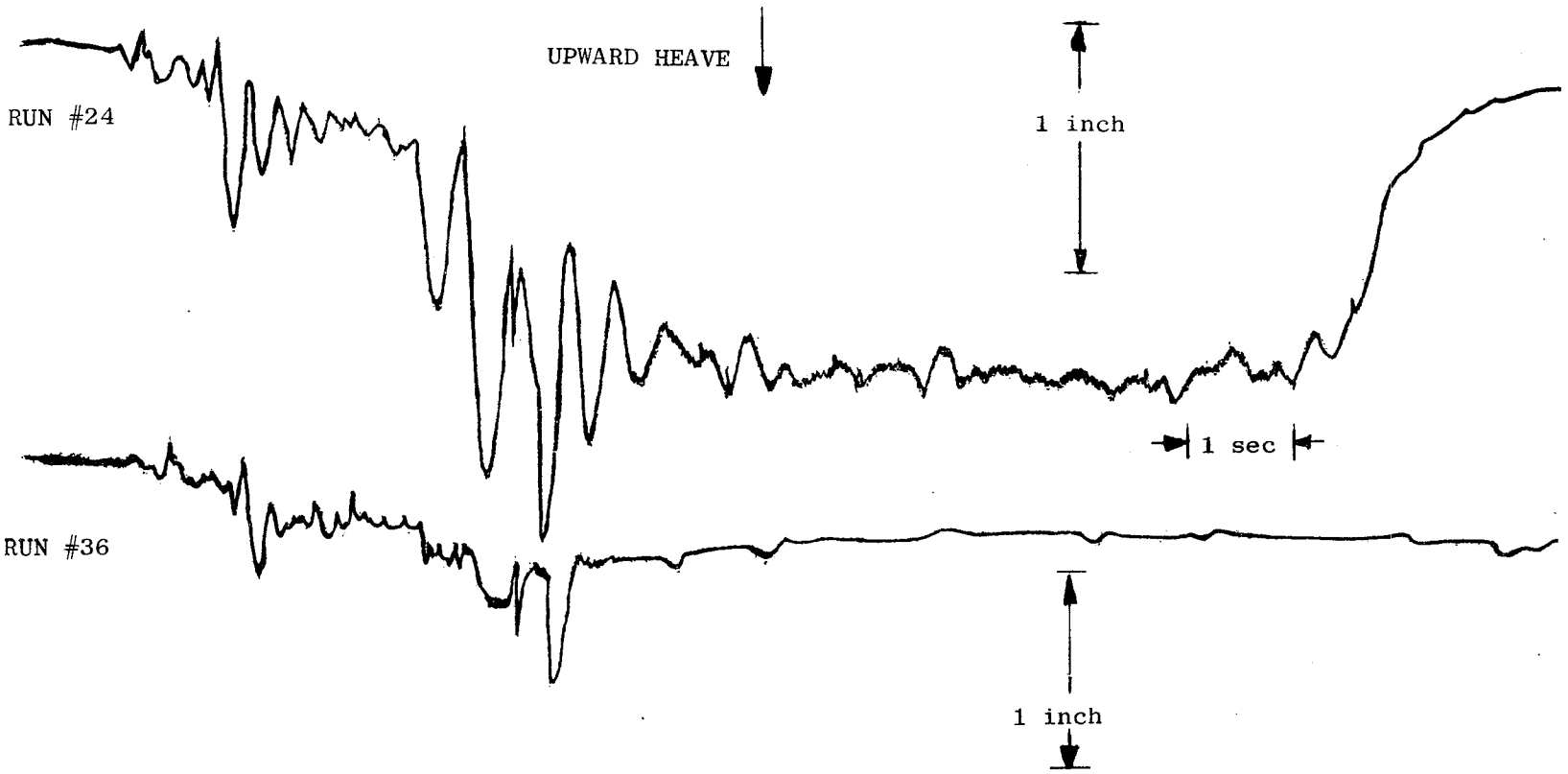

FIGURE 30 COMPARISON OF HEAVE MOTIONS-ACTIVE TEST 36 AND PASSIVE TEST 24

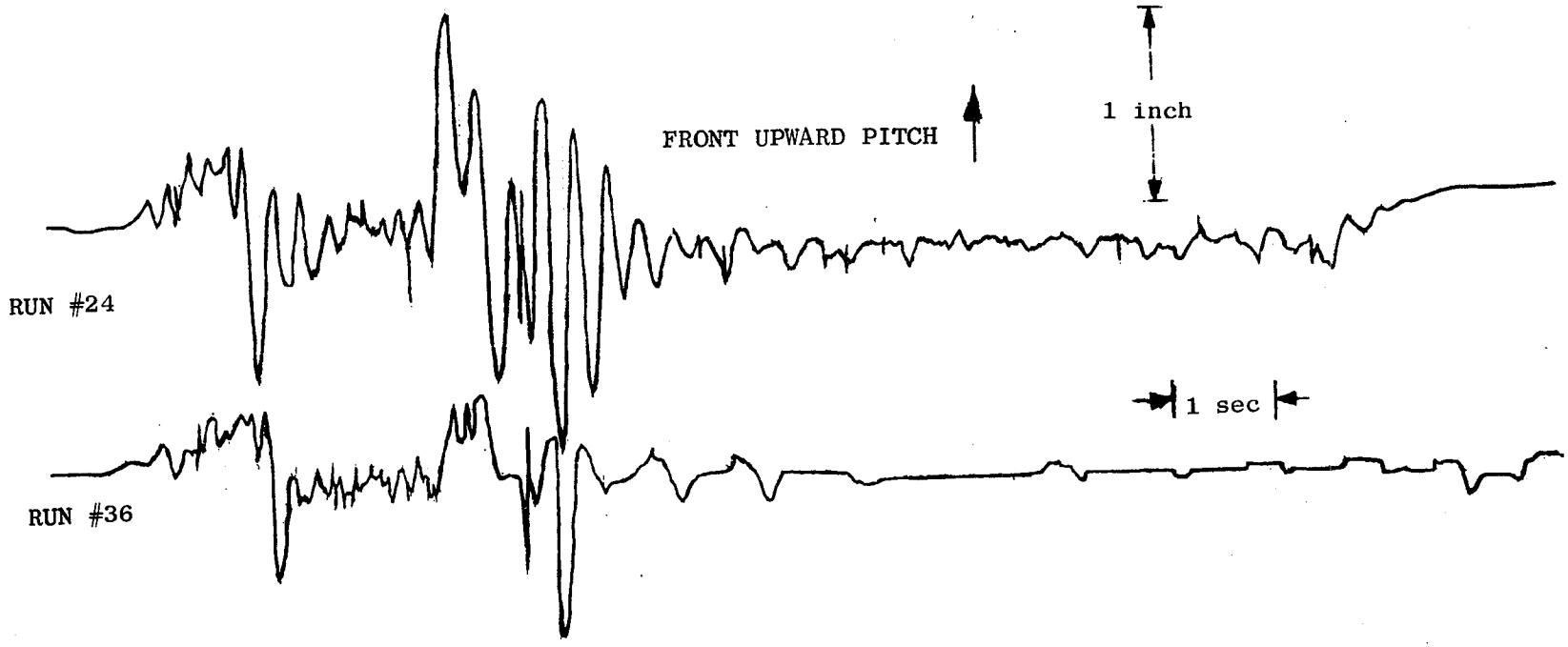

FIGURE 31 COMPARISON OF PITCH ANGLES-ACTIVE TEST 36 AND PASSIVE TEST 24

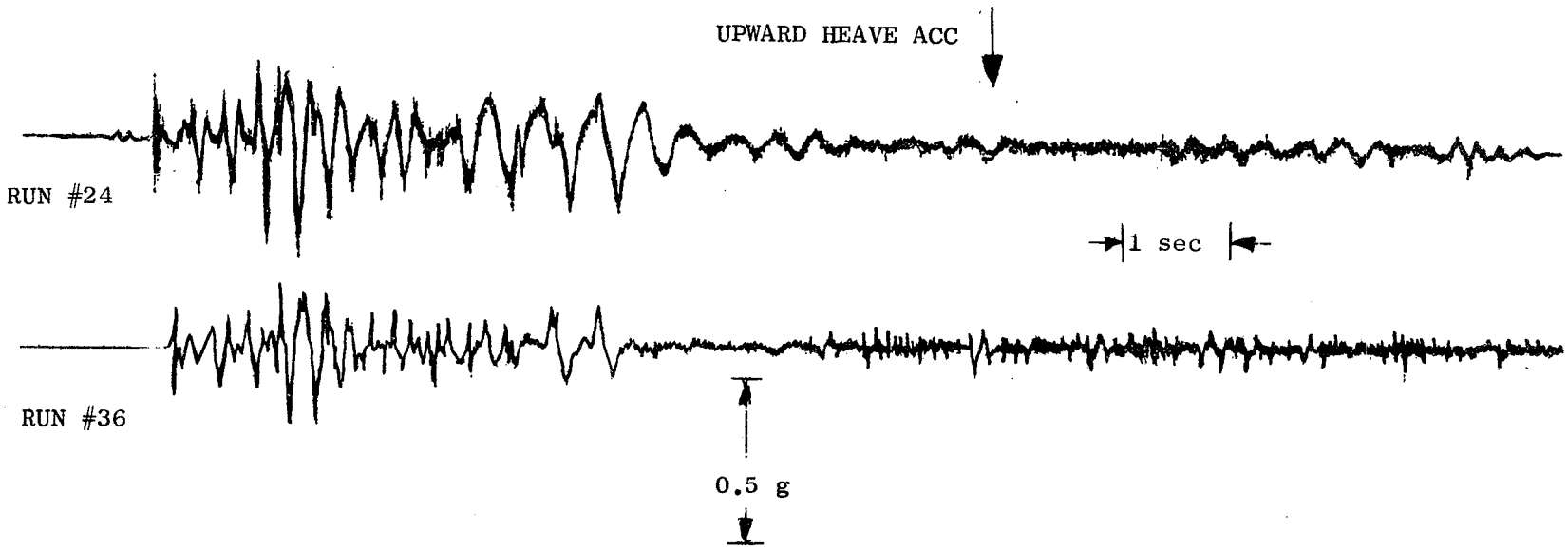

FIGURE 32 COMPARISON OF HEAVE ACCELERATIONS-ACTIVE TEST 36 AND PASSIVE TEST 24

Simulation of Vertical Motions

Vertical motions observed in the experimental tests of the levitated vehicle were simulated on the computer to assess the accuracy of the analytic model. The procedure for modeling these tests and the reasons for this procedure are discussed in the following paragraphs before the results of the simulations are presented.

It was necessary to provide several experimental parameters to the model to obtain correspondence between the model and the actual tests. The velocity of the vehicle and its position on the guideway had to be specified at the beginning of the simulation. Later velocities and positions were obtained by successive integrations of experimentally measured and tape-recorded accelerations which were supplied to the model. Irregularities in the guideway were surveyed and the results retained in the program as a table. The current in the magnets was also tape recorded as a function of time and could have been supplied to the model, but since the current remained relatively constant after levitation was achieved, this additional complication was avoided and the measured current at the start of the simulation was inserted as a constant. The mass and moments of inertia appropriate to the particular experiment were included in the simulation. Finally, the setting of the controls on the active damping system was included for simulations of the active runs.

At the beginning of each simulation, the vertical position at the location of each magnet was assigned an arbitrary value of zero. This is equivalent to referencing the calculated heave, pitch, and roll to the values obtained when the vehicle center of mass is at the equilibrium height, the vehicle is oriented so that each magnet is an equal distance from the surveyed guideway, and the only nonzero velocity is in the longitudinal direction down the guideway. Thus, pitch and roll are not necessarily referenced to a flat horizontal plane since the guideway is

not flat. This procedure, at most, results in a constart difference between the calculated and measured values of these variables.

Simulations were begun immediately prior to the experimental event of primary interest. This permitted a more detailed comparison between the model and the experimental data than could have been obtained if the simulation had been started earlier. The reason for this is that small errors in the measured velocity or acceleration can result in small but significant errors in the position of the vehicle at later times. Similarly, small errors in the computed frequency of oscillation can result in a significant error in phase after a short time. Consequently, the vehicle might be modeled as rising at the time it encountered a downward perturbation, although, experimentally, it might have been falling. Such a phase shift would result in a considerable difference between the calculated and measured accelerations at the perturbation although the model provided a very good approximation. For example, the location of the perturbation must be known within about the length of the magnets (0.3m) to achieve exact correspondence between the experimental and analytical results even if the model is exact. At a velocity of 10 m/s this requires that the velocity be known within 3% for a 1-second test and with increasing accuracy for longer tests. Neither the velocity nor the acceleration was measured with this precision.

Simulation of Standard Guideway Tests

Test 21 was simulated in the above manner. The heave motion for this test was shown earlier in Figure 10 and the heave (center of mass) acceleration was shown in Figure 11. The simulation of the heave data shown in Figure 33 was begun after the vehicle was levitated, as indicated in Figure 10. The experimental and calculated suspension heights are virtually identical, and the amplitude of the largest experimentally observed peaks are of approximately the same amplitude as those simulated,

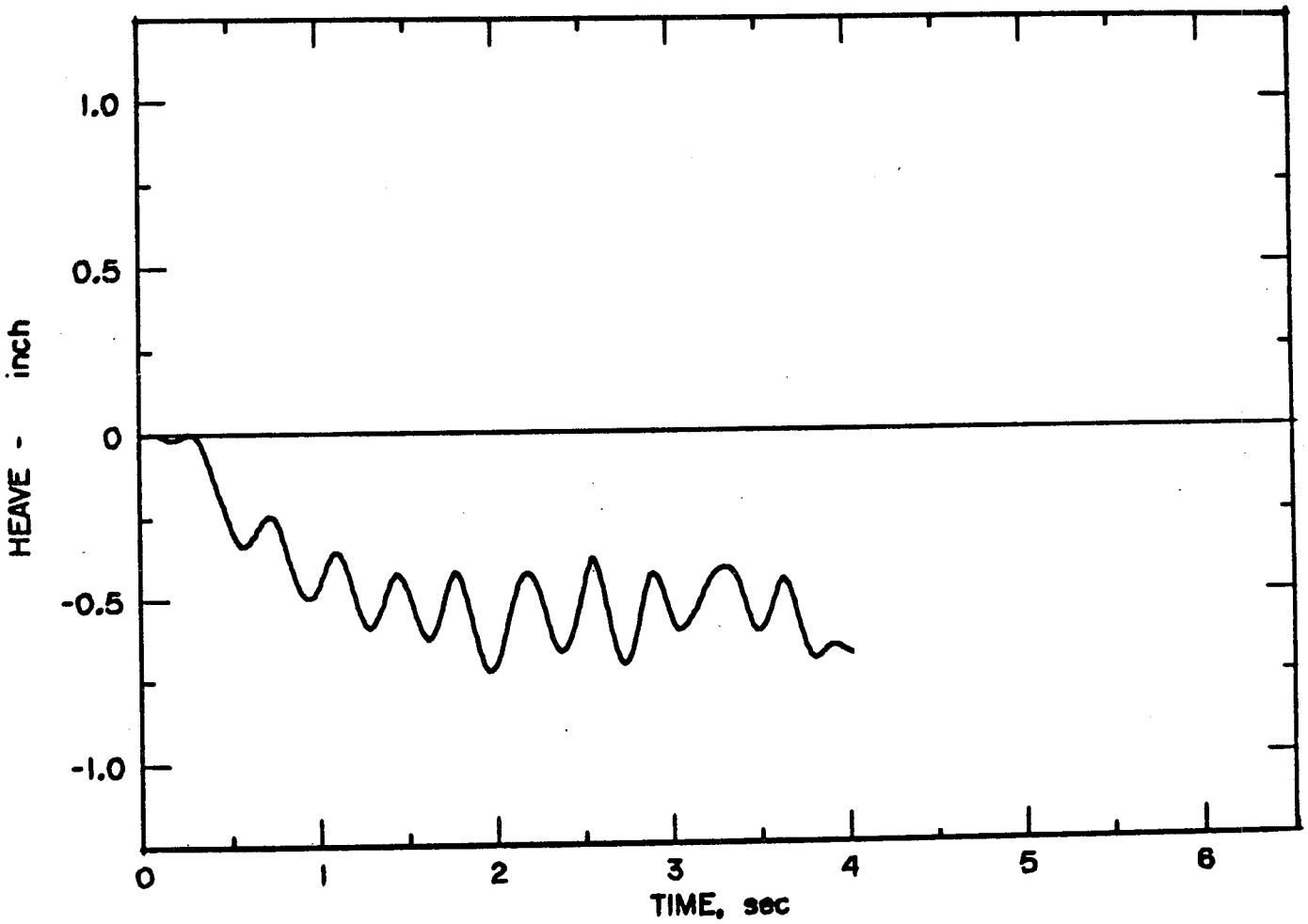

FIGURE 33 HEAVE SIMULATION VERSUS TIME-TEST 21

about 0.5 cm (0.2 inch). This is a variation of approximately 6% in the average height of the magnets above the guideway, 8.2 cm. However, the average amplitude of the simulated oscillations is greater than that observed experimentally. This difference in simulated suspension height variations corresponds to a simulated heave acceleration that is also somewhat larger than actually observed (Figure 34). The frequency of vertical oscillation is the same in each case, within the accuracy that they can be determined from the graphs. Note that the differences in scales tend to emphasize these discrepancies.

The pitch and roll data for this test were presented earlier in Figure 15 and 16, and are simulated in Figures 35 and 36. The simulations reproduce most of the specific features of the experimental data and the amplitudes are very similar.

All of these simulations are very sensitive to both the accuracy of the guideway survey and the precise location of the vehicle on it. Variations in the roll and pitch angle (see page 44 for definition of angles) seldom exceed 0.2 inch (0.5 cm). An error of one-half this amount in the surveyed height would account for the differences in the observed and simulated amplitudes. This precision could not be maintained in the survey over any appreciable distance. In addition, changes in the ambient temperature and the resulting thermal stresses in the guideway were observed to cause slight variations in the guideway profile. Note also that any guideway deformation due to the presence of the vehicle (i.e., vehicle-guideway interaction) is not accounted for.

The use of actively controlled damping coils was simulated using parameters appropriate to Tests 29, 30, and 31 with 3/8, 5/8, and 1 times critical damping, respectively. It was noted earlier that the left rear active control circuit appeared to be generating only about 10% of the current generated in the other active controls. This failure was observed to occur in the right rear magnet in later tests in which

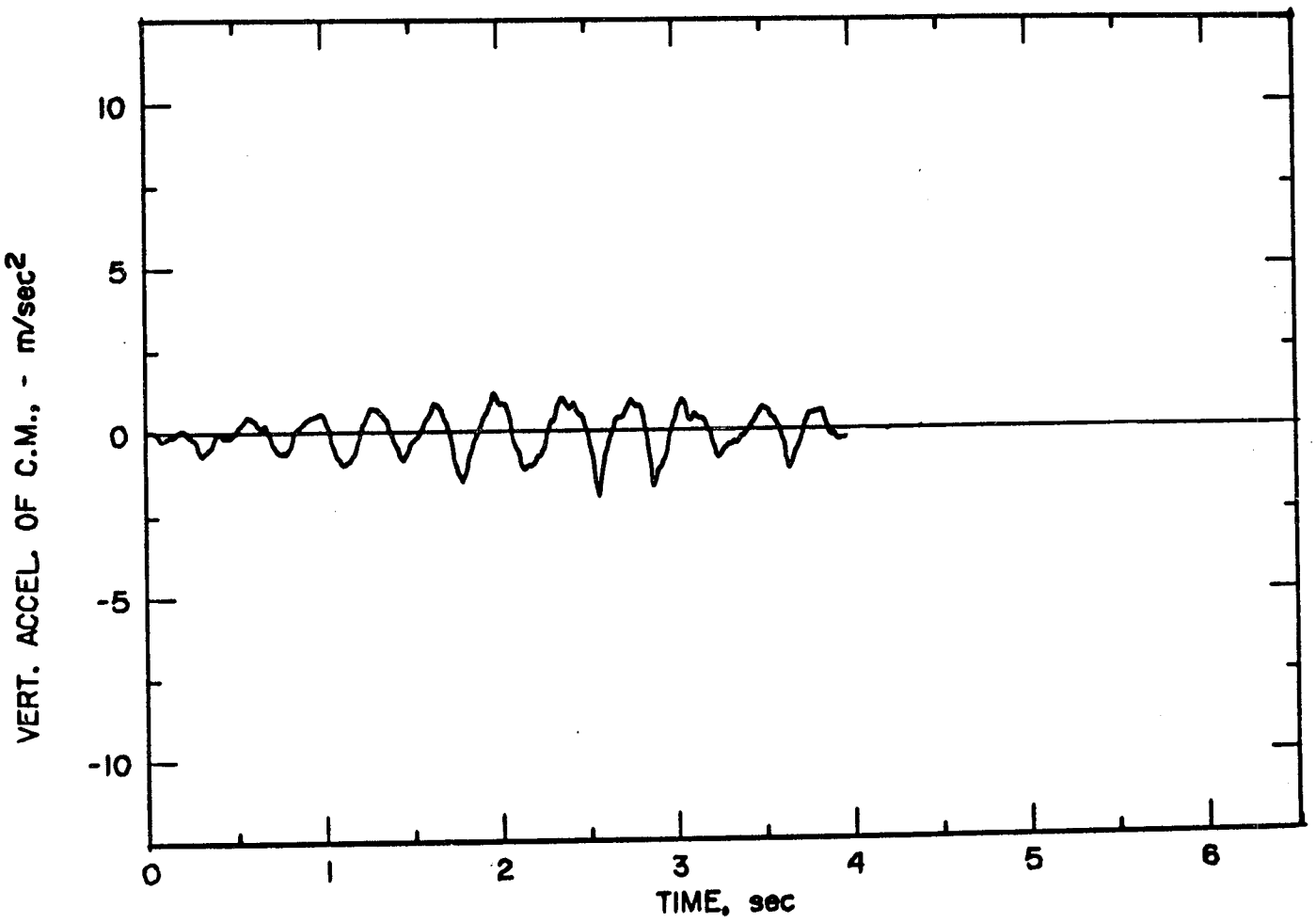

FIGURE 34 HEAVE ACCELERATION SIMULATION VERSUS TIME-TEST 21

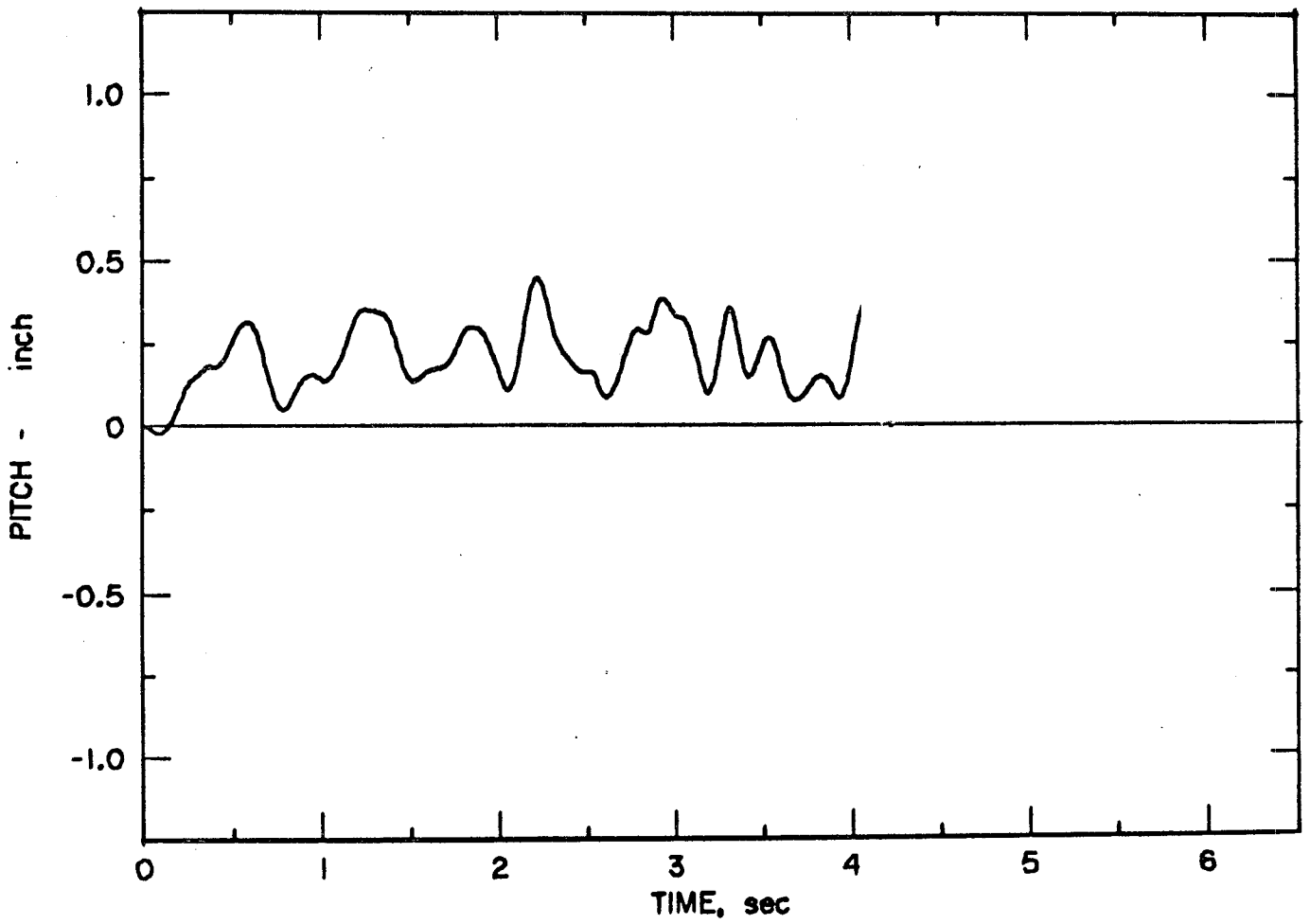

FIGURE 35 PITCH ANGLE SIMULATION-TEST 21

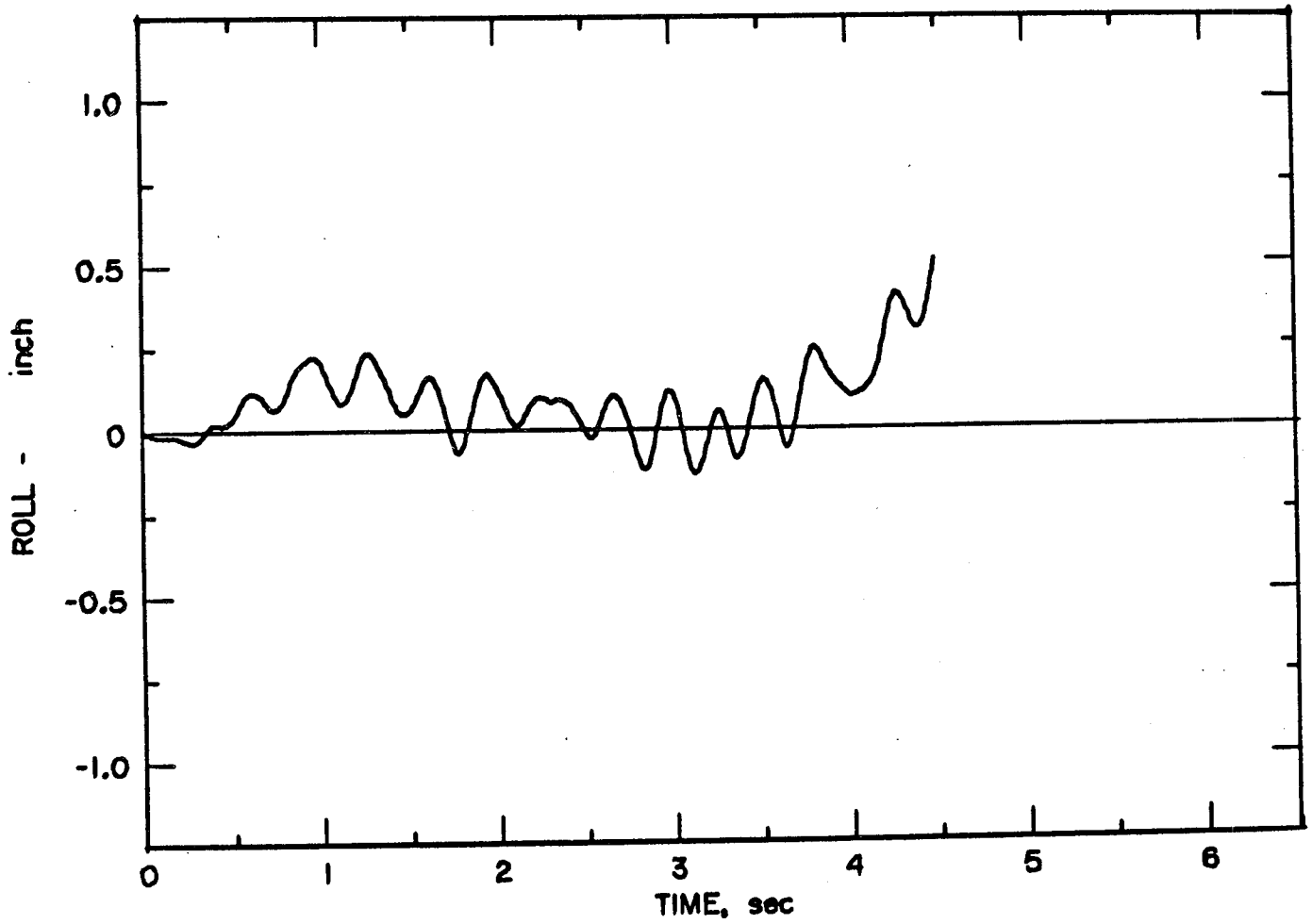

FIGURE 36 ROLL ANGLE SIMULATION-TEST 21

the control current was monitored in all the coils. It is assumed that a similar failure occurred in these earlier experiments and that the magnitude of the failure was the same. In an attempt at a more exact simulation, this effect was modeled by specifying a damping coefficient in the left rear control coil which was 10% of that in the other coils.

The results of the analytic model in the three actively controlled damping tests over the standard guideway are shown in Figure 37 for the heave motion and in Figure 38 for the heave acceleration. These can be compared with the experimental results in Figures 17 and 18. The heave and heave acceleration results are in good agreement with the experiments, although the extent of the perturbation is again overemphasized--leading to speculation that the survey might be faulty in some regions of the guideway. This simulation of faulty operation was required to evaluate the validity of the model, but it is also of interest to determine how the vehicle would have behaved if all the controls had operated properly. To illustrate this, Test 29 was also simulated with the left rear coil operating correctly. The effect of simulating the correct current in each coil in Test 29 is to smooth the curves somewhat and to reduce the accelerations correspondingly. The accelerations in the corrected simulation in Test 29, where the damping of all coils was set at 3/8 of critical, are comparable to those of Test 30 where the damping in three coils was set at 5/8 of critical and in the left rear coil at 10% of this value.

The effect of correcting the control coil current on the pitch angle motion (not shown) was similar to that calculated for the heave motion--the peaks were reduced in amplitude 20% to 30%. The effect on the roll motion, however, was quite pronounced, as shown in Figure 39 with the data from Test 29.

Since the vertical motions over the standard guideway are greatly

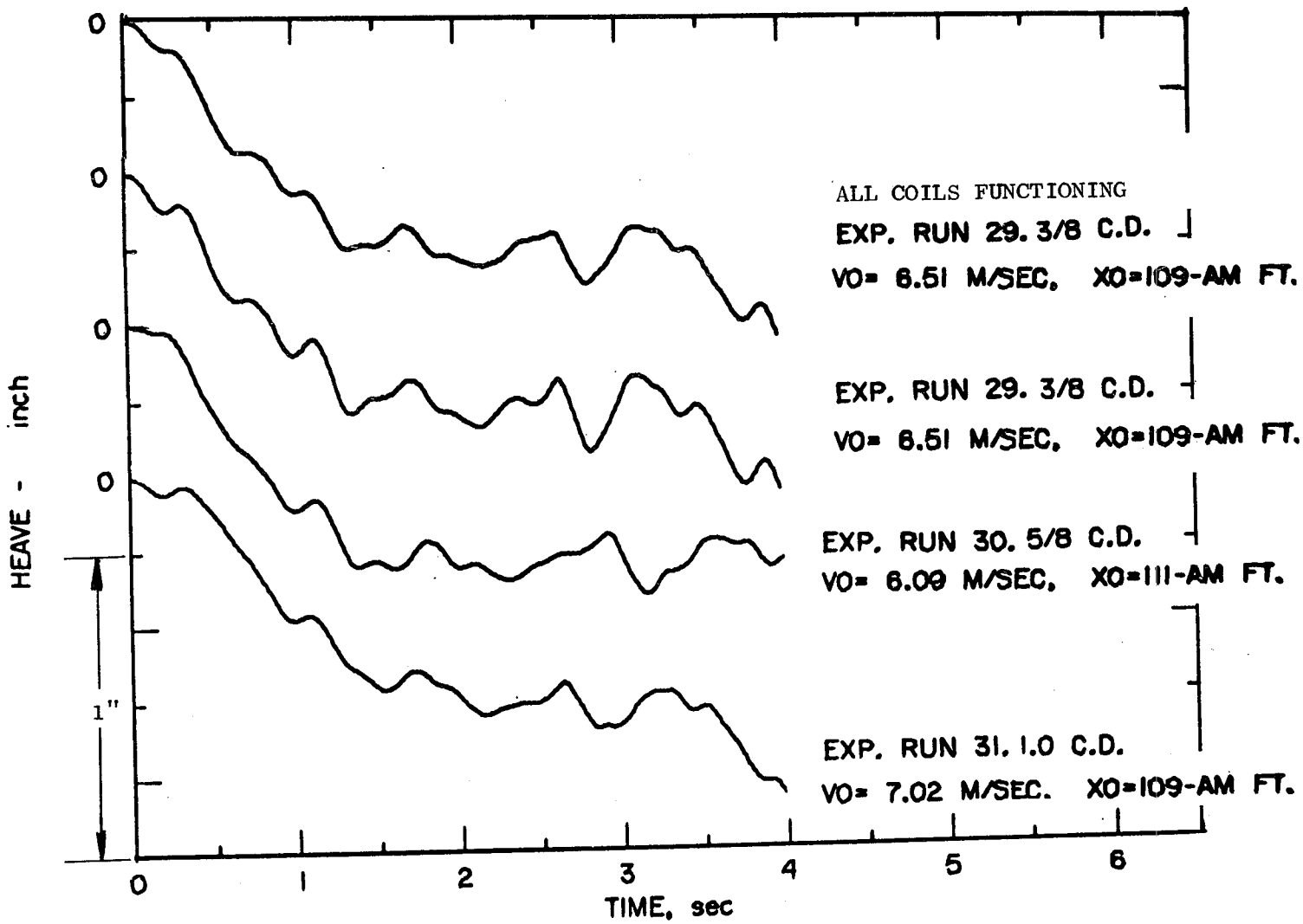

FIGURE 37 HEAVE SIMULATION-ACTIVELY CONTROLLED TESTS 29, 30 AND 31

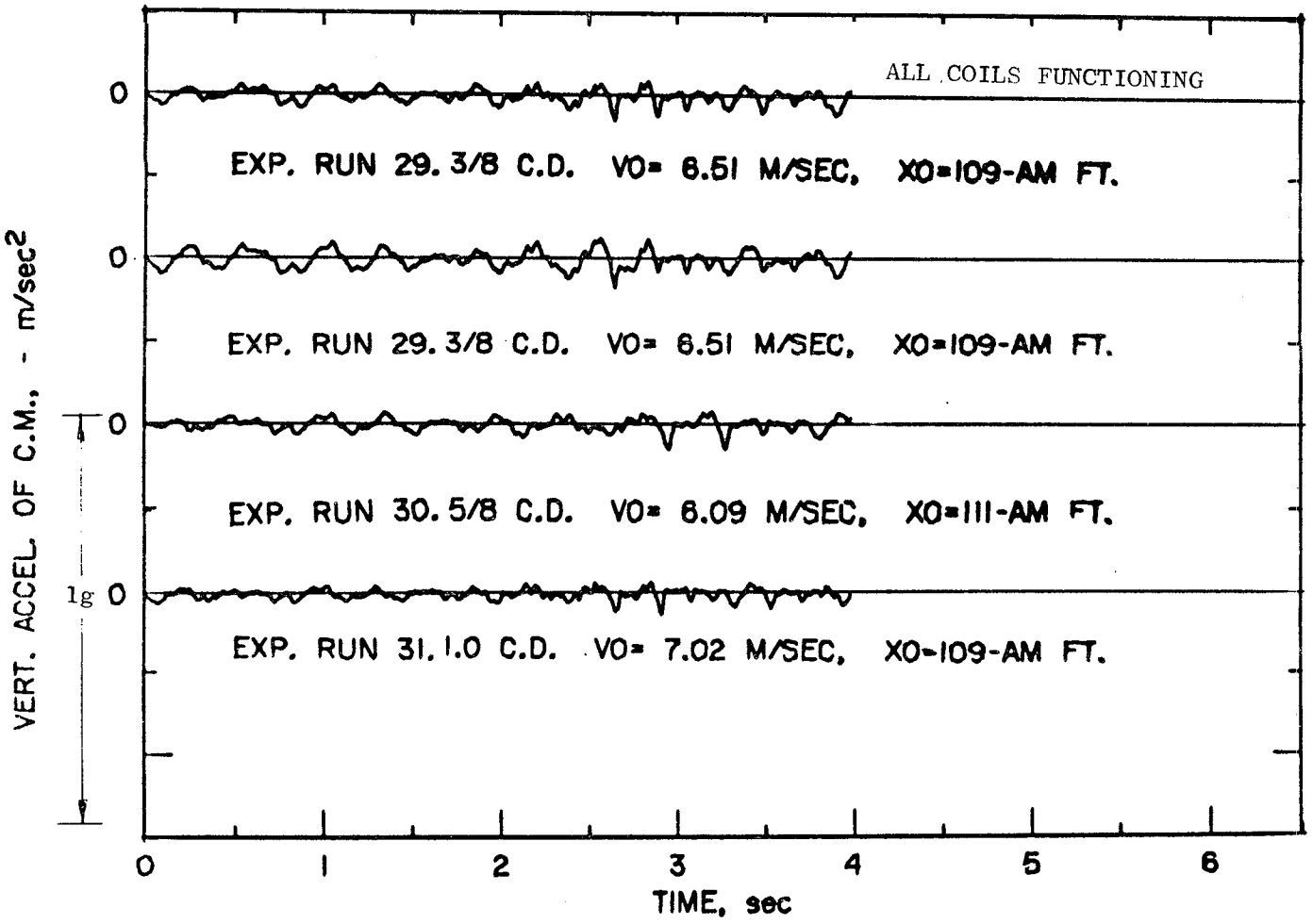

FIGURE 38 HEAVE ACCELERATIONS SIMULATION-ACTIVELY CONTROLLED TESTS 29, 30, 31

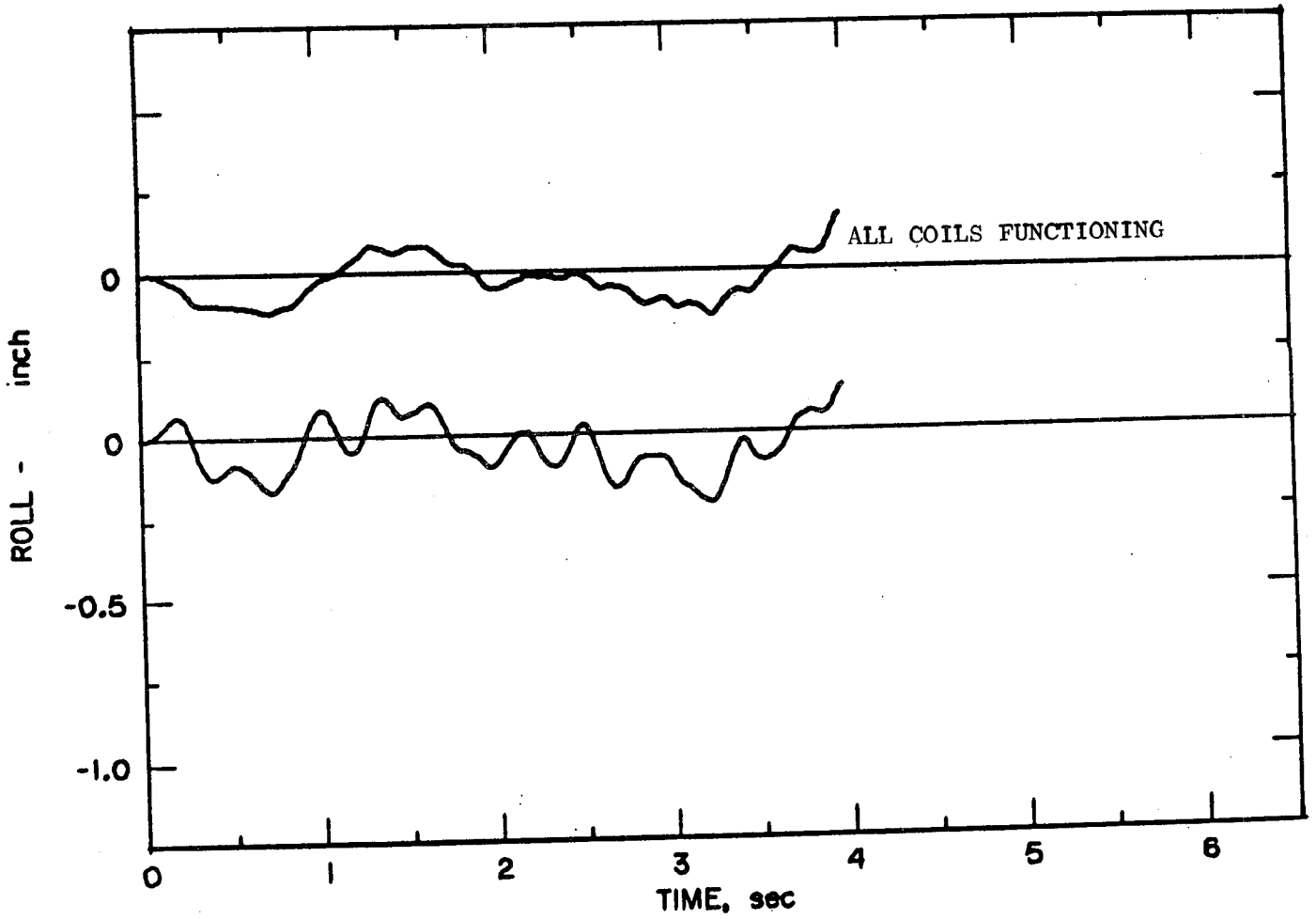

FIGURE 39 COMPARISON OF SIMULATED ROLL MOTION WITH AND WITHOUT DEFECTIVE ACTIVE CONTROL-TEST 29

influenced in the details by the precision of the guideway survey, it is better to compare the experiments and calculations where large known perturbations exist. Such a comparison was made in the tests with the symmetric vertical perturbation.

Simulation of Symmetric Vertical Step Tests

Passive damping Test 23 was simulated on the computer. The heave position data and its computer simulation are shown in Figure 40. The major oscillations and the phase of the oscillations at which the vertical sensors drop off the step are accurately predicted. Toward the end of the simulation, a heave oscillation is simulated that did not occur in the experiments. This is probably caused by an error in the guideway survey. The frequency of oscillation measured from these curves is approximately 2.8 Hz by the simulation and 2.5 Hz from the experiments. The amplitude of the oscillations during the perturbation is simulated as being less than observed, but later, over the unperturbed guideway, the simulated amplitude is greater than that which was observed.

The pitch simulation, Figure 41, also reproduces the major characteristics of the data, but is inaccurate in the amplitudes of the oscillations. The same simulation was performed assuming the guideway to be perfectly flat and is shown in Figure 42. The pitch amplitudes in this latter simulation are in better agreement with the experimental data than those in which the surveyed shape of the guideway was included. This again suggests that one source of discrepancy between the experiments and the simulation is the error in the guideway survey.

It was found that the amplitudes of the oscillations were very sensitive to the initial conditions for the simulations. For example, an error of one centimeter in equilibrium height can result in a factor of two differences in the amplitude of pitch oscillations. Further, the amplitude of the oscillations while traversing the perturbation is influenced

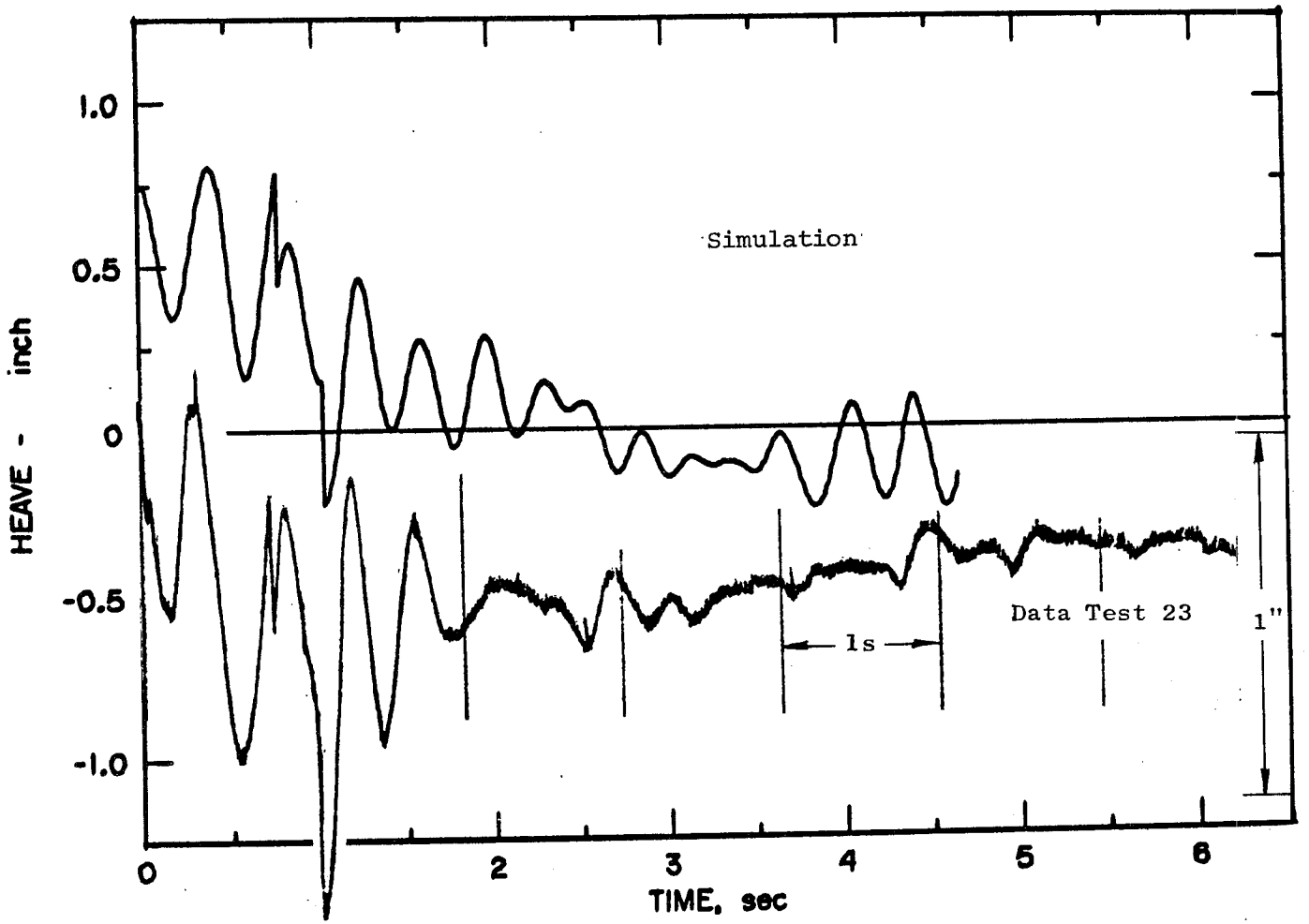

FIGURE 40 COMPARISON OF SIMULATED AND EXPERIMENTAL HEAVE MOTIONS-TEST 23

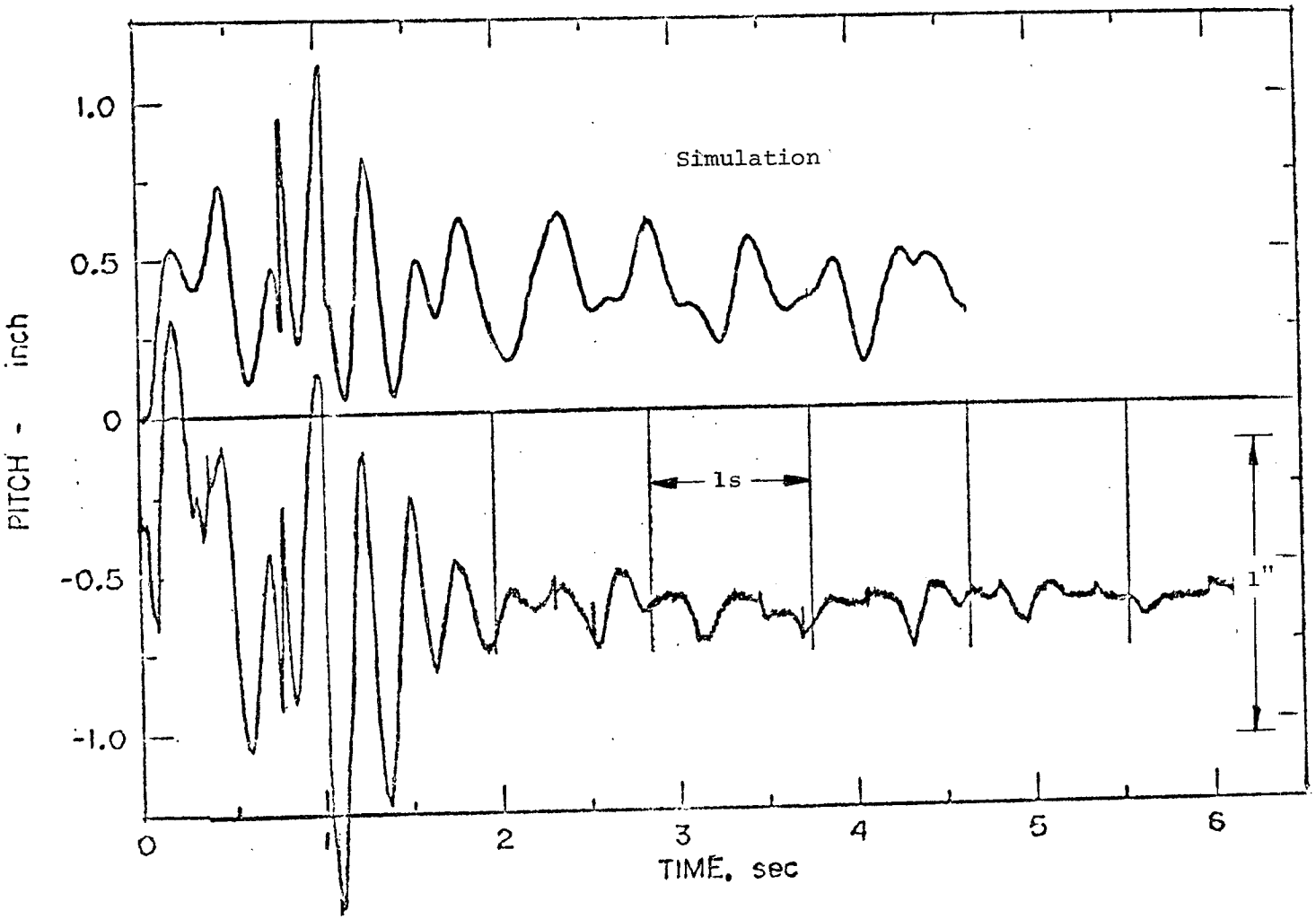

FIGURE 41 SIMULATION OF EXPERIMENTAL RUN 23 (UPPER CURVE) INCLUDING TRACK PERTURBATIONS AND TEST DATA (LOWER CURVE).

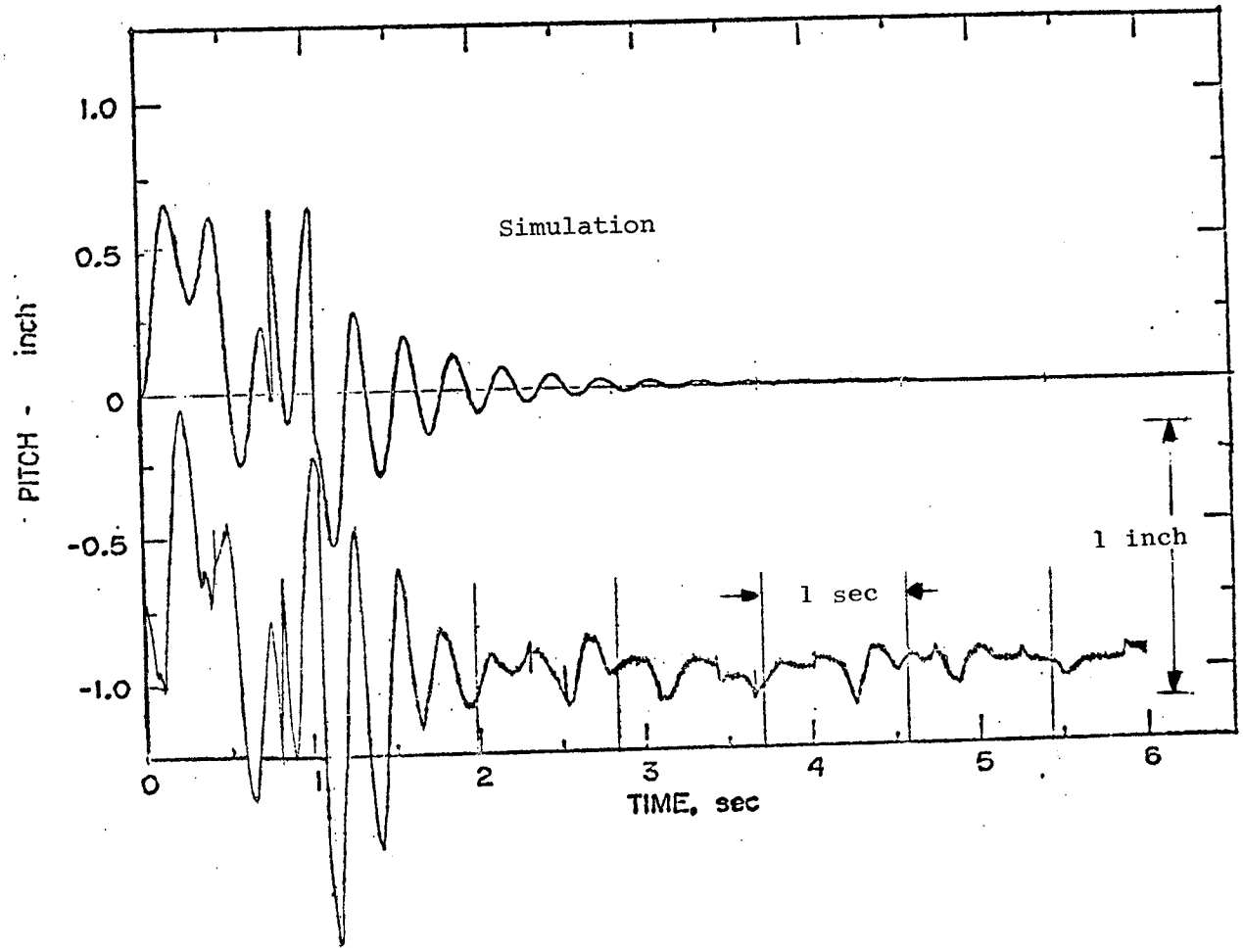

FIGURE 42 SIMULATION OF EXPERIMENTAL RUN 23 (UPPER CURVE) AND TEST DATA (LOWER CURVE). NO TRACK. VO= 7.93 m/sec.

by the modeling of the step in the guideway. As discussed earlier, the guideway was modeled to have a taper equal in length to the length of the magnet. This assumption appears to be sufficient to reproduce the character of the measured motion, but may not be sufficiently detailed to reproduce, for example, the amplitude of the measured accelerations. The heave acceleration and its simulation for Test 23, shown in Figure 43, suggest that the acceleration when traversing the step was in fact larger than that modeled. No variations in the modeling of the step perturbation were made during the analysis.

The experimental results for Test 34, the vertical step perturbation with active damping on the vehicle, were also simulated using the computer model and the active damping model. The active damping system was modeled as having no interaction with the passive damping coils, although the passive coils continued to provide damping both experimentally and in the model. It is reasonable to expect that the passive coil reacted against the active system and reduced its effectiveness to an undetermined extent.

The pitch motion from this test and its simulation are shown in Figure 44. As before, the left rear active control was modeled as defective as was ascertained after the experiments. The simulation is very good, both in the characteristic motions and in the amplitudes. As discussed above, the reference values for the measured and calculated values of pitch differ by a constant.

Measured and calculated heave motions are shown in Figure 45 for Test 34. The calculated increase in height is a result of the method used for setting the current in the magnets for computational purposes and is of no significance. The experimentally determined heave motion is slightly more pronounced than that calculated while passing over the perturbation, and is less perturbed than that calculated further down the

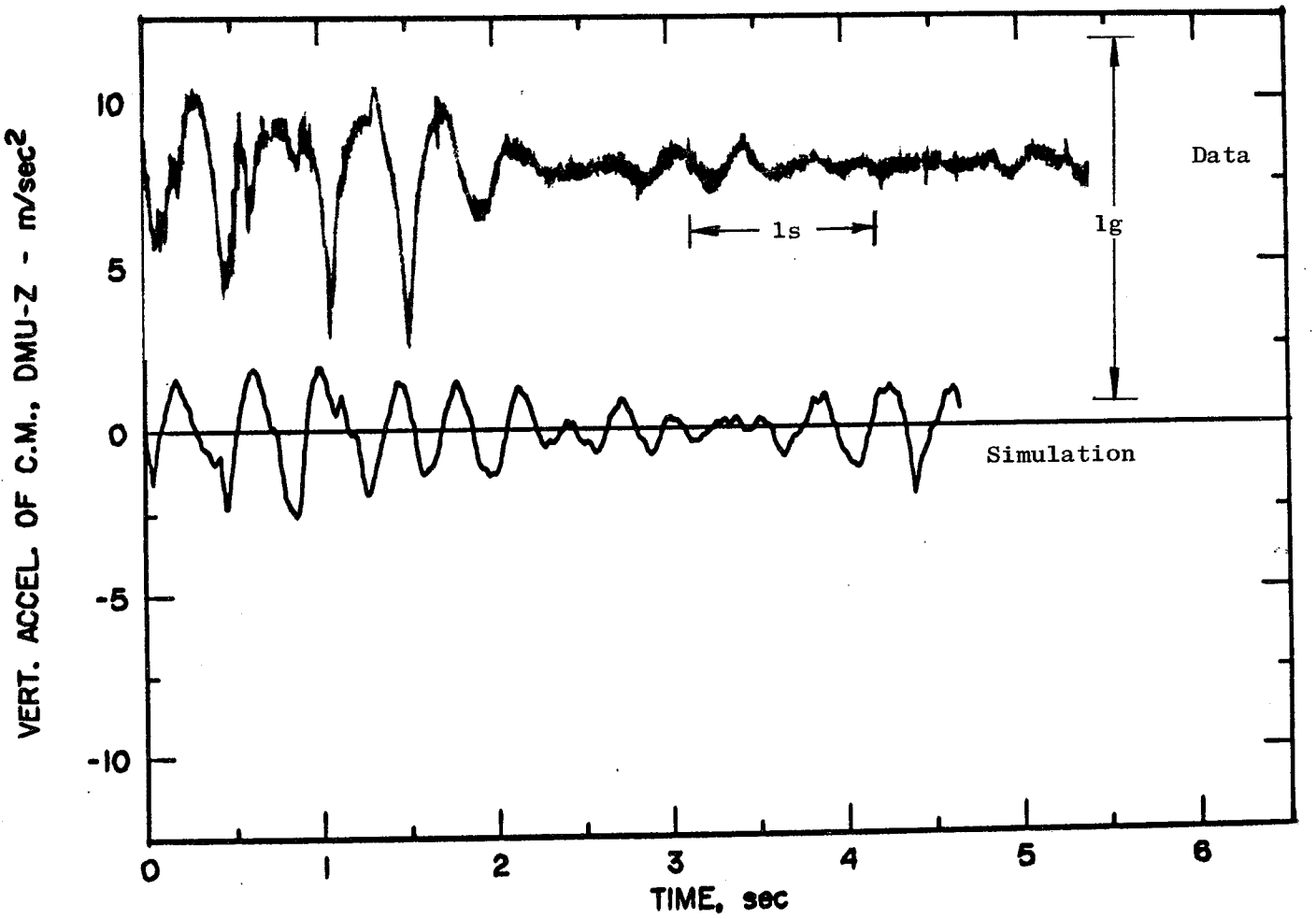

FIGURE 43 SIMULATED AND MEASURED VERTICAL ACCELERATIONS: TEST 23

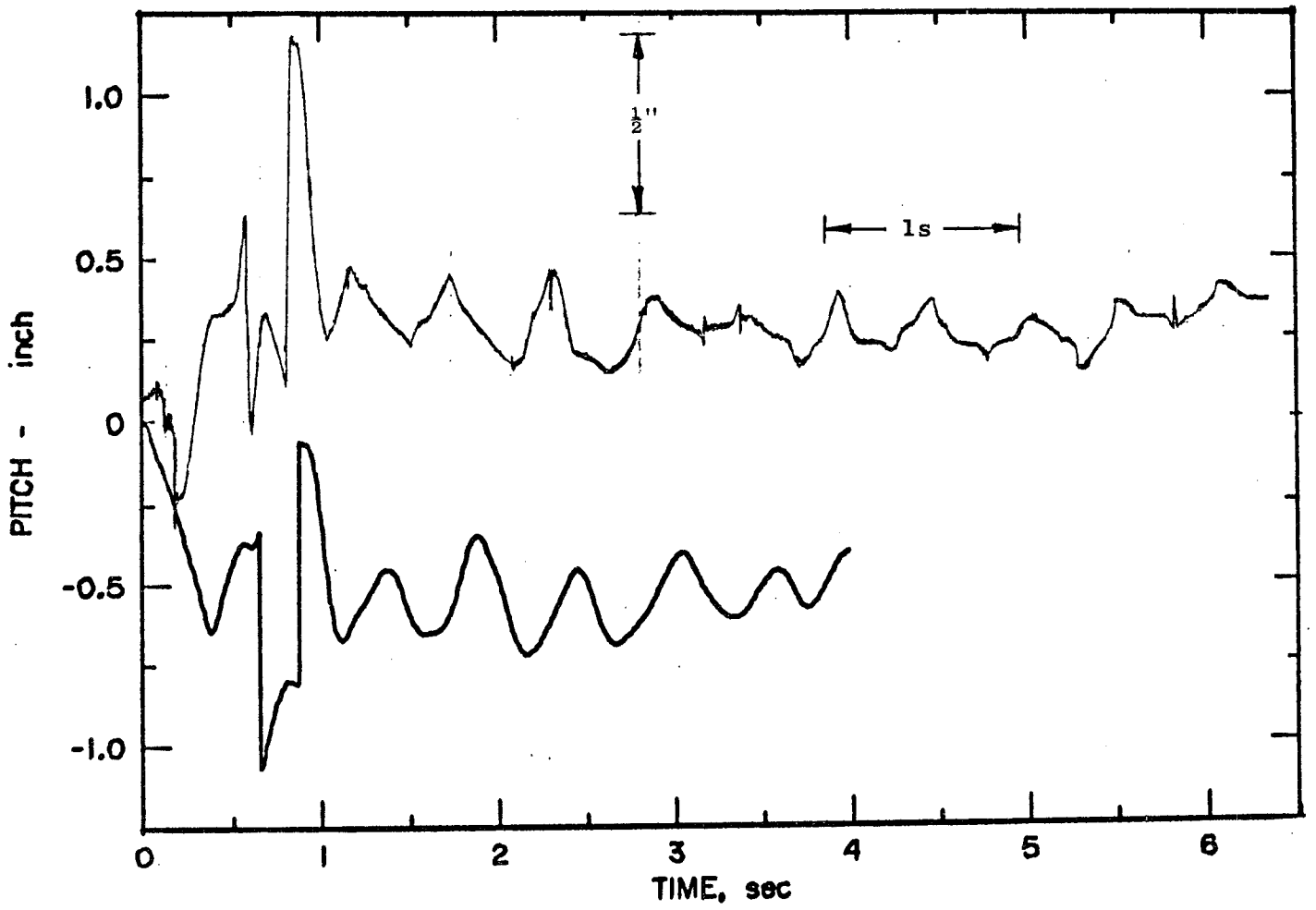

FIGURE 44 SIMULATED (LOWER CURVE) AND MEASURED (UPPER CURVE) PITCH MOTION: TEST 34, CRITICAL DAMPING, ACTIVE.

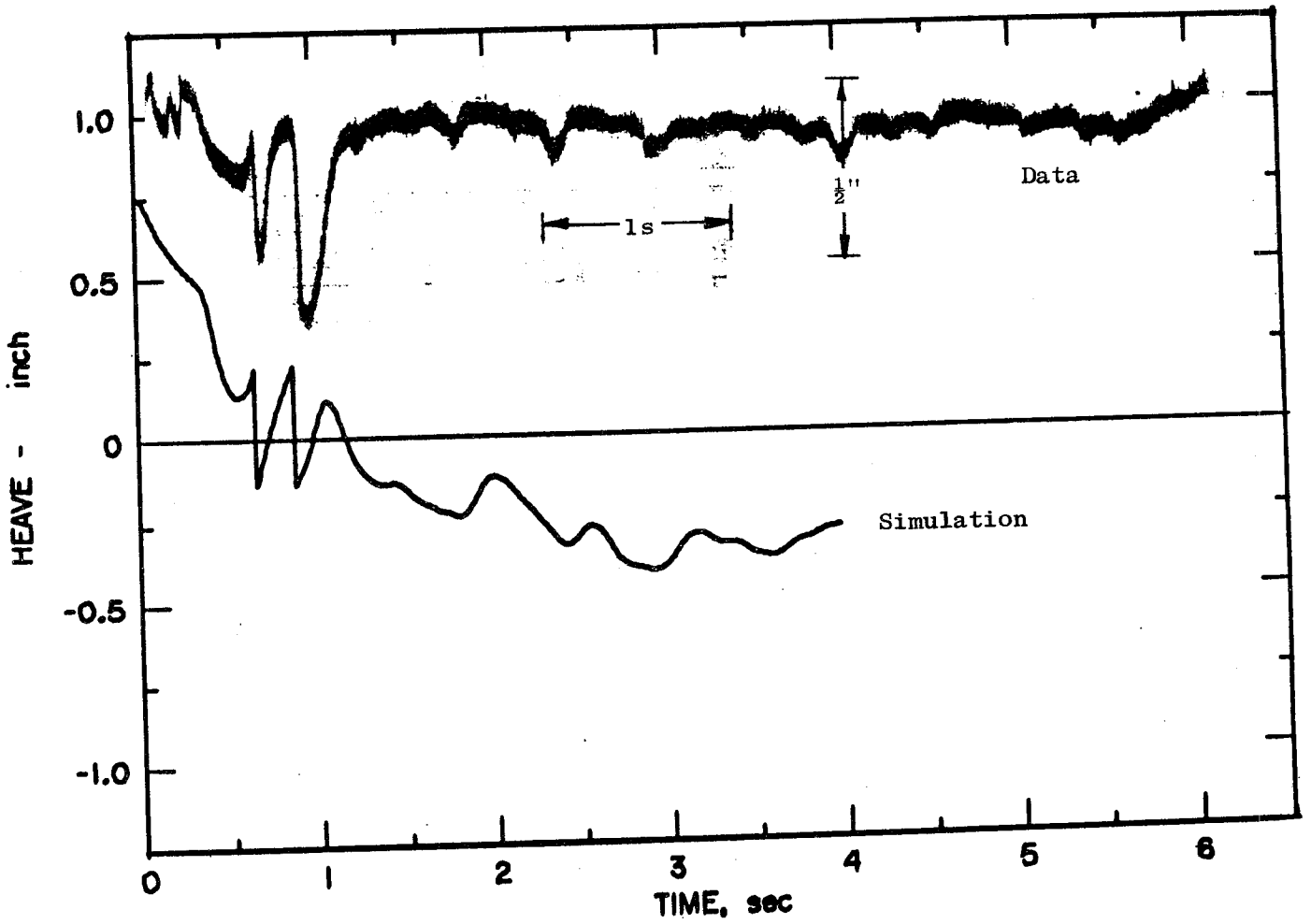

FIGURE 45 SIMULATED AND MEASURED HEAVE MOTION, TEST 34

guideway. The calculated increase in suspension height is caused by a slightly high acceleration input to the model. A comparison of the measured and modeled roll motion is shown in Figure 46 and is in good agreement in all respects.

These simulated motions are in good agreement with the experimental data, considering the accuracy with which the data were known and the small effort devoted to the simulations. A more detailed analysis would have been profitable.

Lateral Motion Tests

Heave, pitch, and roll motions of the levitated vehicle on the standard guideway were discussed earlier in this chapter. The other motions of the vehicle measured in these tests were slip and yaw. These lateral motions were of particular interest in that the active and passive damping systems were specifically designed to produce damping of the vertical motions. Any damping in the lateral direction was incidental.

The approach throughout this program has been to achieve a fundamental understanding of the behavior of magnetically levitated vehicles. If the damping in one mode is thoroughly understood, the same principles can be applied to other modes. This has led to a concentration of efforts on the vertical oscillations.

Although damping effects have not been calculated in the lateral direction, the guidance force has been studied theoretically and experimentally and can be well approximated at all velocities and lateral distances. These forces arise from the interaction of the real magnet and its mirror image in the vertical plates of the guideway. Since

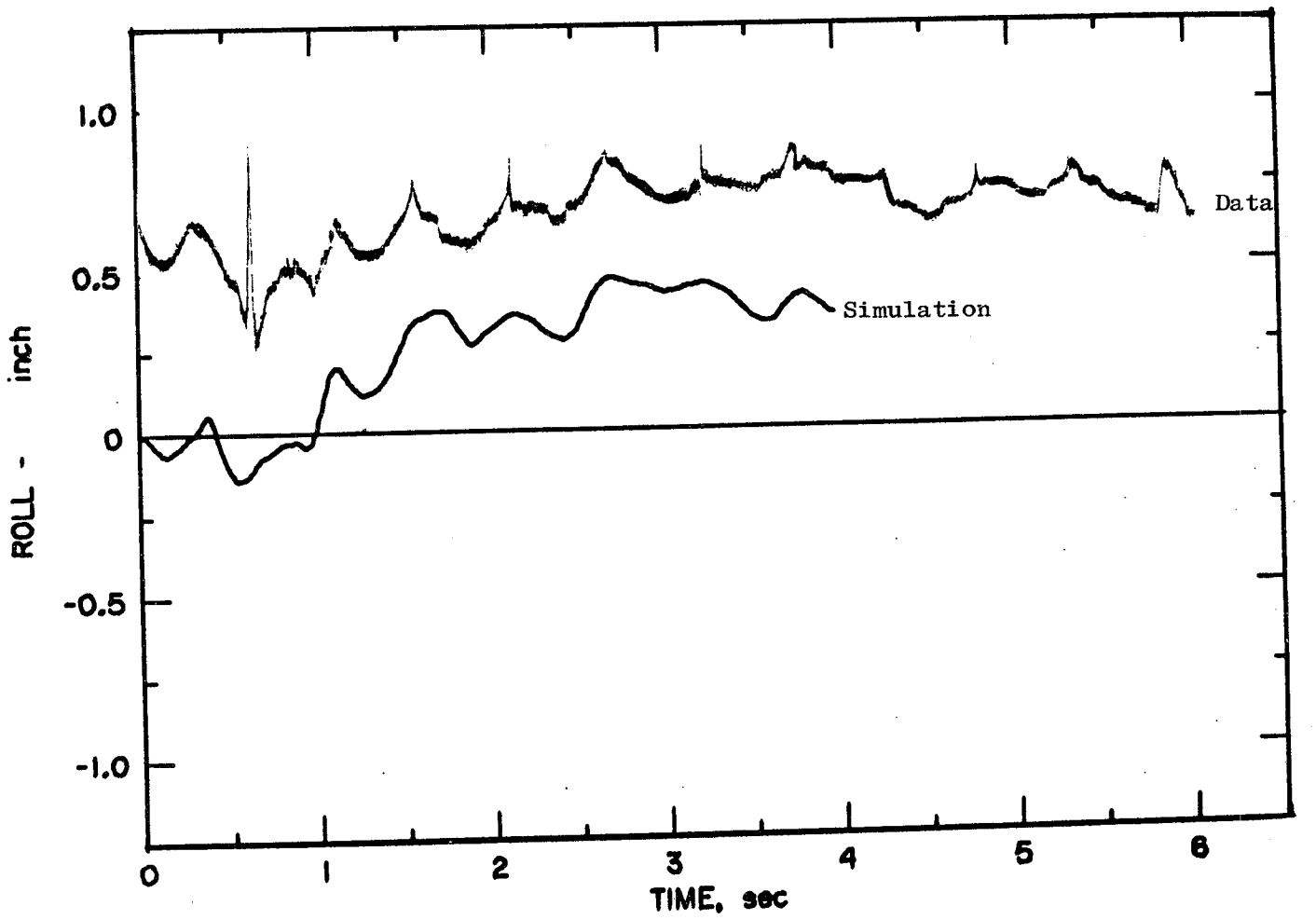

FIGURE 46 MEASURED AND SIMULATED ROLL MOTIONS, TEST 34

equal but oppositely directed forces are generated on each side of the vehicle in equilibrium, no net force is exerted on the vehicle when it is centered in the guideway. Any deviation of the vehicle from equilibrium results in a force restoring the vehicle to its equilibrium position. Even though the net force on the vehicle is zero, the force on each of the magnets can be appreciable and always exceeds the net guidance force.

Similarly, the damping force in the lateral direction depends on the interaction of the damping coil (active or passive) with the image of the suspension magnet. Currents can be induced in the passive damping coil by any motion of the vehicle in the lateral direction just as they are induced in the vertical direction. The damping force produced by the induced currents will be in such a direction as to oppose the motion, and the forces in each of the passive coils will act cooperatively to dampen lateral motions.

Lateral motions were observed in all the tests performed, but for completeness data will be presented on the same tests used in discussing the vertical motions in the standard guideway.

Lateral slip and yaw motion during Test 21 are shown in Figure 47. Similar data for Test 16 are shown in Figure 48. As was the case in the vertical motions, the perturbations in these tests can be identified with irregularities in the guideway in the lateral direction. Corresponding data for the active Tests 29, 30, and 31 could not be obtained since one of the lateral sensors was damaged in the asymmetric step test immediately preceding these runs.

The best comparison of these data is again afforded by PSD analyses. Figures 49 through 53 show the PSD generated in these tests. By comparing Figures 49 and 50 with Figures 12 and 13, it can be seen that the lateral PSD's are lower by 5-6 dB than the vertical PSD's for these passive tests.

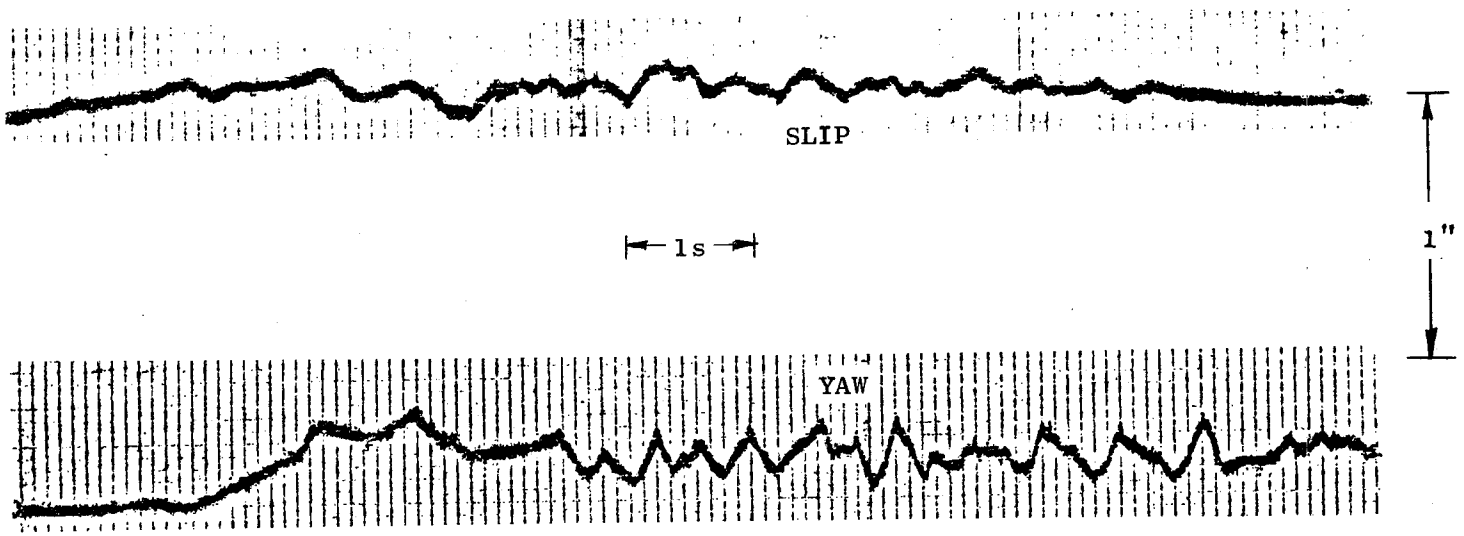

FIGURE 47 SLIP AND YAW MOTIONS, TEST 21

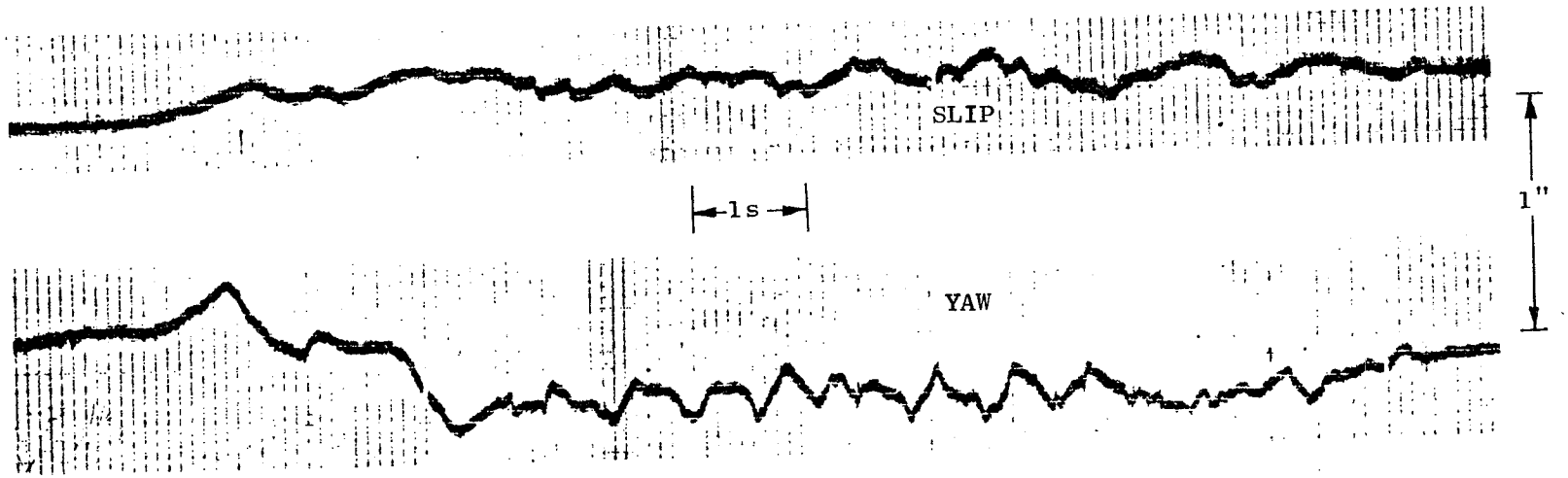

FIGURE 48 SLIP AND YAW MOTIONS, TEST 16

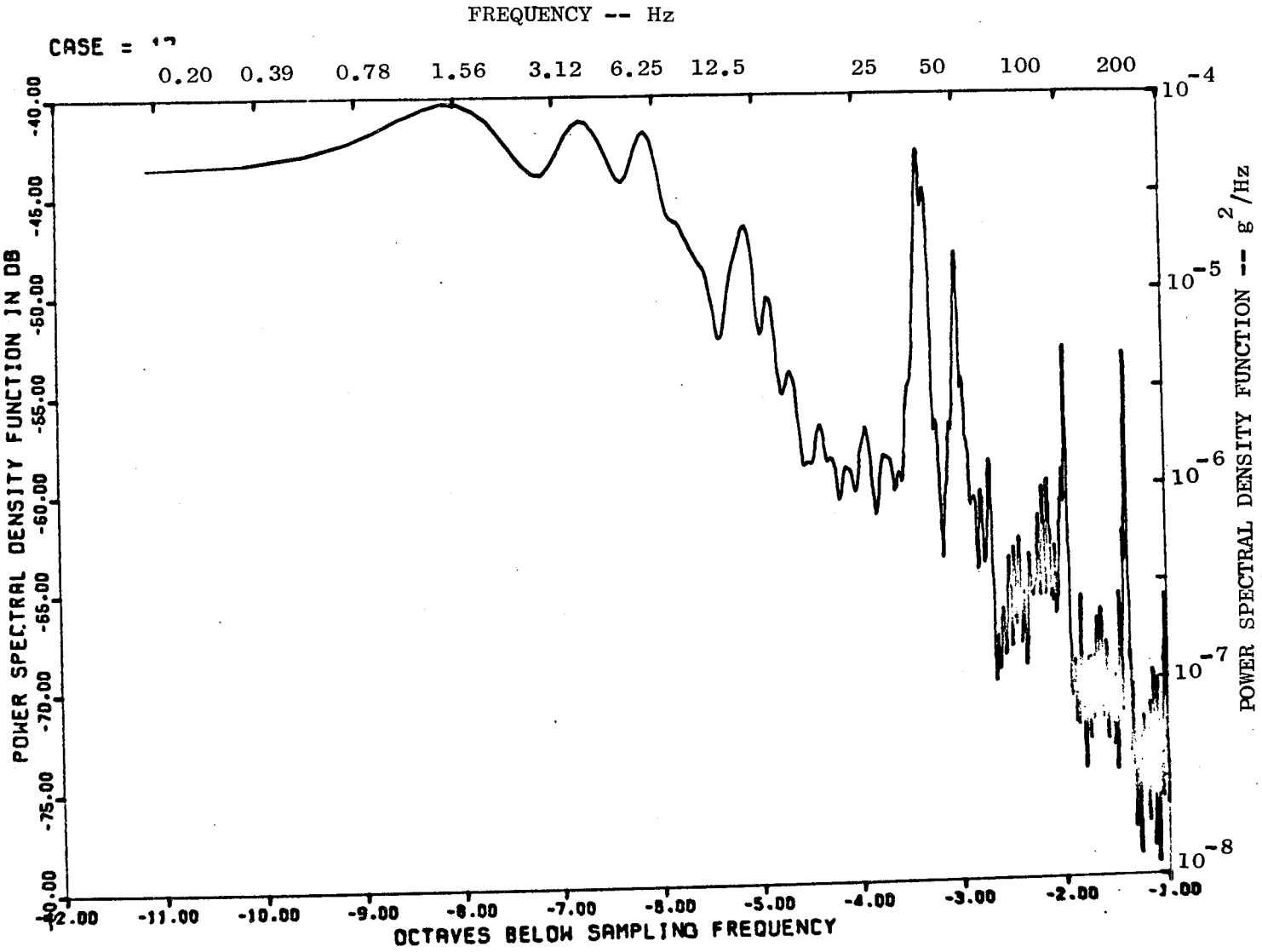

FIGURE 49 POWER SPECTRAL DENSITY FUNCTION - TEST 16

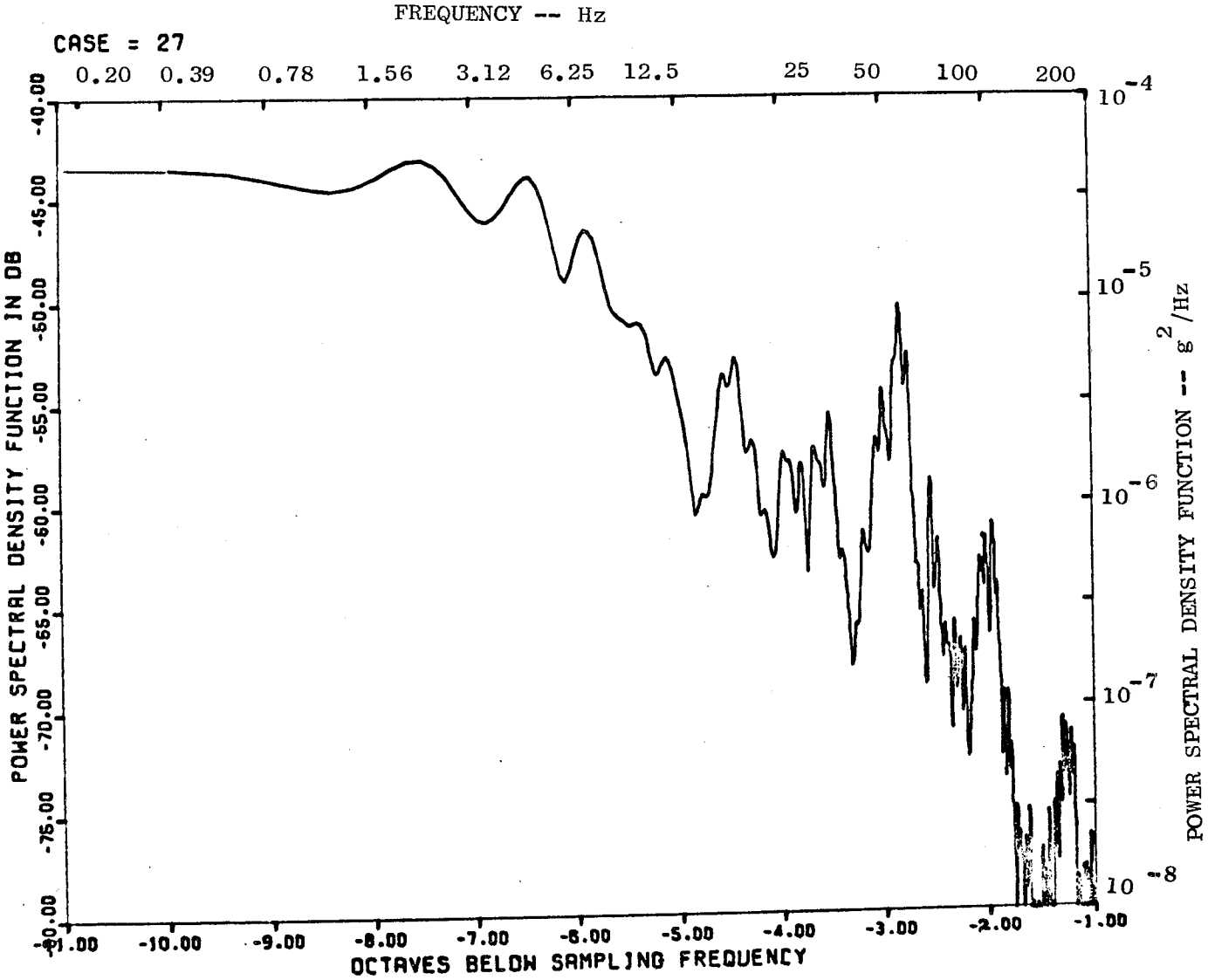

FIGURE 50 POWER SPECTRAL DENSITY FUNCTION - TEST 21

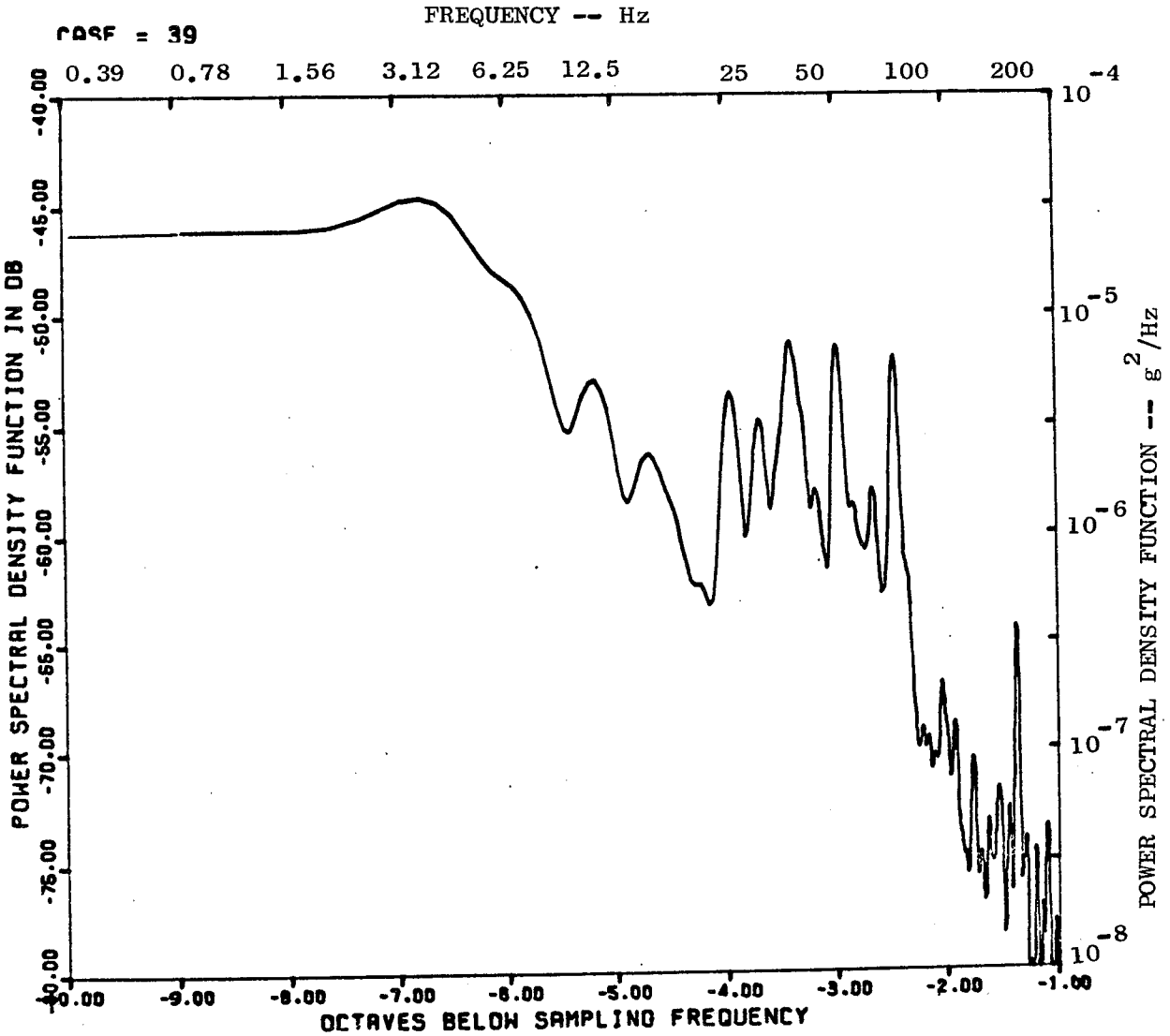

FIGURE 51 POWER SPECTRAL DENSITY FUNCTION - TEST 29
ACTIVE DAMPING - 3/8 CRITICAL

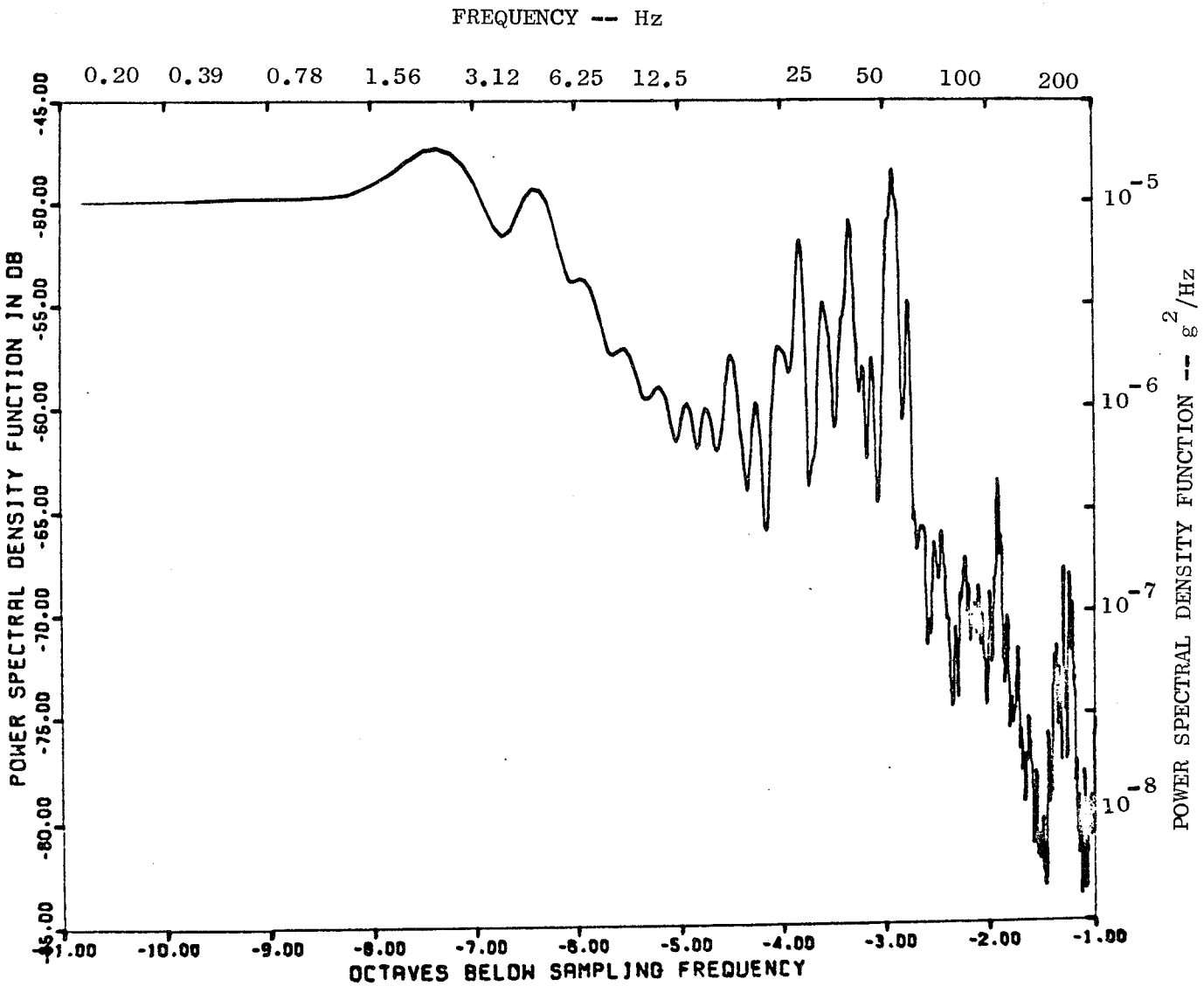

FIGURE 52 POWER SPECTRAL DENSITY FUNCTION - TEST 30
ACTIVE DAMPING - 5/8 CRITICAL

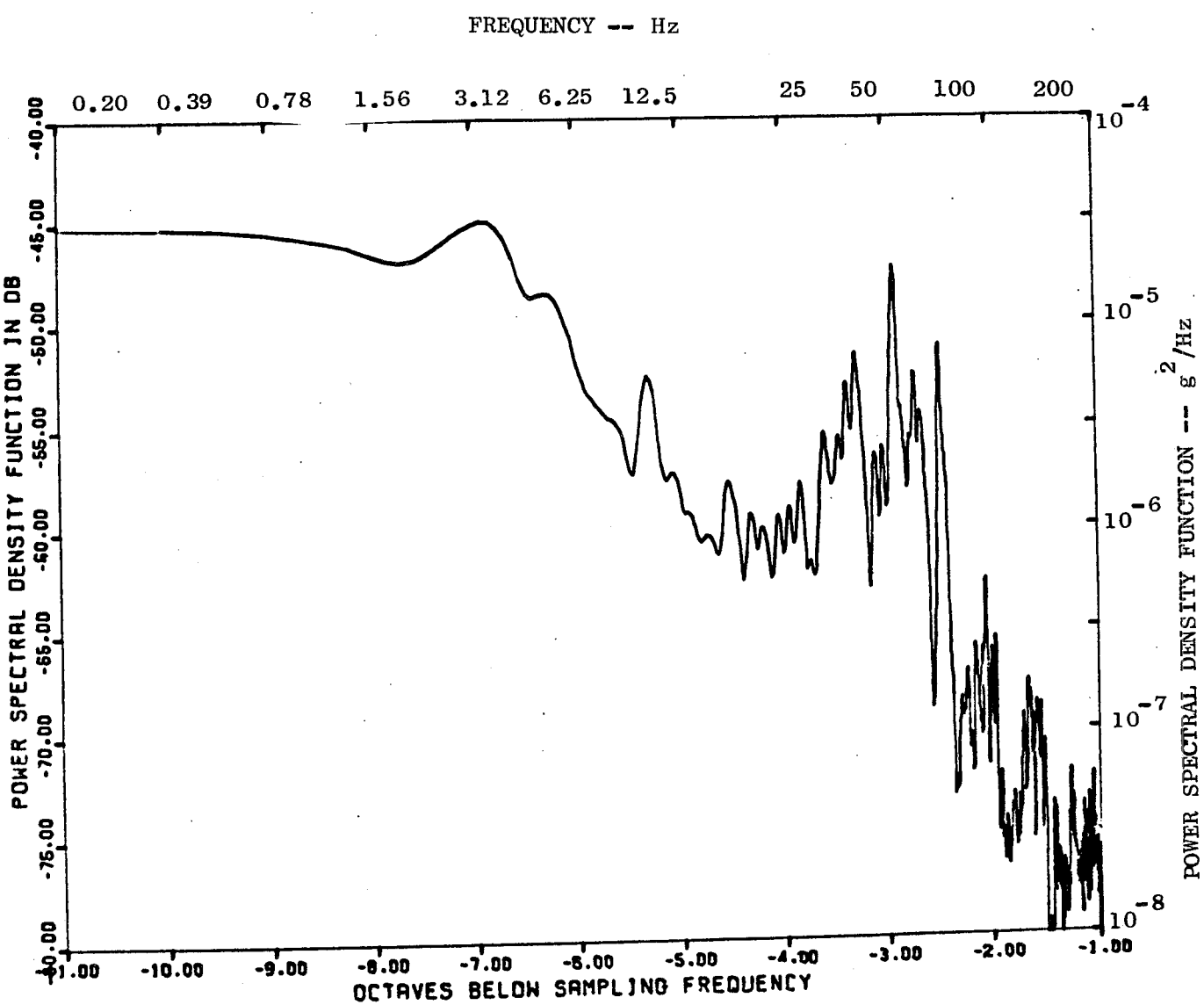

FIGURE 53 POWER SPECTRAL DENSITY FUNCTION - TEST 31
ACTIVE DAMPING - CRITICAL

Figures 51 through 53 show that the active damping controls reduced the lateral accelerations slightly and resulted in vertical and lateral PSDs of about the same magnitude (see Figures 19 through 21). The comparisons cannot be made in great detail since the errors in calibrating the accelerometers are squared in calculating the PSDs.

The characteristics of these tests are summarized in Table 3.

Table 3

LATERAL CHARACTERISTICS OF TESTS OVER STANDARD GUIDEWAY

Experiment	Damping	v(m/s)	I(A)	PSD Peak (g^2/Hz)	Peak Frequency
16	NA	9.5	87-91	1.0×10^{-4}	1.48
21	NA	8.8	85	5.0×10^{-5}	2.19
29	$\frac{3}{8}$ CD	13.5	~ 100	4.0×10^{-5}	3.66
30	$\frac{5}{8}$ CD	10.4	~ 100	2.0×10^{-5}	2.42
31	CD	12.2	~ 100	3.2×10^{-5}	3.40

Lateral Step Tests

In the previous symmetric vertical tests, a large perturbation was used to excite particular vehicle motions in order to study the growth of any instabilities that might develop. Similarly, the objective of the lateral tests was to excite only lateral oscillations that could develop into instabilities in yaw and slip motions. The method used for achieving lateral oscillations was to levitate the vehicle while offset from the center of the guideway and allow the vehicle to return to the center of the guideway through lateral guidance forces. This lateral test was accomplished by forcing the vehicle to the left side

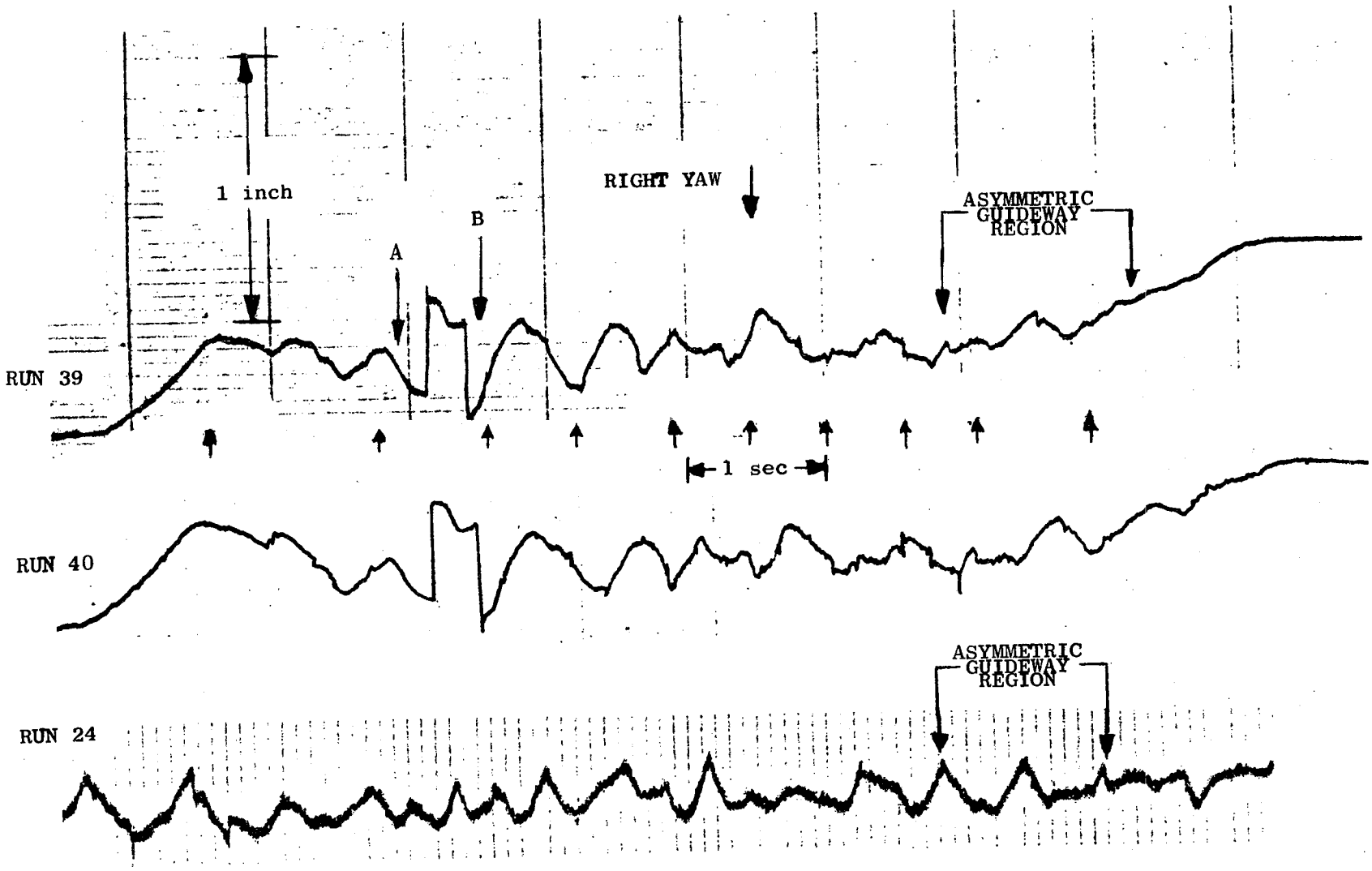

FIGURE 54 YAW MOTION-TESTS 39, 40, 24

of the track for a distance of 14.6 m (48 feet) by using a 3/4-inch wooden offset on the right side. After the vehicle levitated, it passed the offset and yawed to the right with the right front lateral sensor indicating a discontinuous jump, as shown in the yaw motion, after point A of Figure 54. The right rear lateral sensor then passed the offset with a discontinuous jump. A short time later the rear magnets cleared the offset (point B of Figure 54) and resulted in a yaw to the left as the guidance forces centered the rear of the vehicle. This perturbation only excited a yaw motion in the vehicle and thus provided a test for both the growth of instabilities and mode coupling.

Two passive lateral tests were made (Nos. 39 and 40) with the active coils and active controls on-board. This required considerably more current in the lift magnets than used in the earlier passive tests since the weight was increased and a greater suspension height was necessary to provide clearance with the active coils installed. The current was further increased during Test 40 to emphasize the lateral guidance forces. The appropriate parameters in the region of the perturbation for these tests are listed below.

Test	z_o (cm)	v_o (m/sec)	I(A)
39	9.6	7.6	110
40	10.0	6.4	118

The heave, pitch, and roll motions for Test 39 are shown in Figures 55, 56, and 57. The heave motion is similar to that of the earlier passive standard guideway tests. The pitch and roll motions indicate the usual track perturbations, with the exception of an unexplained step during deceleration of the vehicle.

Figure 54 shows the yaw motion for Tests 39 and 40, including the lateral step. The latter part of Test No. 24 over the standard guideway

is shown for comparison (I = 95A, v_o = 8.3 m/sec, z_0 = 9.0 cm). For these tests the shock-mounted side bumpers, normally used to protect the dewars from rubbing the guideway, were pulled back to a point where the dewars could actually contact the sides of the guideway. This contact did not occur, as evidenced by the absence of any lateral acceleration spikes (e.g. Figure 59) indicating a sufficient guidance force. On both lateral tests the yaw motion displays an oscillation after the lateral perturbation.

The frequencies of the yaw oscillations were 1.4 Hz and 1.27 Hz for Test 39 and 40, respectively. The track perturbations, indicated by the arrows in Figure 54, are quite close to this frequency (1.24 Hz and 1.05 Hz, respectively), suggesting that this might be the source of the oscillation. This is further supported by the fact that both tests have almost identical features for yaw. It should be noted that if the lateral track perturbations are not symmetric, the sensors can give an artificial yaw and slip motion, even when the vehicle is not oscillating. The magnitudes of the yaw oscillations in these tests are comparable to those of Test 24. Following the lateral perturbations, the oscillations die out in less than two cycles, indicating that even when the vehicle is driven both with a lateral offset, and periodic perturbations, no instability developed.

Figure 58 shows the slip (lateral) motion for Tests 39 and 40 compared to Test 24. There is no appreciable difference except for a right slip on Tests 39 and 40 in the 12.2 m (40 ft) region where a 7 cm aluminum plate has been added to the height of the left sidewall of the guideway. For the higher current test (Test 40), the right slip is more pronounced. This feature was not distinguishable in the data for the active tests with currents on the order of that for Test 39. Figure 59 shows the heave acceleration and lateral acceleration for Test 39. The data are insufficient to determine any appreciable effects resulting from the lateral offset and the lateral track perturbations. Other tests

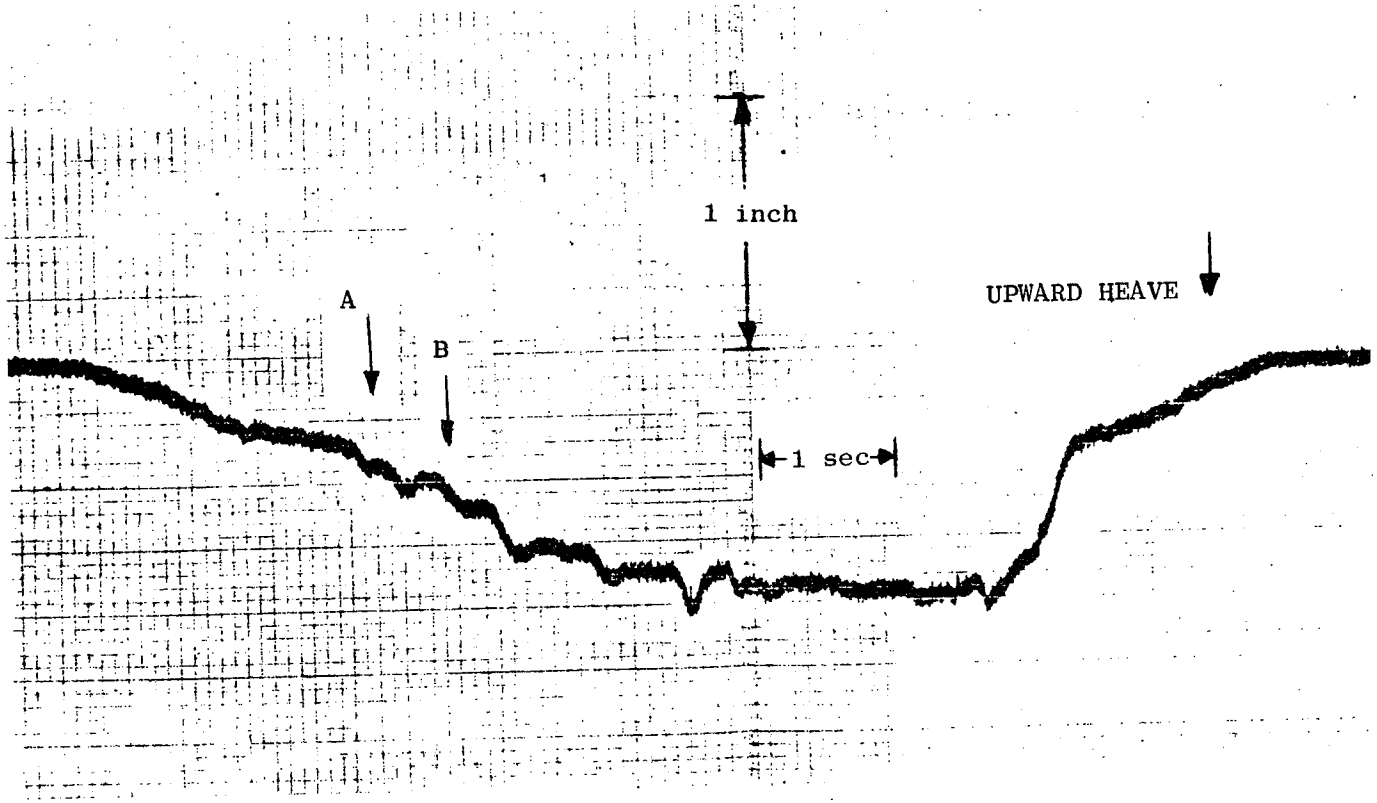

FIGURE 55 HEAVE MOTION-TEST 39

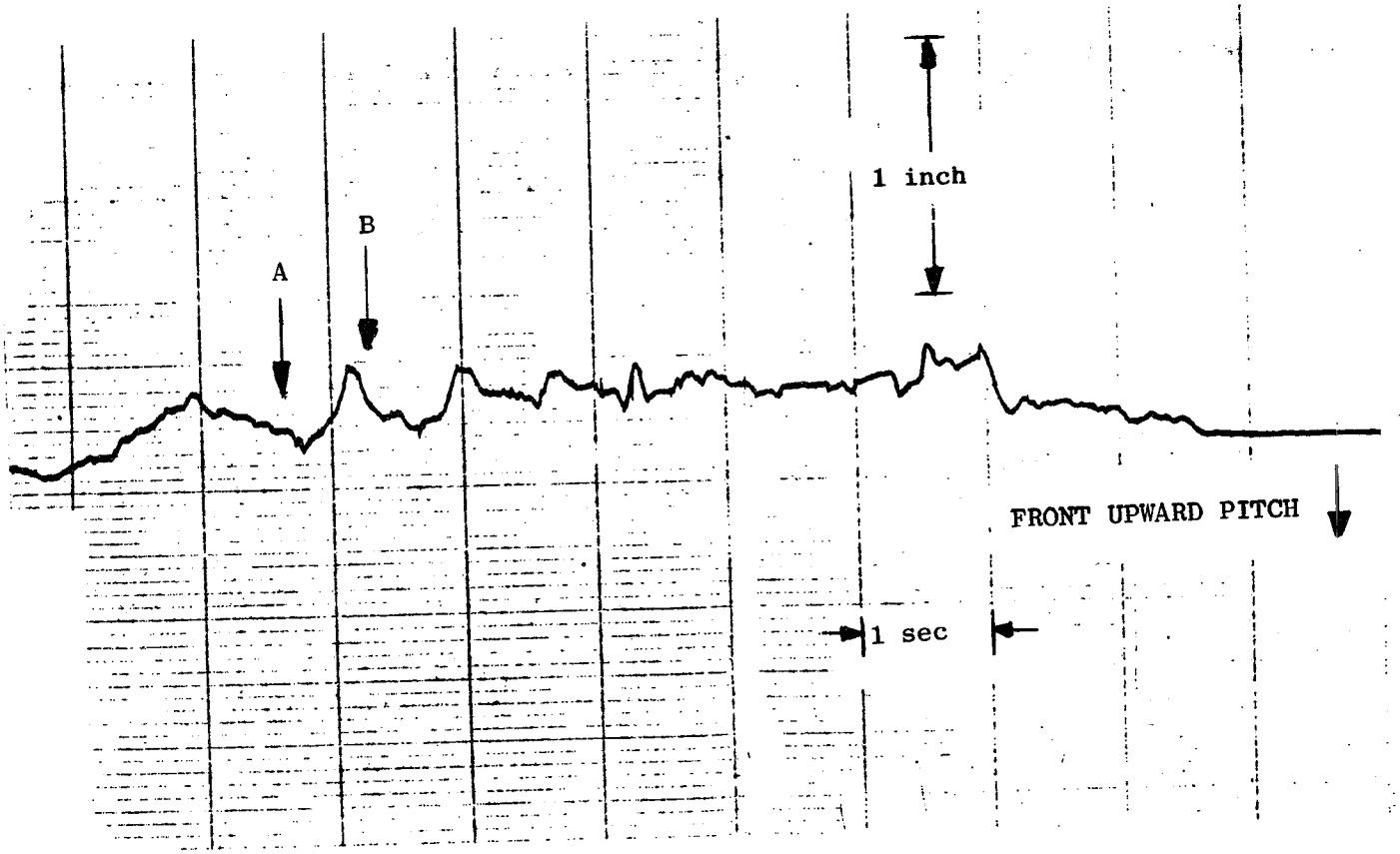

FIGURE 56 PITCH MOTION-TEST 39

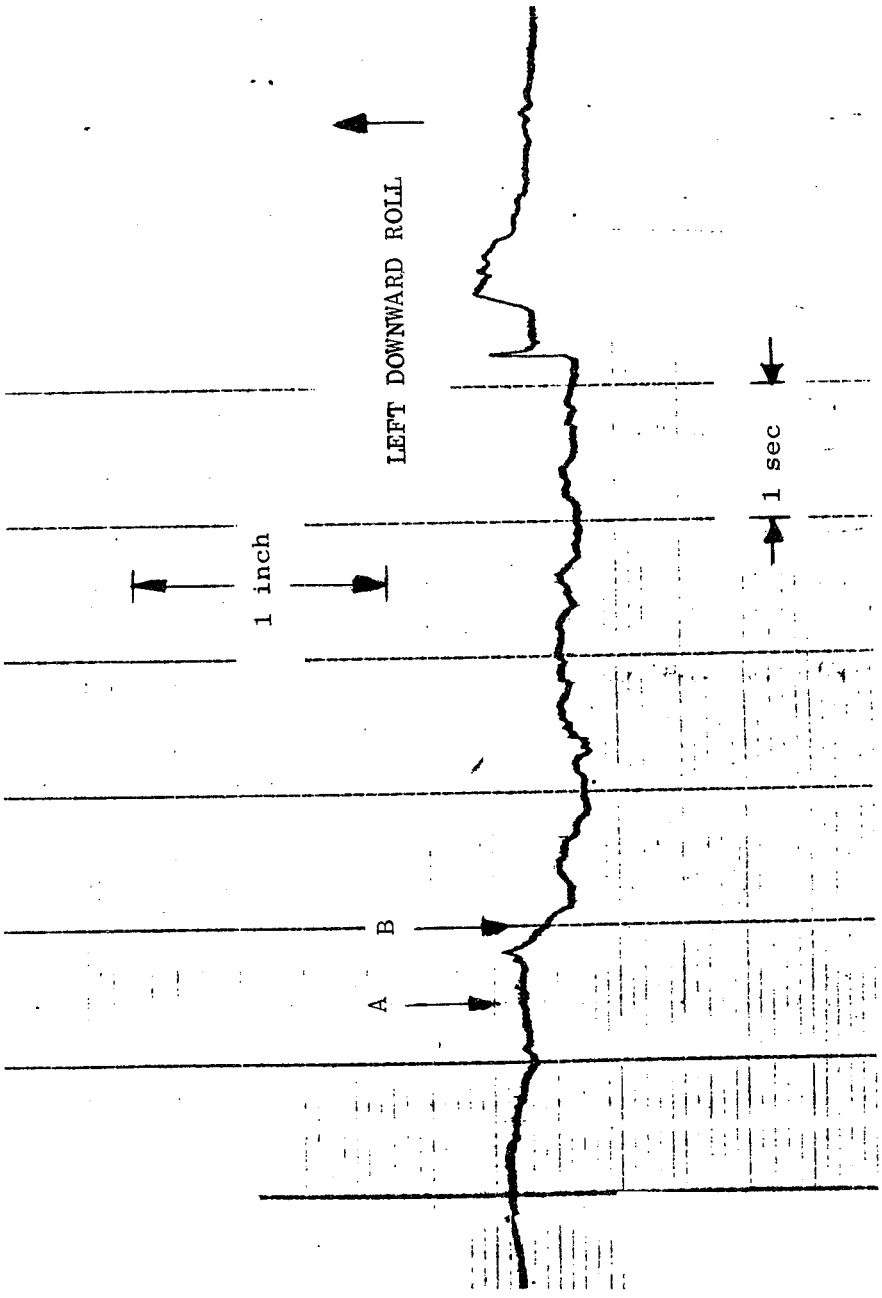

FIGURE 57 ROLL MOTION-TEST 39

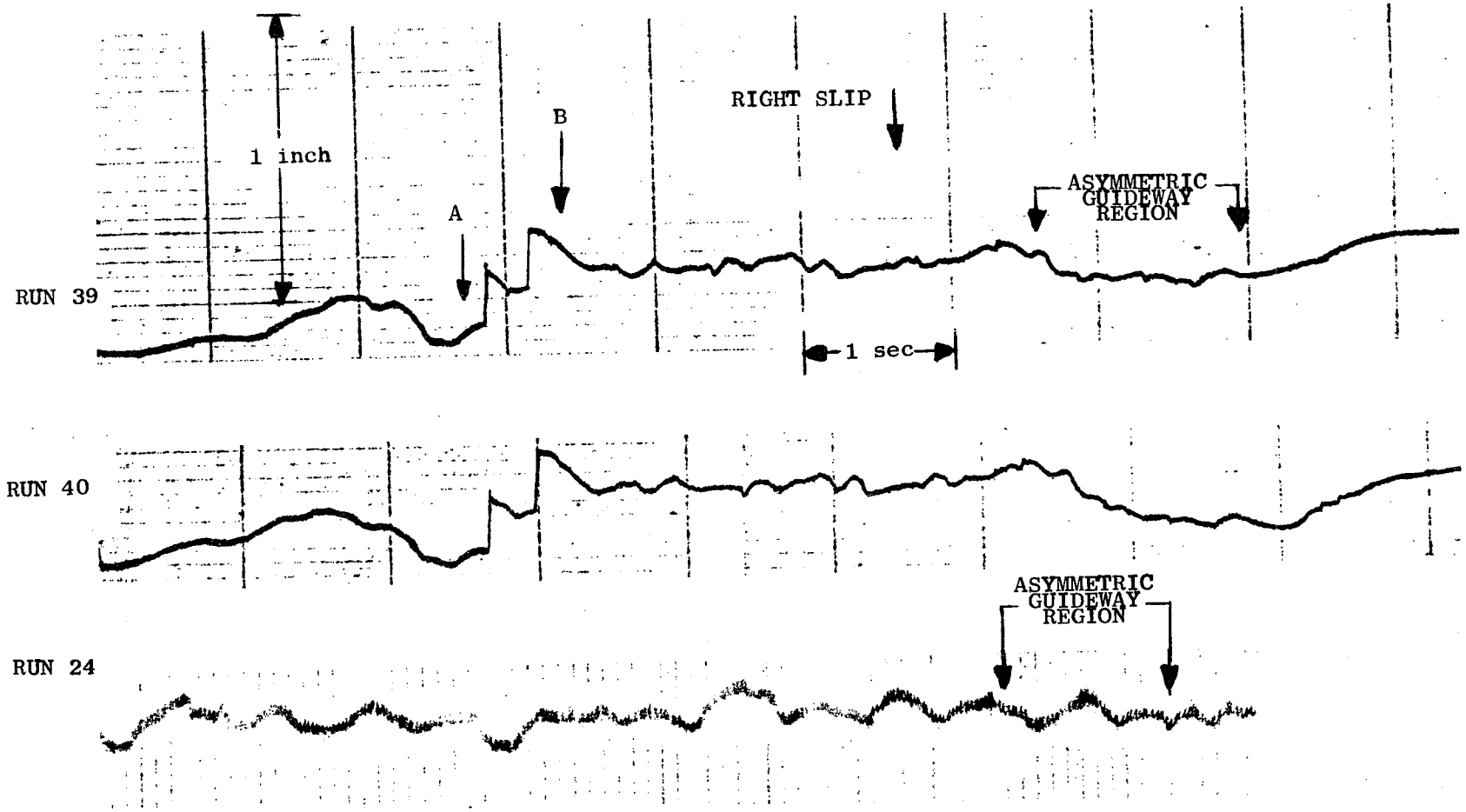

FIGURE 58 SLIP MOTION-TESTS 39, 40, 24

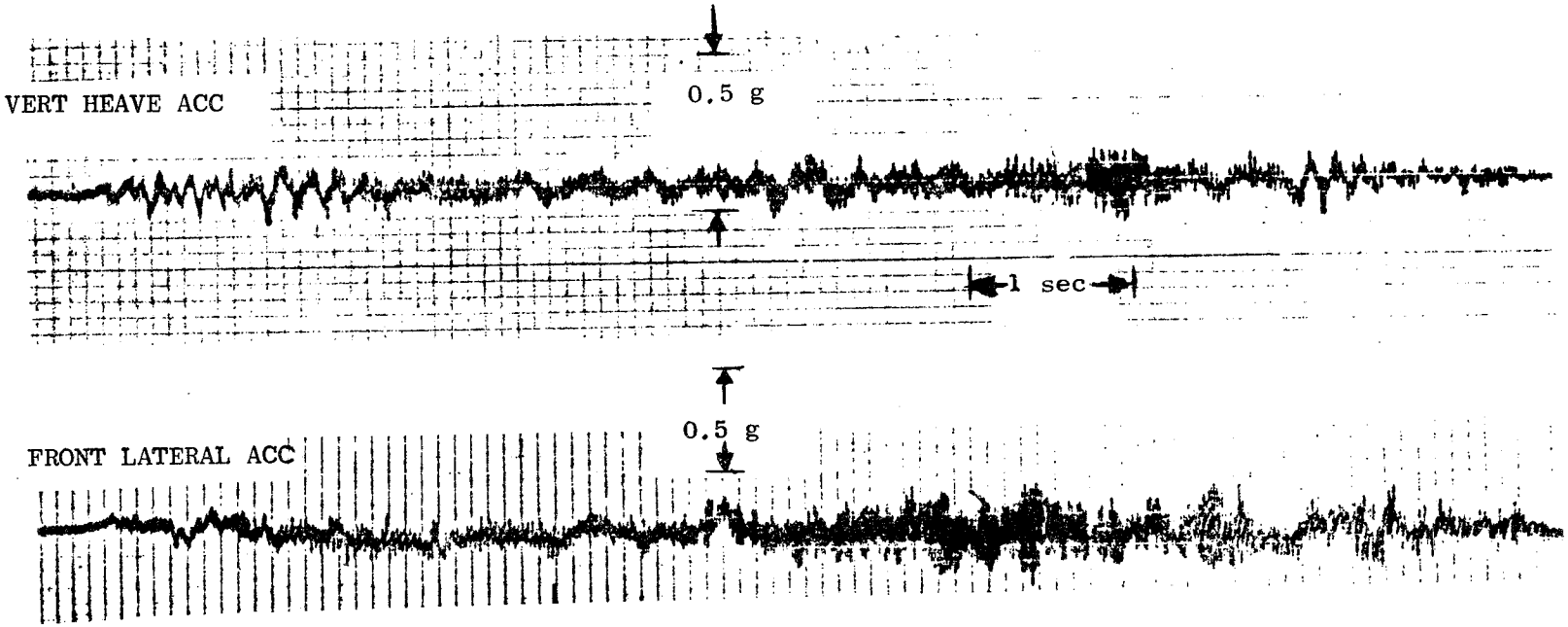

FIGURE 59 HEAVE AND LATERAL ACCELERATION-TEST 39

indicated a direct correspondence between lateral perturbations and lateral accelerations, but this feature was not apparent in the data.

No simulations were performed for these tests because the lateral guidance damping forces have not been modeled and incorporated into the computer program. It would be of great interest to investigate such forces in conjunction with a lateral track survey (obtained from the track profile) and changes in the height of the guidance plates. It may then be possible to simulate the observed right slip motion discussed earlier.

In conclusion, the lateral step perturbation stimulated yaw and slip in the vehicle's motion. No instabilities developed, and only a possible yaw motion from the lateral track perturbations was observed.

Asymmetric Step Tests

The objective in performing these tests was to investigate the stability of the magnetically levitated test vehicle after a perturbation that resulted in an extreme attitude and stimulated multiple modes of oscillation. These were the most severe tests to which the vehicle was subjected. The criterion used in assessing the stability of the vehicle was the damping of oscillations. If oscillations in any mode increased in amplitude as a function of time after the perturbation, the vehicle would be judged to be unstable. Such an instability could arise from either inadequate damping or coupling of the energy from one mode into another.

These tests were performed by levitating the vehicle over two 6.1 m (20 feet) aluminum plates placed end to end on one side of the standard guideway. These were the same plates used in the symmetric step tests and were identical to those used in constructing the guideway. When the vehicle dropped off the step, motion was observed in five of the six possible

degrees of freedom. The last degree of freedom--longitudinal motion--was also noted to be affected by the perturbation (as monitored by the longitudinal accelerometer), but these data were not sufficient for analysis.

A total of three passive (Nos. 26, 27, and 28) and two active (Nos. 37 and 38) asymmetric step tests were conducted. The two active tests were performed with $1/\sqrt{2}$ critical damping settings on the active damping controls.

At no time, in any of these five runs, did a growth of oscillation amplitude occur in any of the five degrees of freedom measured. No oscillation in any test, either active or passive, with an amplitude larger than the track perturbations, persisted for more than $1\text{-}\frac{1}{2}$ cycles.

The high degree of stability of the vehicle and the comparative effects of active and passive damping on this stability can be seen in Figures 60 through 65. Figure 60 compares the heave motion of Tests 27 (passive) and 37 (active). After the rear magnets dropped off the perturbation at point D, the vehicle's heave motion was damped in 1-1/2 cycles using passive damping and in less than one cycle using active damping. It was in this series of actively damped tests that the defect in the right rear active damping control was discovered.

The pitch motions for these same tests are shown in Figure 61. As in earlier tests over the symmetric step, the amplitudes of the pitch oscillations are comparable in the actively and passively damped tests. No instability was noted in either test. The observed heave and pitch frequencies and damping time constants are comparable to those observed in the symmetric step tests.

Roll motions are shown in Figure 62 for these experiments. A complication occurred in the passive tests that had an effect on the

roll motion and perhaps affected the details of some of the other motions. The roll of the vehicle permitted the right rear lateral position sensor to come out of the guideway. Being spring-loaded, the sensor extended above the vertical plate on the right side of the guideway where it held that side artificially high for a distance of about 10 m before the vehicle dropped back into the guideway. This unintentional perturbation might have contributed to the large roll oscillation in the passive tests. This difficulty did not arise in the active Tests 37 and 38. The frequency of roll oscillation and the damping time for this roll mode were determined from these hindered data.

Figure 63 shows the slip motion for the same tests. A brief slip oscillation is noted in the passive test with a frequency of 2.3 Hz. It is interesting that the same oscillation did not occur in the actively controlled damping test although active control was provided only in the vertical direction. It was noted in an earlier section that bumpers were provided in the lateral direction to avoid the possibility of damage to the dewars. The oscillations shown in this figure are well within the limits placed on the lateral motions by these bumpers.

Yaw motions occurring in these same two tests are shown in Figure 64 and indicate very similar motions in both the actively and passively damped tests. Heave accelerations are shown in Figure 65 and are typical of the results found in the symmetric step tests, with the actively controlled damping tests being quieter. The parameters obtained from these tests are summarized in Table 4. These frequencies and time constants are obtained over at most, two cycles and should only be considered as estimates.

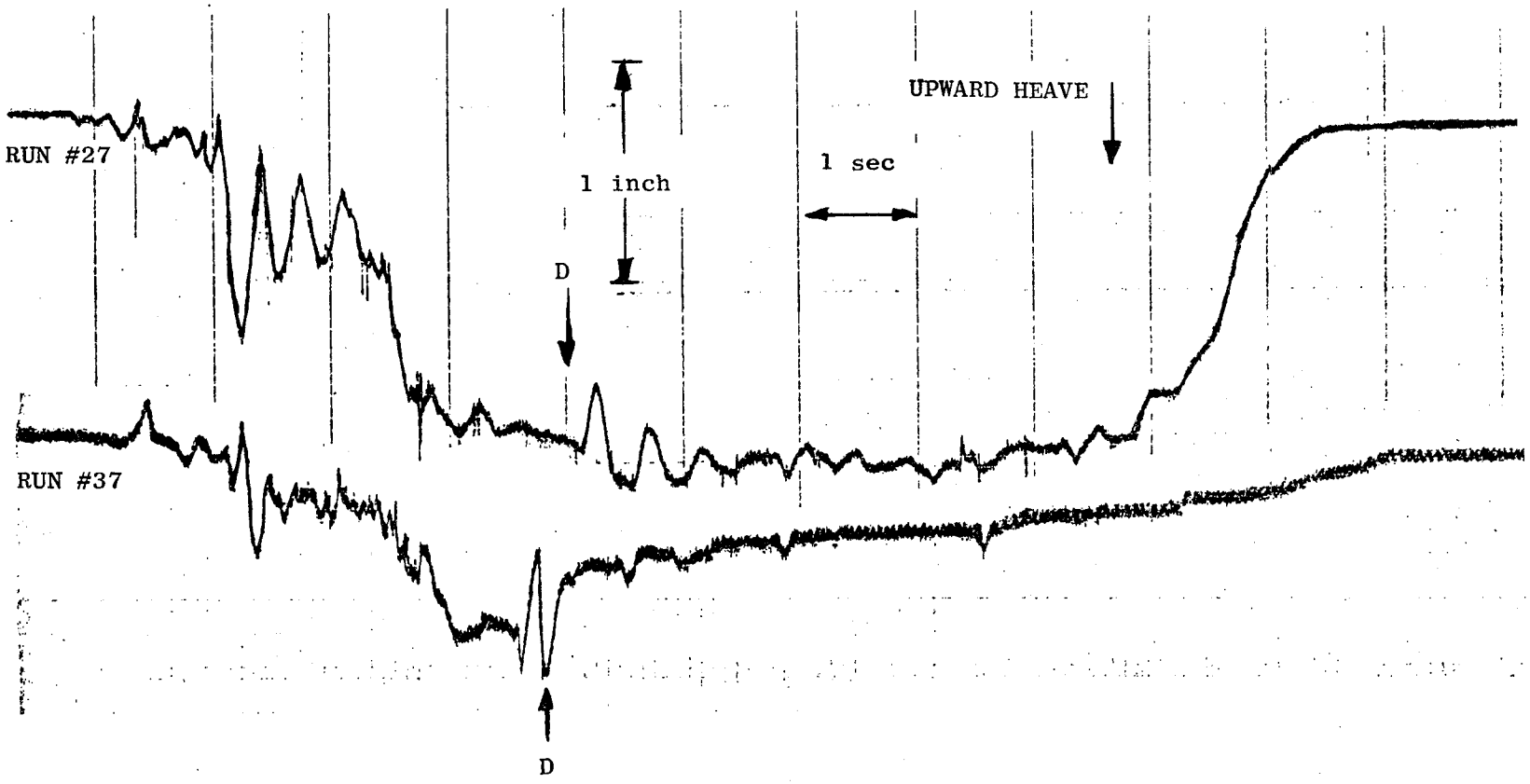

FIGURE 60 HEAVE MOTION-TEST 27, 37

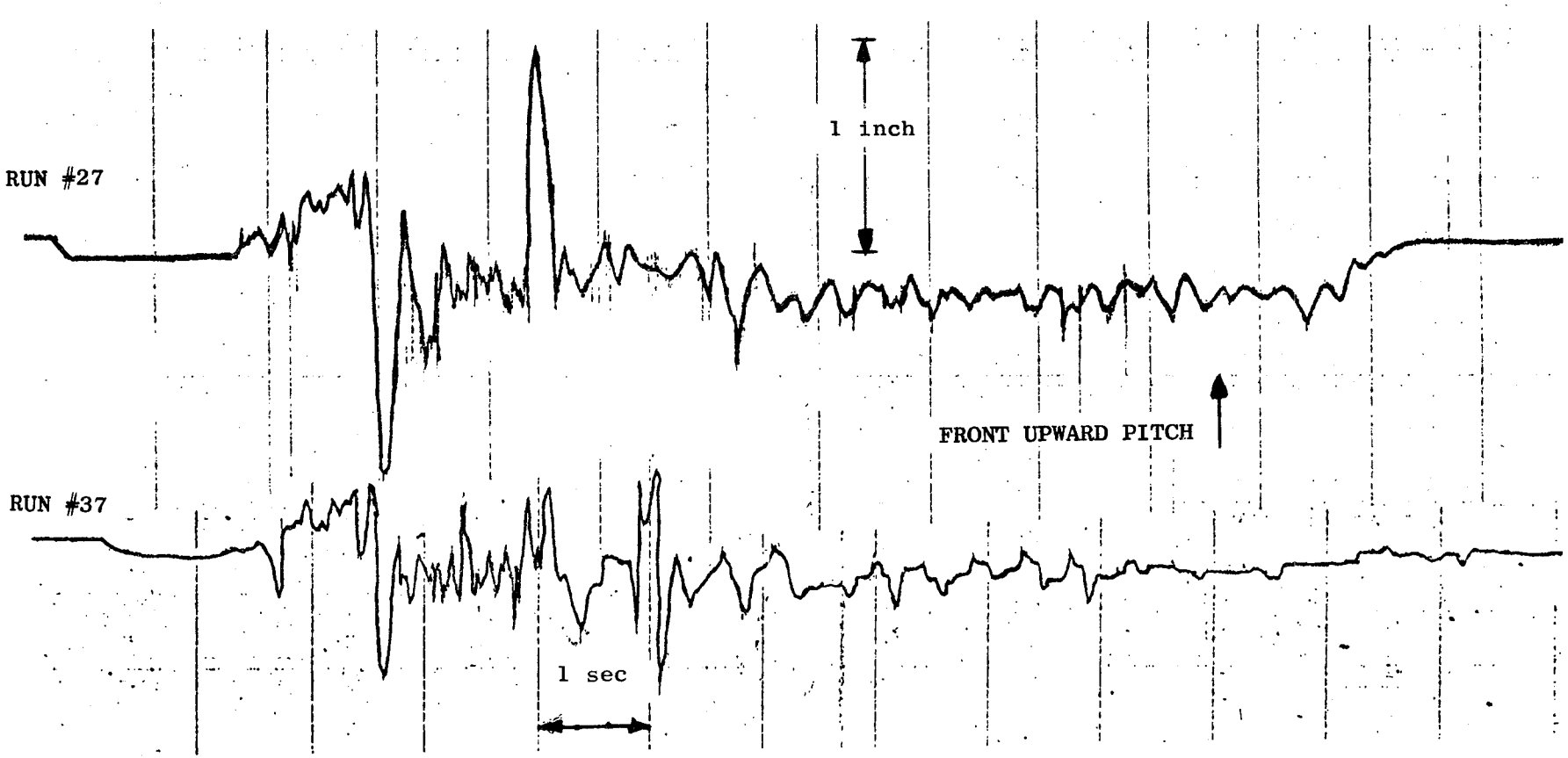

FIGURE 61 PITCH MOTION-TEST 27, 37

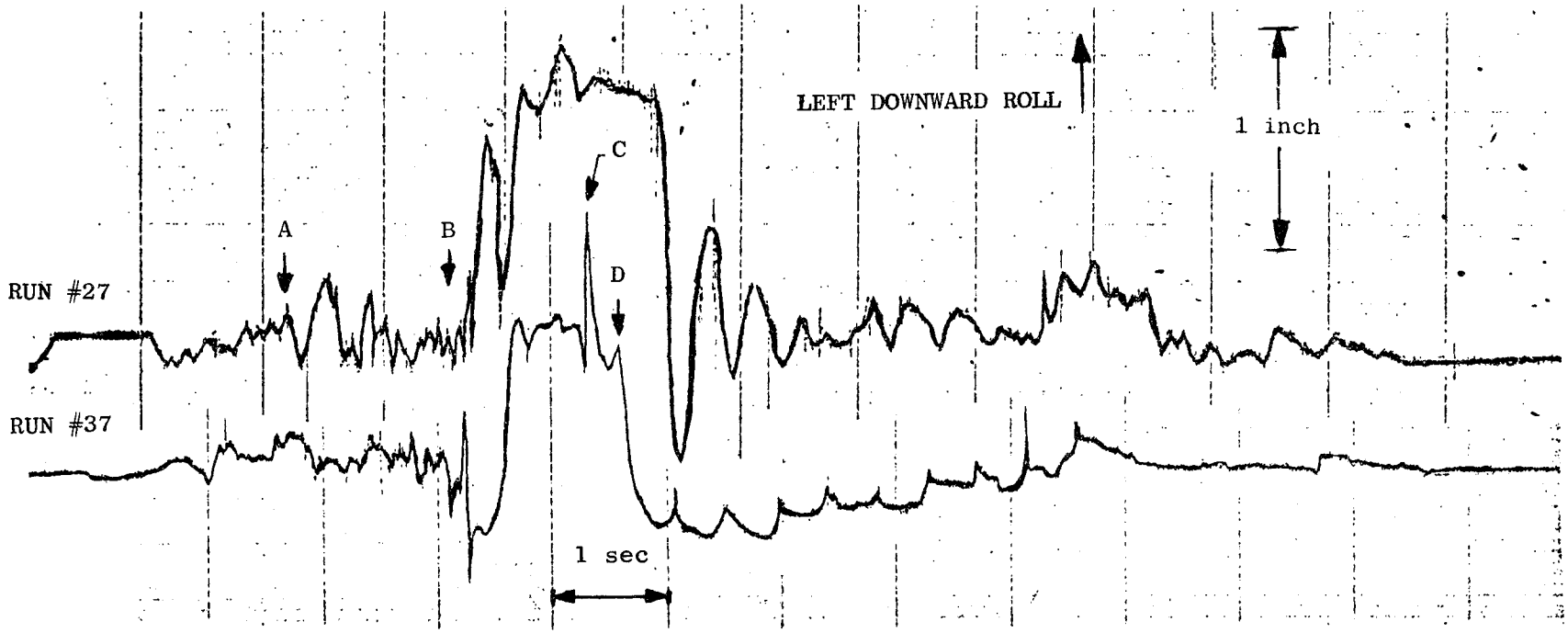

FIGURE 62 ROLL MOTION-TEST 27, 37

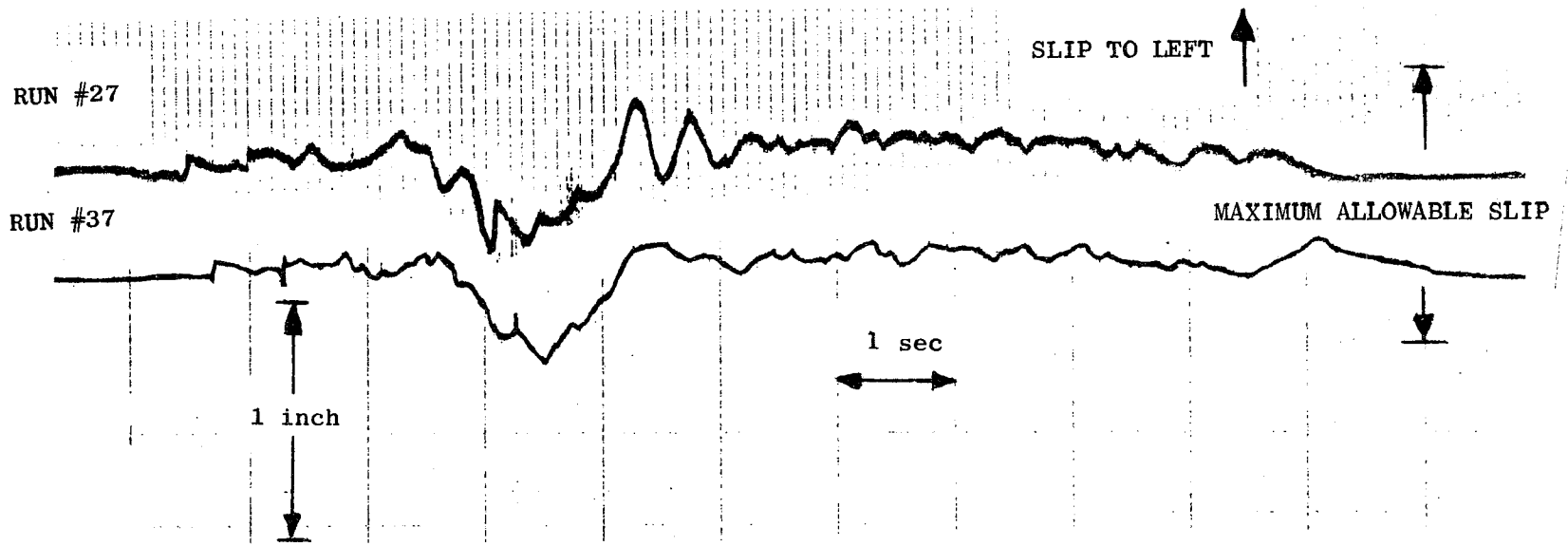

FIGURE 63 SLIP MOTION-TEST 27, 37

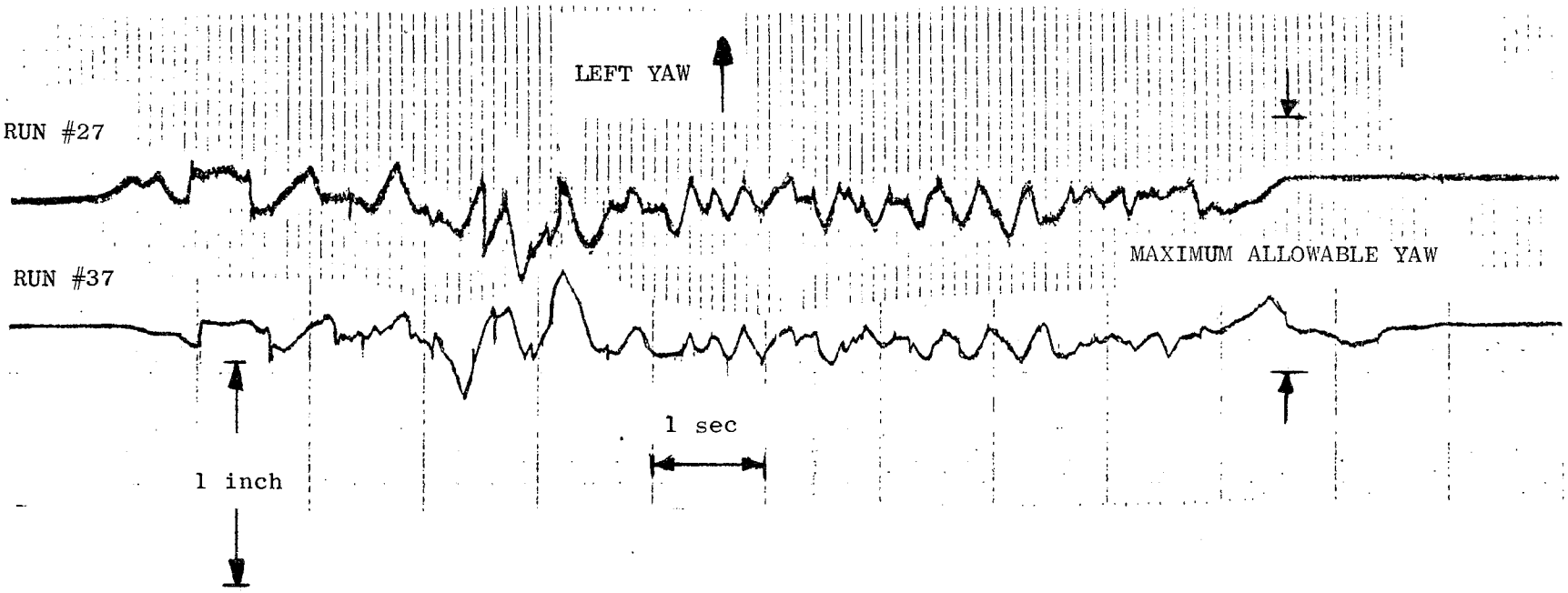

FIGURE 64 YAW MOTION-TEST 27,37

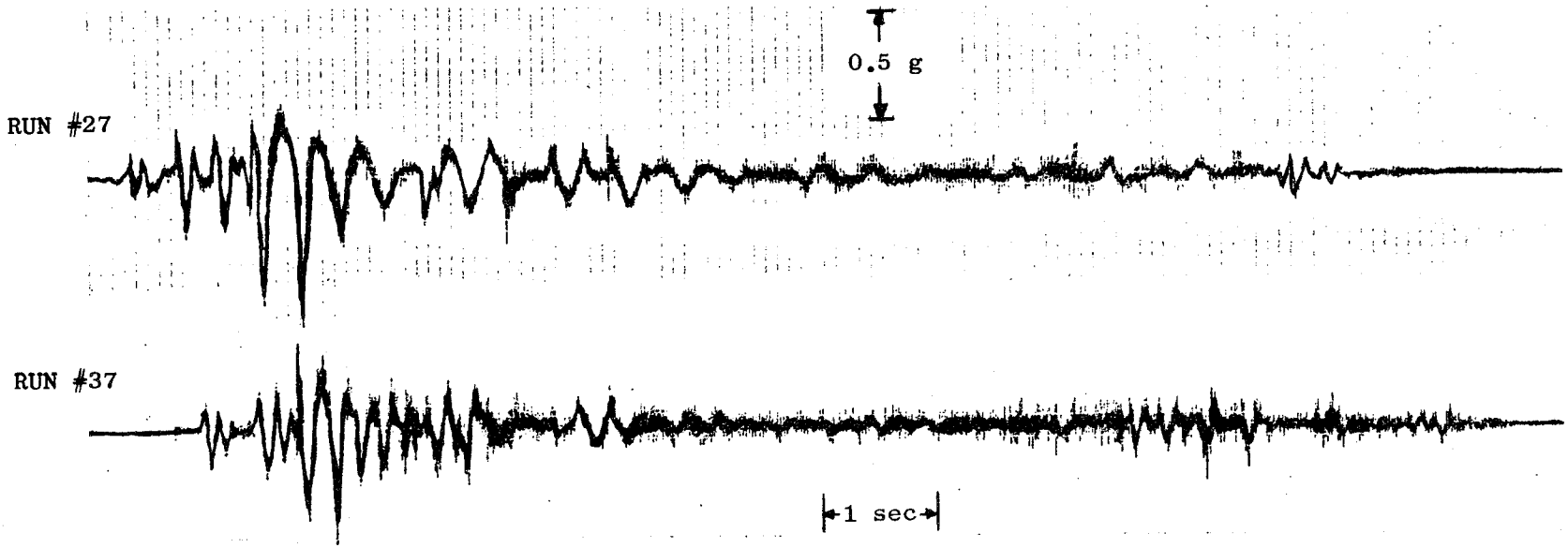

FIGURE 65 HEAVE ACCELERATION-TEST 27, 37

Table 4

PARAMETERS ASSOCIATED WITH ASYMMETRIC STEP TESTS

Run #	Active Damp. Set	z_o †* (cm)	v_o * (m/sec)	I* (A)	f_{pitch} (Hz)	τ_{pitch} (sec)	f_{heave} (Hz)	τ_{heave} (sec)	f_{roll} (Hz)	τ_{roll} (sec)
26	None-passive	9.2	11.7	95	3.5(?)	NA	2.2	0.73	2.3	0.32
27	None-passive	9.8	13.5	96	3.2(?)	NA	2.1	0.55	2.4	0.39
28	None-passive	9.4	9.5	96	3.3(?)	NA	2.1	< 0.5	2.1	< 0.47
37	70.7% C.D.	9.7	14.3	104	2.10††	No oscillation	NA	< 0.38	2.3 ††	NA
38	70.7% C.D.	9.0	7.1	104	1.10††	No oscillation	NA	< 0.29	1.2 ††	NA

† $z_o = \Delta z_o +$ {5.9 cm for Runs 26-28 / 8.2 cm for Runs 37,38} where Δz_o is the actual levitation height of the vehicle.

*Measured in region immediately after point D of Figure 60.

††Frequency caused by track perturbations at 20 foot intervals; $f = 20 \text{ ft.}/v_o$.

Simulation of Asymmetric Step Tests

The asymmetric step tests were performed by placing two additional aluminum plates on one side of the guideway. To avoid damage to the vertical sensors, plywood of the same thickness as the aluminum was placed on both sides of the guideway preceding the additional aluminum plates. This asymmetry in the height of the surfaces on which the vertical sensors rolled leads to apparent motions in the data that do not occur in the vehicle. When the left side vertical sensors drop off the plywood, the sensors indicate an increase in suspension height on that side and give a false indication of heave and roll.

The plywood sheets were not simulated in passive Test 26, leading to a simulation of the left side of the vehicle being higher than the right by 3/4 inches. This caused an indication of a roll to the right when in fact the vehicle was level, as shown in Figure 66. This figure also shows that the vehicle caught on the side of the guideway as discussed earlier and did not drop back to the level position immediately upon traversing the downward step on the right side of the guideway. A simulation of this event was not attempted; the computed curve assumes the correct experimental behavior. The basic characteristics of the curves are similar, except the roll damping in the experiments is greater than that calculated. The simulation, in this case, did not include the track perturbations so the simulated decay of the roll motion could be seen more clearly. The calculated frequency of roll oscillation, about 3.2-3.3 Hz, is considerably higher than the observed frequency of about 2.5 Hz. The slight differences in the scales should be noted.

The heave motion and vertical accelerations of this test and the simulations of them are in reasonable accord as shown in Figures 67 and 68.

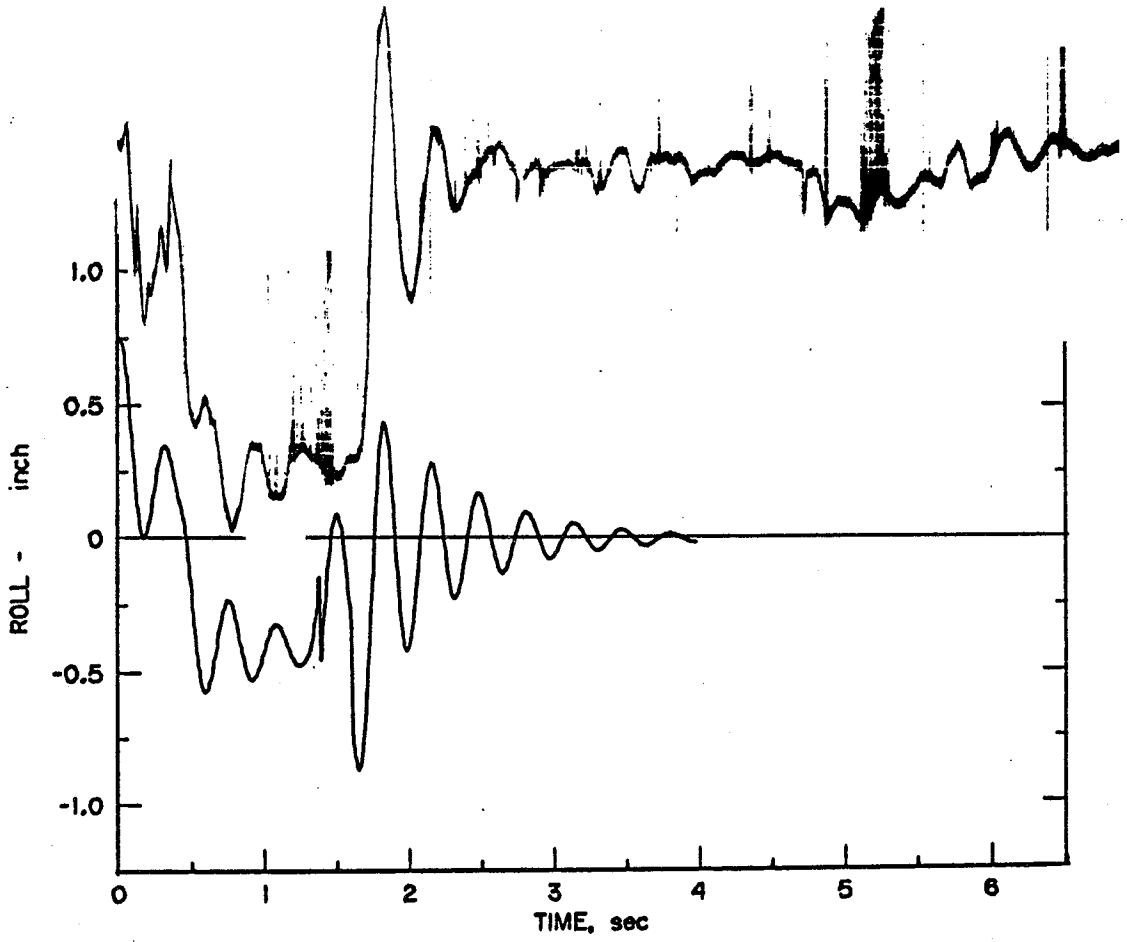

EXP. RUN 26. ROLL, PASSIVE DAMP., V0=8.08 M/SEC, X0=48-AM FT.

FIGURE 66 ROLL MOTION, TEST 26

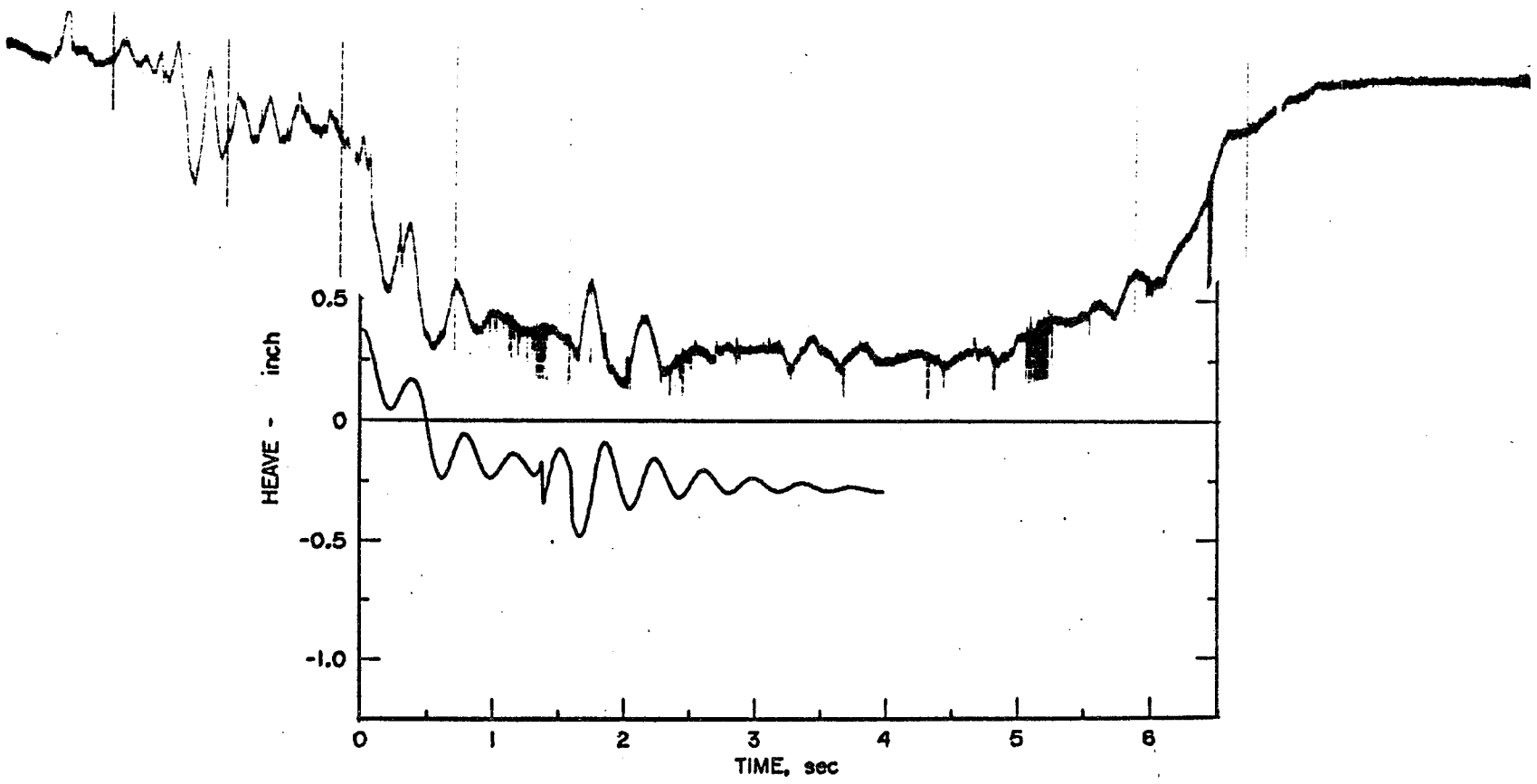

FIGURE 67 HEAVE MOTION, TEST 26

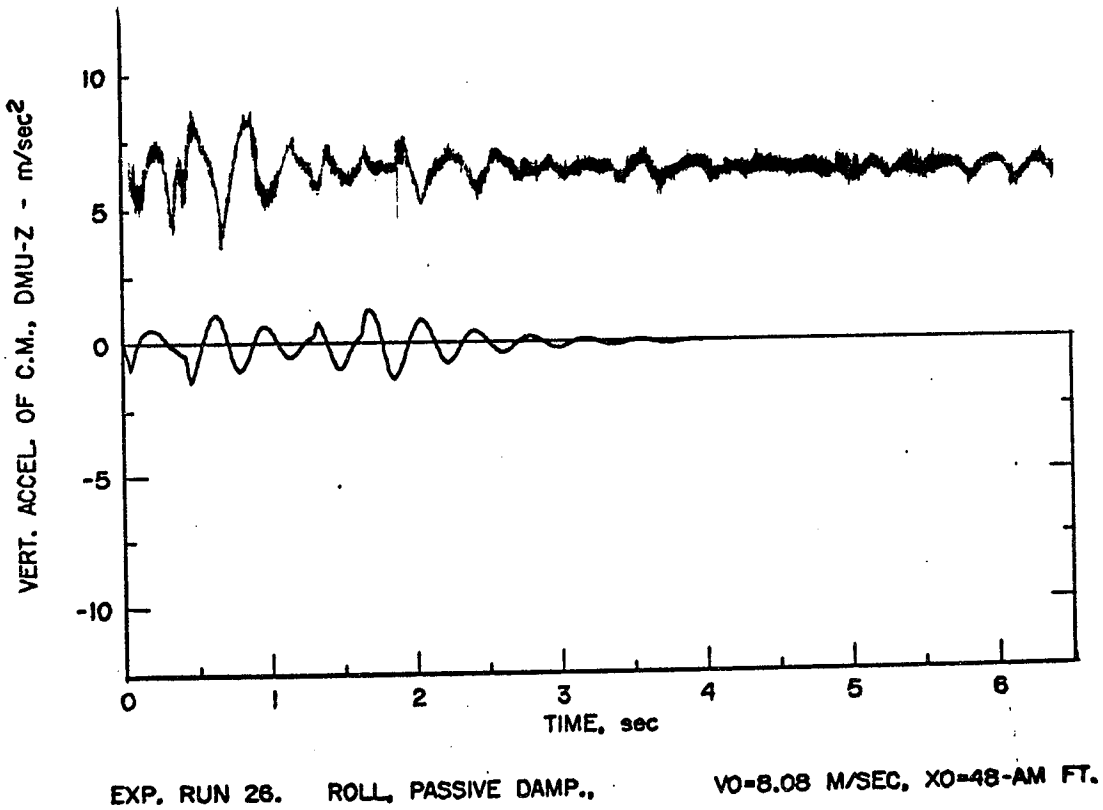

FIGURE 68 VERTICAL ACCELERATION, TEST 26

The same experiment was performed using active damping in two tests as discussed in the preceding section. Test 37 with 70.7% of critical damping was simulated on the computer. Sensor P6, the left rear vertical sensor was found to be defective so the pitch and roll motions were determined from the right side and front sensors respectively. This procedure contributes no error in pitch and roll, but introduces a slight error in reconstructing the heave motion using only one rear sensor. The heave motion was taken to be the sum of the front vertical sensor outputs plus twice the right rear vertical sensor output. To permit direct comparison, this same function was simulated.

The roll motion and its simulation are shown in Figure 69. As expected, the simulated roll falls toward zero faster than the experimental roll because the sensor caught on the guideway during the test. Other than this discrepancy, there is little difference in the two curves.

The measured and simulated pitch and heave motions are shown in Figures 70 and 71 respectively. It should be noted that the scales for the simulated and experimental curves differ slightly. The pitch motion appears to have more structure than that simulated in the early portions of the run. This suggests that one of the sensors might have bound momentarily before releasing and following the guideway.

The analogous curves for the heave motion are shown in Figure 71. The vertical motion of the vehicle following the asymmetric step is overemphasized and the heave position incorrectly increases rather than decreasing as observed. These discrepancies seem to arise from an error in the digitized accelerations, probably a dc offset. The exact source and nature of this problem has not been identified.

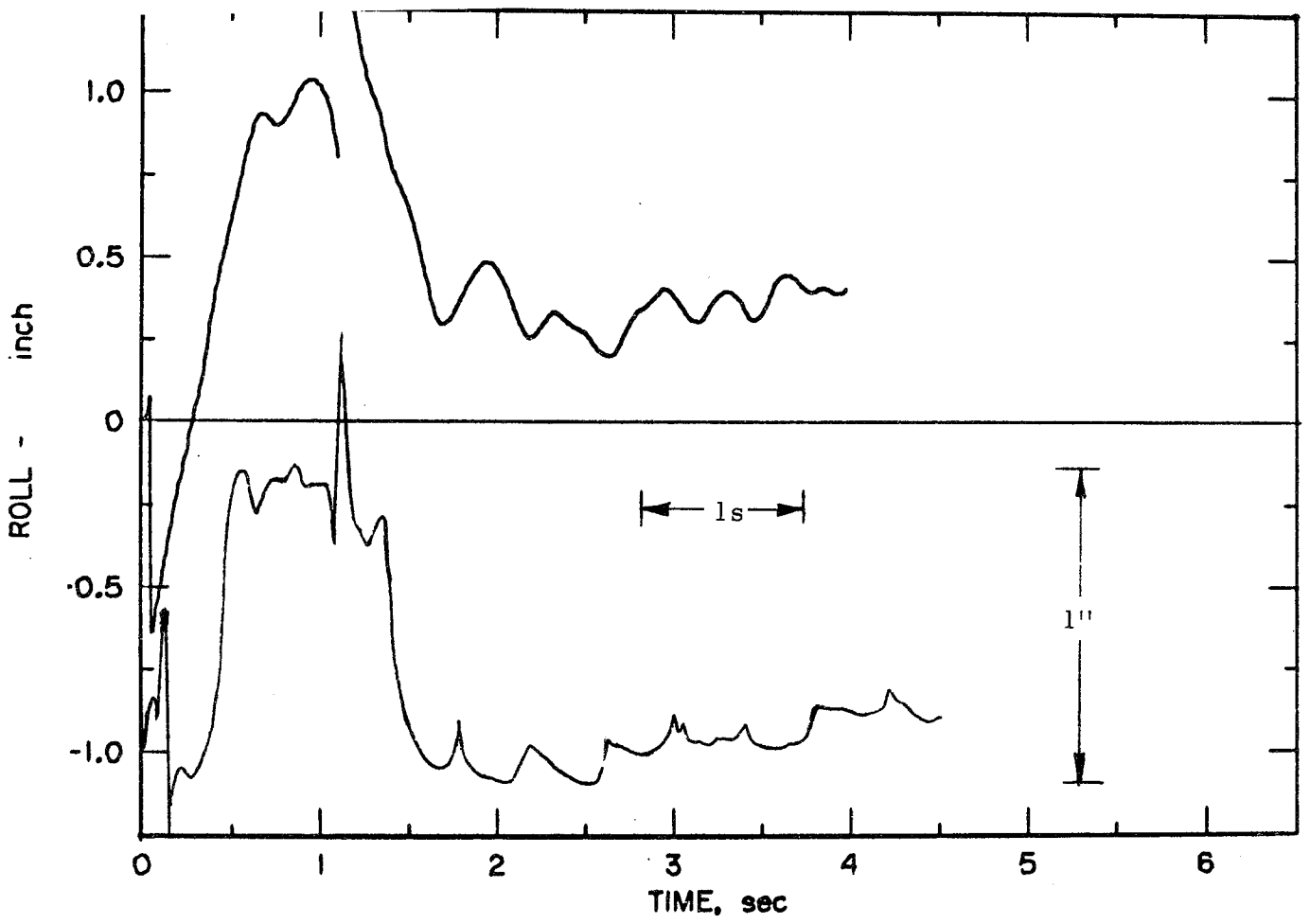

EXP. RUN 37. ROLL, ACTIVE DAMP., TRACK, V0=11.09, X0=48-AM FT.

FIGURE 69 ROLL MOTION, TEST 37

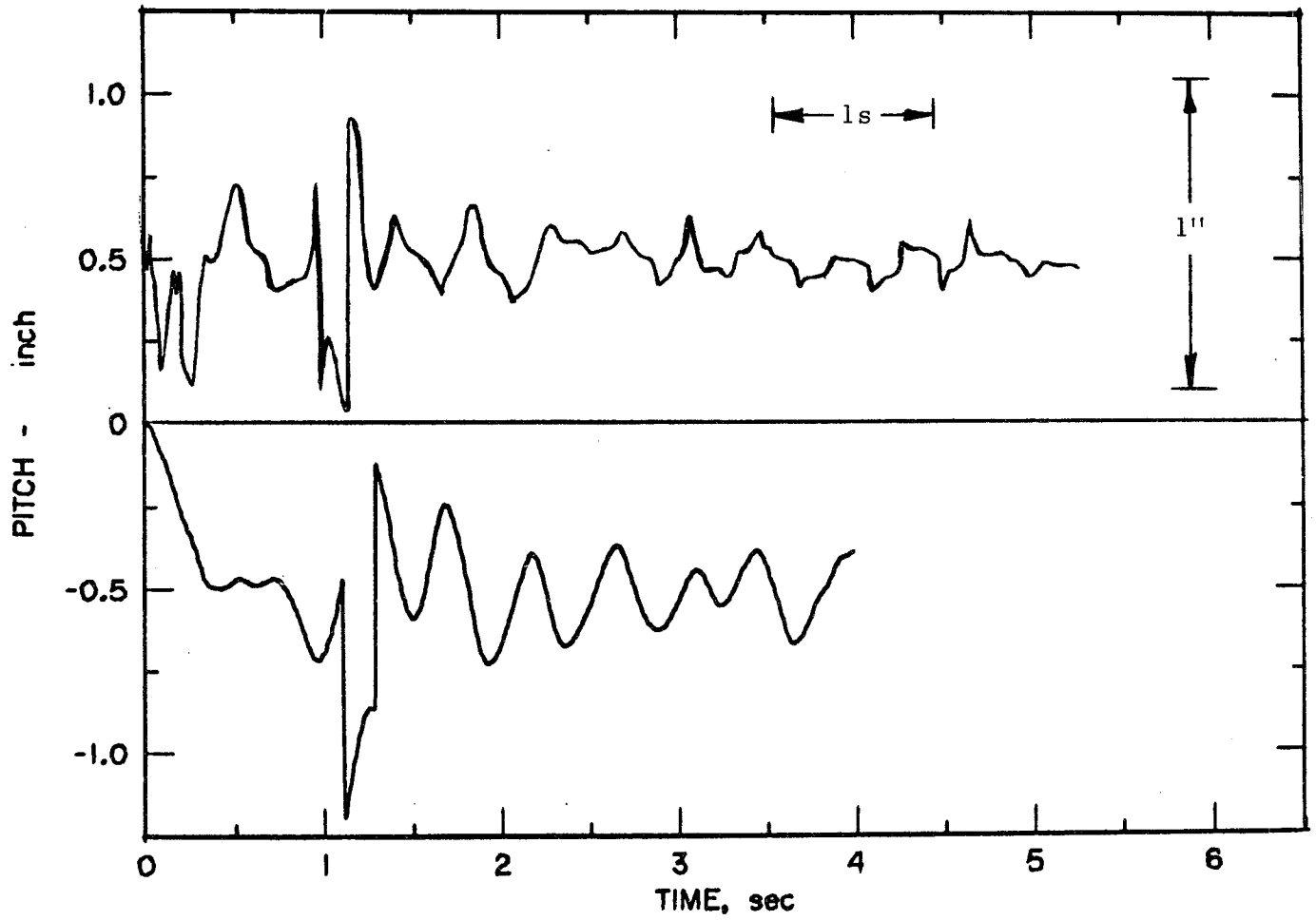

FIGURE 70 PITCH MOTION , TEST 37

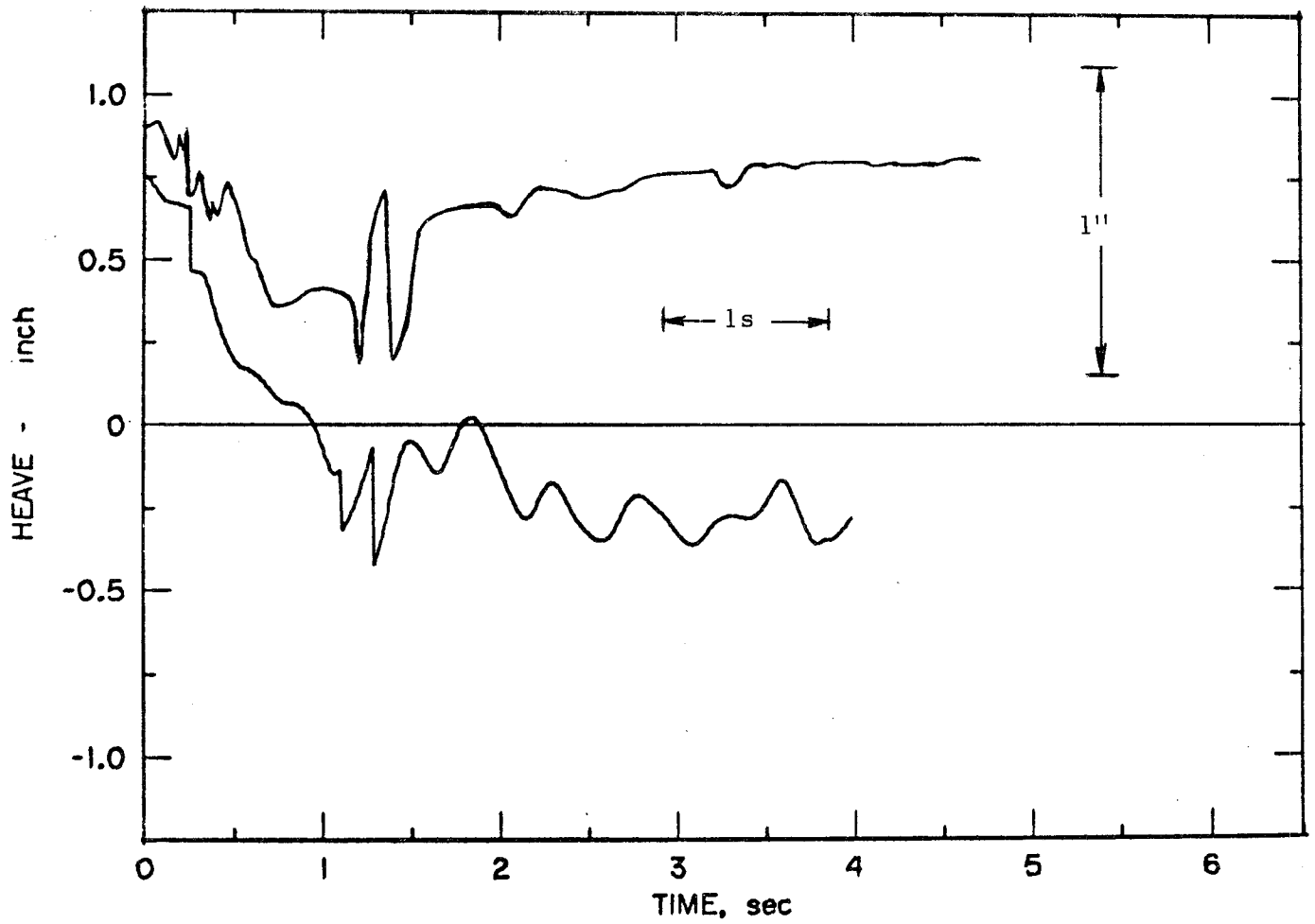

FIGURE 71 HEAVE MOTION, TEST 37

Mode Coupling Investigation

One of the concerns in establishing the stability of a MAGLEV vehicle is the coupling of energy from one mode of oscillation to another. The energy transferred into a particular mode, together with energy already residing in that mode, may be too great for the available damping -- leading to an unstable oscillation.

Many forms of mode coupling exist in this type of suspension and guidance system. Experimentally, none of these resulted in unstable oscillations. Some of the more prominent forms of coupling, neglecting aerodynamic effects, are discussed in the following paragraphs.

It is well established that in both the vertical and lateral directions the repulsive force and the associated drag force increases as the distance between the magnet and the guideway decreases. This is true whether the magnets are powered by a constant current source or are short circuited to operate in the persistent current mode. In the latter case, however, the force-distance curve varies more rapidly since the magnet current increases as the separation distance decreases.

Consider first the simple case of yaw induced by roll. If the vehicle is centered in the guideway but rolls, an increased drag force is experienced by the magnets on the side with the smaller clearance, leading to unbalanced drag forces on each side of the vehicle and a yaw motion. A slip motion similarly results in an increased drag force caused by the increased guidance interaction on one side and a decreased interaction on the other side of the vehicle. Thus, slip and yaw and roll and yaw are coupled via the drag force. The drag force decreases at high velocity and the severity of this coupling should be decreased. This coupling is expected to be maximized at the drag peak.

Similarly, heave motions are coupled to the longitudinal acceleration via the drag force. Any oscillatory change in suspension height results in an oscillatory drag force and, under a constant propulsive force, will result in an oscillatory longitudinal acceleration. Since the magnets, and therefore the drag force, are below the center of mass of the vehicle, this drag force can result in a pitch oscillation as well. In the vehicle tested in this program, this coupling is expected to be small since the magnets are only a short distance below the center of mass.

Summarizing the drag force couplings, roll and slip are coupled into yaw, and heave and pitch are both coupled into the longitudinal acceleration. It is of course important to note that the fact that a coupling exists is not sufficient to cause an instability if damping is present. It is only when the coupling is excessively strong that an instability might occur.

Another source of mode coupling is the magnetic image that results from the reflection of the guidance and lift images through their planes of symmetry. This image is located on a straight line connecting the image and the real magnet and passing through the intersection of the vertical and horizontal plates of the guideway. Unlike the lift and guidance interactions, this image results in an attractive force. This interaction is greatest when the vehicle magnet is close to the corner of the guideway and results in a reduction in both the lift and guidance forces. The interaction with this image is sometimes referred to as the side-bottom interaction.

The side-bottom interaction can cause the vehicle to loose lift on one side in an extreme slip configuration, leading to a roll and a decrease in suspension height. It could also lead to a coupling of pitch into yaw if the drag varies in this location, and possibly to a

slip instability if the lateral force decreased sufficiently. This interaction was discussed in our first report* but has not been explored in detail. In all the tests to date, this interaction has not played a major role. Its effect on larger vehicles with other magnet configurations should be explored.

The non-linearity of the forces with the vertical height can also lead to a coupling of modes of oscillation. If the vehicle rolls or pitches, two magnets move closer and two move farther from the conducting surface. Assuming the vehicle to be rigid and rotating about the center of mass, the upward and downward displacements are equal. The forces, however, do not vary linearly so the increase in force on the lower magnets is greater than the decreases in force on the higher magnets. This increase in net force in the vertical direction must be accompanied by a change in vertical acceleration and position.

The major purpose in this program was to search for the growth of instabilities in a MAGLEV vehicle. While the tests reported herein did not exhibit any growth of instabilities, it is of particular interest to examine these tests for coupling that might cause an instability to develop. In order to examine this possibility experimentally, it is desirable to examine tests in which only one mode is excited and search for coupling into different modes. This ideal type of experiment was not performed since it was decided at the outset that a direct search for instabilities was more important than detailed tests of mode coupling. The experiments were therefore designed primarily to test stability.

In the actual tests, not less than two modes were stimulated. Consequently, the vertical step tests which excited only pitch and heave motions, and the lateral step tests, which excited only slip and yaw motions were examined for mode coupling. Both the active and passive tests were examined for mode coupling brought about by passive and active damping. The following possible modes were examined for coupling

* Reference 1

in the vertical step tests for both passive and active damping:

1) Heave coupled into slip, roll, magnet current and longitudinal acceleration, 2) Vertical acceleration coupled into lateral acceleration, and 3) pitch coupled into yaw and roll. For the passive lateral step tests the following modes were examined for coupling: 1) Slip coupled into heave, roll, and magnet current, and 2) yaw coupled into roll and pitch.

The data were photographed onto transparencies for direct point by point comparison. Test Nos. 24 and 36 were used primarily for the passive and active vertical step cases, and Test No. 39 was used for the lateral step case. In general the experimental results showed that track irregularities were reflected in all motions. There was a definite coupling between the heave and longitudinal acceleration, and the heave and magnet current. The active tests indicated less coupling than the passive tests as would be expected. More specifically, the track perturbations gave an apparent coupling into many modes, mainly because the lateral and vertical perturbations are concurrent. The current in the magnets increased about 5% upon full levitation for both the active and passive tests, which indicates a coupling between heave and magnet current. The active tests indicated no other coupling distinguishable from the track perturbations.

The passive tests showed a direct coupling bewteen longitudinal acceleration and magnet current in the region of the step perturbation, with an oscillation frequency on the order of the heave frequency. A very slight indication of coupling from roll to heave and roll to pitch also existed in the region of the step perturbations.

A roll motion occurred near the end of Test 39, probably caused by a track perturbation. No corresponding motions were observed in either

the slip or heave motions. A slight coupling of roll and yaw was noted in this portion of the test. Another slight coupling was noted between yaw and pitch in the vicinity of the lateral offset in Test 39. All other features were correlated with track perturbations.

In conclusion the experimental results showed track irregularities were reflected in all motions. There was a definite coupling between the heave and longitudinal acceleration and heave and magnet current. Subtle coupling of other modes may not have been detected because of the track perturbations. At no time, in any of the tests, did the coupling show any growth that led to an instability. In every case observable coupling decayed in a few cycles.

VI CONCLUSIONS

A study was made of the motion of a small-scale, magnetically levitated test vehicle which traversed several types of guideway perturbations. Some of these perturbations were as great as 25% of the equilibrium suspension height of the vehicle and stimulated all possible modes of oscillation. In every case, the vehicle's motion was found to be stable with either active or passive damping.

Although the results were not extrapolated to a full-size vehicle, no reason was found to expect that a full-scale vehicle would experience an instability under the circumstances investigated. This study did not include aerodynamic effects that will be of much greater importance at expected operational speeds of 500 kmph.

It was found experimentally that the use of active damping to reduce vertical accelerations resulted in a similar reduction in lateral accelerations. This suggests a strong coupling between the damping coil and both the horizontal and vertical guideway plates.

The vertical motion of the vehicle measured in these tests was simulated with an analytic model initiated in the previous phases of this program and extended in the present phase. The simulations were in very good agreement in the case of actively controlled damping, but were somewhat less satisfactory in simulating passively damped tests. An analysis of this discrepancy was not made.

The use of active damping coils with currents proportional to the absolute vertical velocity of the vehicle resulted in a significant improvement in ride quality over that obtained with passive damping coils. Specifically, the peak from the heave motion in the power

spectral density of vertical acceleration was found to be a factor of ten lower for active damping than for passive damping.

VII RECOMMENDATIONS

The experimental and analytical results presented in this report show that the test vehicle developed no unstable motions in any of the five degrees of freedom measured using either passive or active damping. They also show that the damping and ride quality were improved by using active damping coils. The work performed in this task constitutes a survey rather than an in depth study of the stability and damping of MAGLEV vehicles. While the results and conclusions are accurate as expressed in this report, they are susceptible to misinterpretation if applied to other vehicles.

Our recommendations apply to both the experimental and analytical work on MAGLEV. A strong interaction between these two categories is essential, and it is recommended that they be performed concurrently.

The passive damping system provided stability to the vehicle motions, both experimentally and analytically, but more damping was observed than was calculated. The source of this discrepancy should be identified and corrected to provide greater confidence in extrapolations to other vehicles. More detailed experiments should be performed to assess the damping in the lateral direction, especially in the yaw mode where stability might be marginal. After the discrepancy in the passive vertical damping is clarified and corrected, this formulation of the passive damping should be adapted to the lateral direction and included in the analytical model.

The experiments and analyses showed that the ride quality could be improved by the use of active damping. However, only absolute velocity feedback was used for controlling the active currents and was not optimized. Absolute acceleration and position feedback as well as feedback of position and velocity relative to the guideway and combinations of these feedback variables should be explored, first analytically and then

experimentally. These parameters are of great economic significance since they determine the tolerances that must be maintained in the guideway and therefore affect both construction and maintenance costs.

The active damping experiments that were performed were difficult to interpret since, with one exception, the controls were set close to critical damping and no appreciable oscillations occured. These settings should be made to achieve less damping where analyzable oscillations occur and systematically varied to investigate the ride quality of the vehicle over a range of feedback variables and for various combinations of feedback parameters. To obtain the greatest precision from these measurements, the guideway should be carefully aligned to remove irregularities over a distance corresponding to at least two oscillations, i.e. about 12 m, before and after the perturbation to permit equilibrium to be established.

The interaction of the active and passive damping systems should be analyzed and incorporated into the analytic model.

A parameter of considerable significance is the variation of the damping time with suspension height. To achieve a significantly greater height, stronger magnets must be used and the height of the sidewalls must be increased.

The analytic model should be modified to include the side-bottom image of the suspension magnet since this interaction accounts for some of the coupling between the vertical and lateral motions. A correlation should be made between the guideway roughness parameter and a deterministic specification of roughness so that simulations of typical revenue guideways can be made. In addition, the option of converting the output of the analytical model to PSD form should be included.

The interaction between the dynamics of the guideway and the vehicle should also be investigated. The analytic model should be modified to incorporate the effects of dynamic motions of the guideway and to determine the effect of this motion on ride quality. This modification is particularly important in that it can be used to determine specifications of guideway support structures. This modeling should be checked and confirmed on the existing guideway by direct experimentation in which a range of guideway flexibilities and spans between supports are examined.

It is recommended that guideway curves be included in the analytic model and that the effects of curves be simulated with the experimental facilities. Aerodynamic forces should be included in the model in anticipation of simulation requirements that will arise in the future.

With the above experiments providing confidence in the modifications to the analytic model, extrapolations should be made to a variety of full scale vehicles to determine their characteristics and to determine where any improvements might be required. The analysis should then be extended to assess the dynamic motion and acceptability of an on-board linear induction motor and the effects of operating in multiple vehicle train units.

It is strongly recommended that each of these studies be performed in depth to avoid costly design or experimental errors in the future. To provide timely inputs to later phases of the FRA MAGLEV program, it is recommended that such a program be initiated immediately and be completed by June, 1976. If the results of the recommended program are available by this date, they can be used in designing the MAGLEV research vehicle and guideway that are to be evaluated at the High Speed Ground Test Center in Pueblo, Colorado.

REFERENCES

1. Coffey, H. T., F. Chilton and L. O. Hoppie, The Feasibility of Magnetically Levitating High Speed Ground Vehicles; NTIS Report* No. PB 210-505, February, 1972.

2. Chilton, F. and H. T. Coffey, Magnetic Levitation: Tomorrow's Transportation. The Helium Society Symposium Proceedings, The Helium Society, Washington, D.C.,1971 p. 288.

3. Coffey, H. T., F. Chilton and L. O. Hoppie, Magnetic Levitation for Tomorrow's Transportation. Applications of Cryogenic Technology, Vol. 4 Xyzyx Publishing Co., Los Angeles, 1972, p. 275.

4. Coffey, H. T., F. Chilton and L. O. Hoppie, Magnetic Levitation of High Speed Ground Vehicles. 1972 Applied Superconductivity Conference, Annapolis, Maryland, IEEE Publication No. 72 CH0682-5-TABSC, 1972, p. 62.

5. Hoppie, L. O., F. Chilton, H. T. Coffey and R. C. Singleton, Electromagnetic Lift and Drag Forces on a Superconducting Magnet Propelled Along a Guideway Composed of Metallic Loops. 1972 Applied Superconductivity Conference, Annapolis, Maryland, IEEE Publication No. 72 CH0682-5-TABSC, 1972, p. 113.

6. Coffey, H. T., J. D. Colton and K. D. Mahrer, Study of a Magnetically Levitated Vehicle. NTIS Report PB 221696, February, 1973

7. Coffey, H. T., SRI Magnetic Suspension Studies for High Speed Vehicles. Advances in Cryogenic Engineering, Vol. 19, 1974. To be published.

8. Reitz, J. R., L. C. Davis, D. F. Wilkie and R. H. Borcherts, Technical Feasibility of Magnetic Levitation as a Suspension System for High Speed Ground Transportation Vehicles. NTIS Report PB-210506, 1972.

* NTIS Reports available from National Technical Information Service, Springfield, Va. 22151

9. Reitz, J. R., R. H. Borcherts, L. C. Davis, T. K. Hunt and D. F. Wilkie, Preliminary Design Studies of Magnetic Suspension for High Speed Ground Transportation. NTIS Report No. PB 223237, March,1973. See this report for additional references to papers published by the Ford Scientific Research Laboratories on this subject.

10. Wilkie, D. F., Dynamics, Control and Ride Quality of Magnetically Levitated High Speed Ground Vehicle. Transportation Research, Vol. 6, 1972 p. 343.

Appendix A

VEHICLE MOTIONS AND INSTRUMENTATION

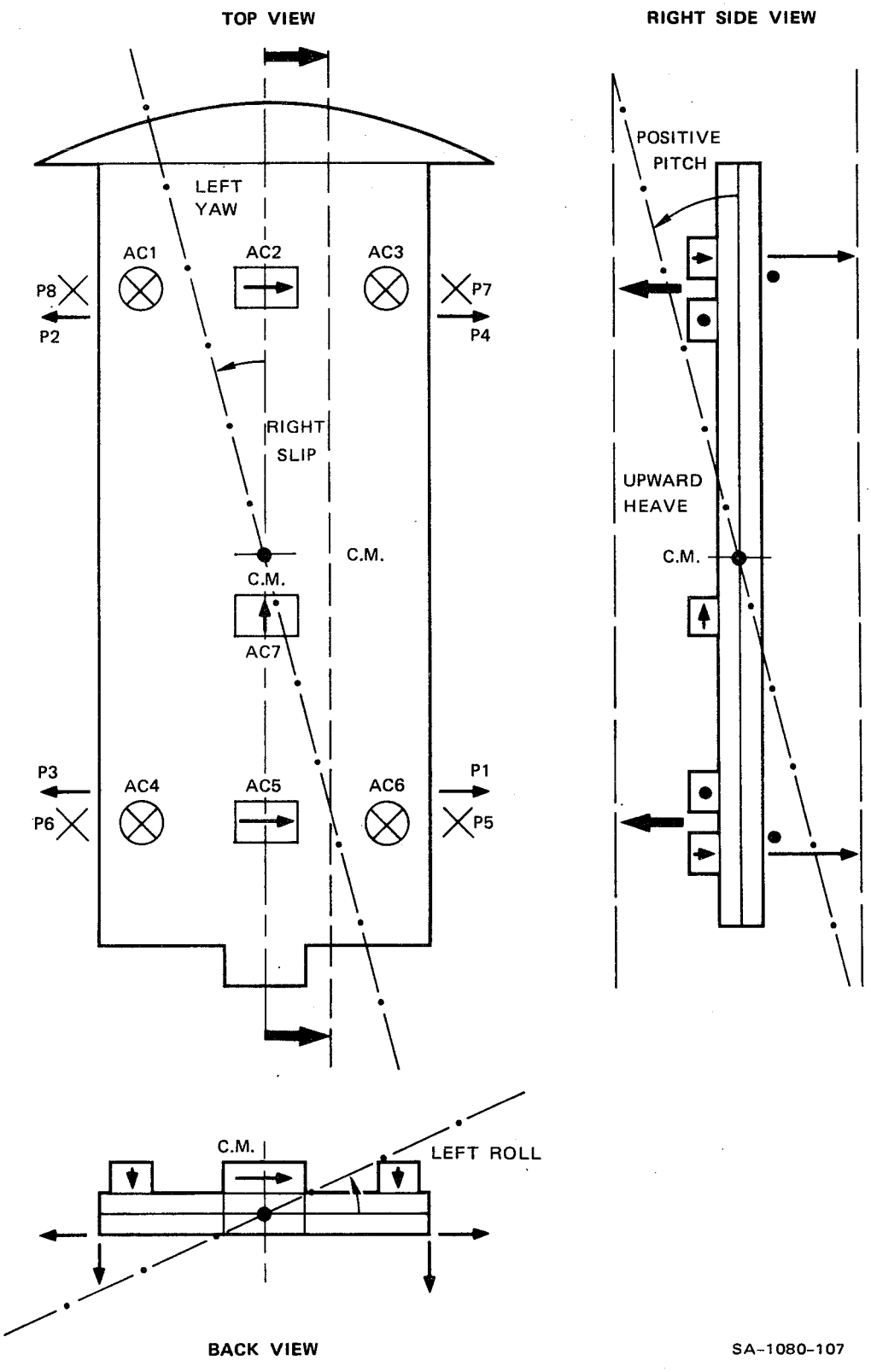

FIGURE A-1 VEHICLE MOTIONS AND INSTRUMENTATION

Appendix B

ACTIVE DAMPING CONTROL CIRCUITS

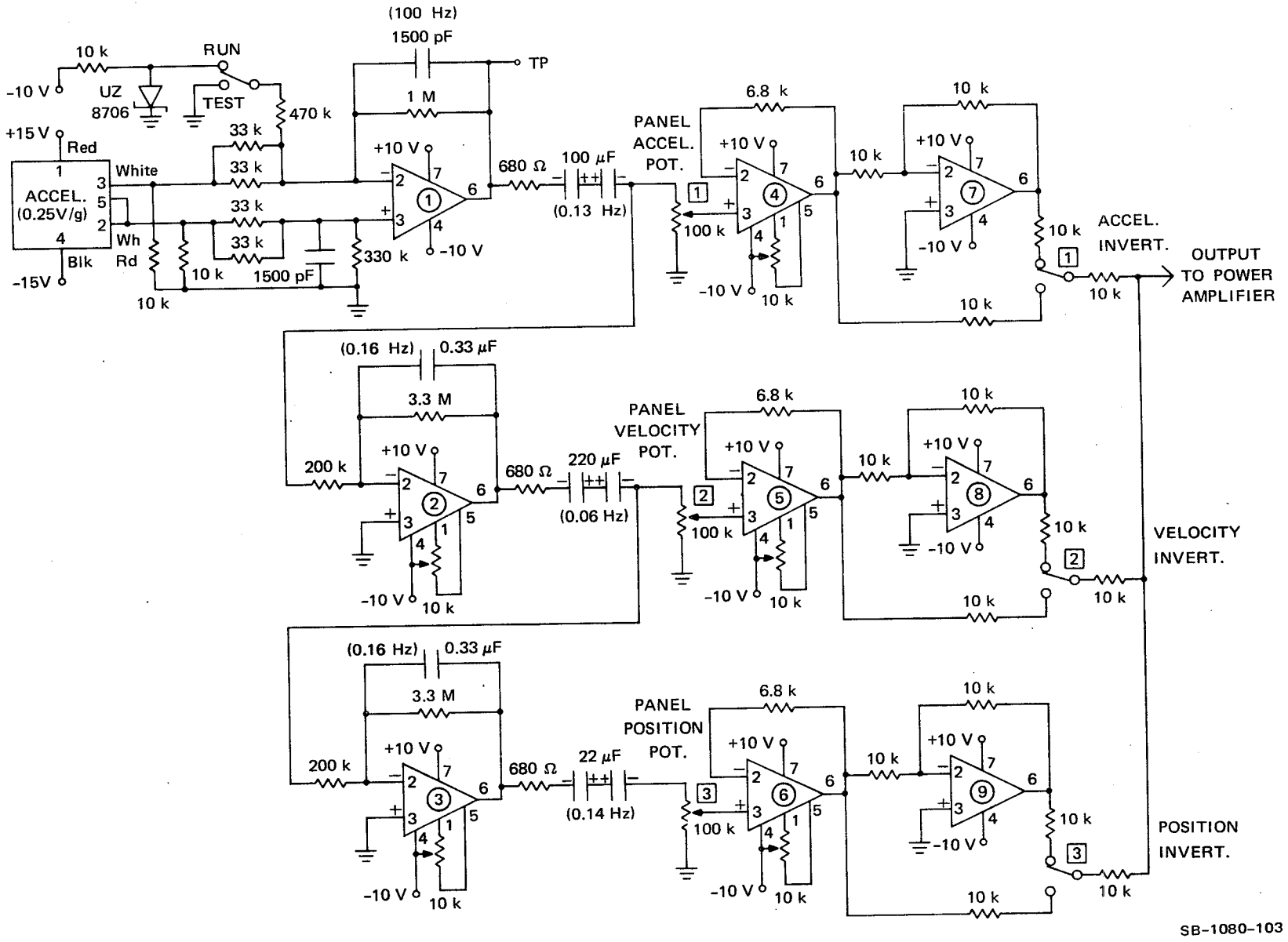

FIGURE B-1 PREAMPLIFIER (ALL OPAMPS ARE μA741)

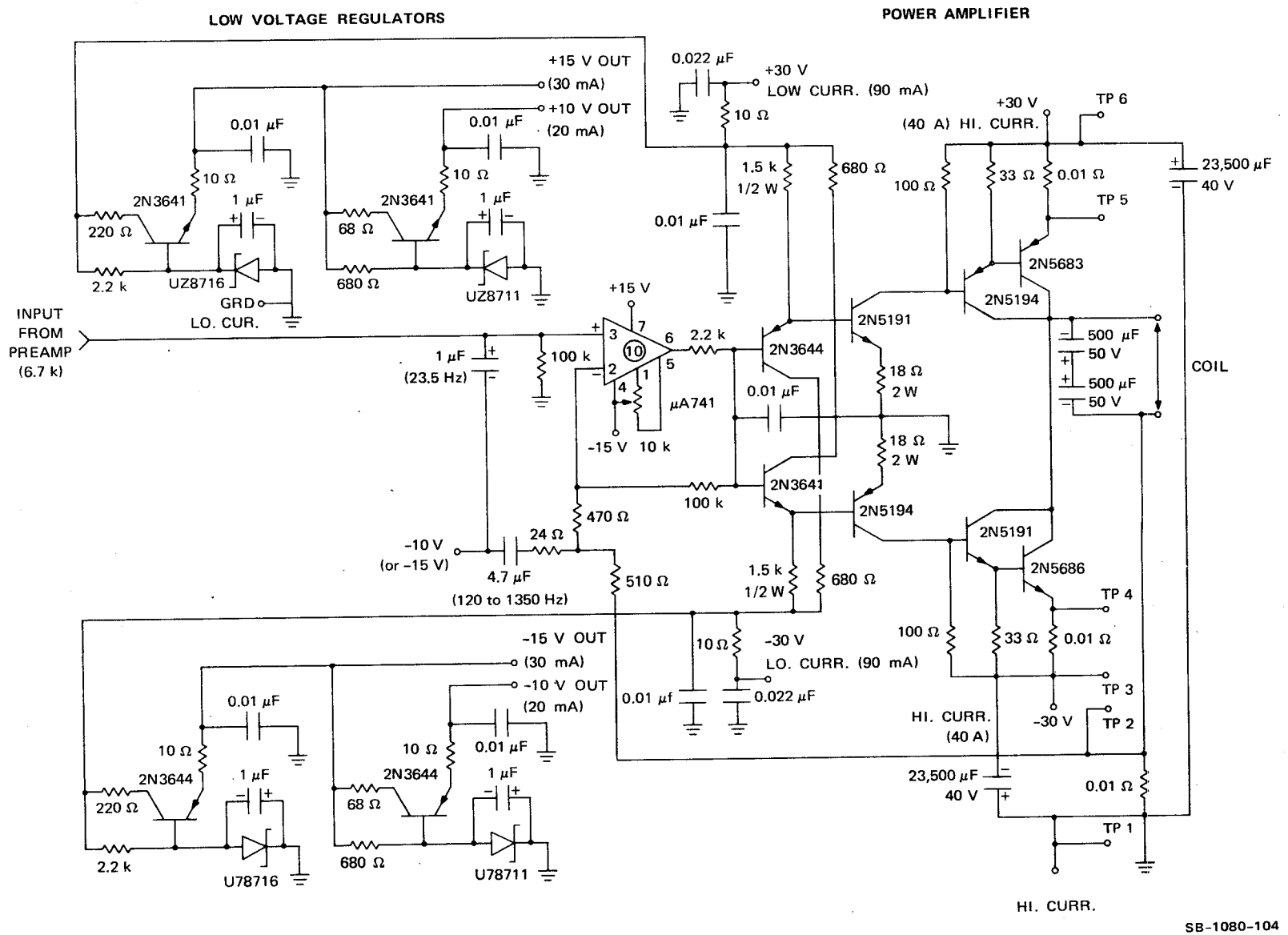

FIGURE B-2 POWER AMPLIFIER

REVISED* INPUT STAGE TO GIVE HIGHER INPUT
IMPEDANCE AND BETTER COMMON MODE REJECTION

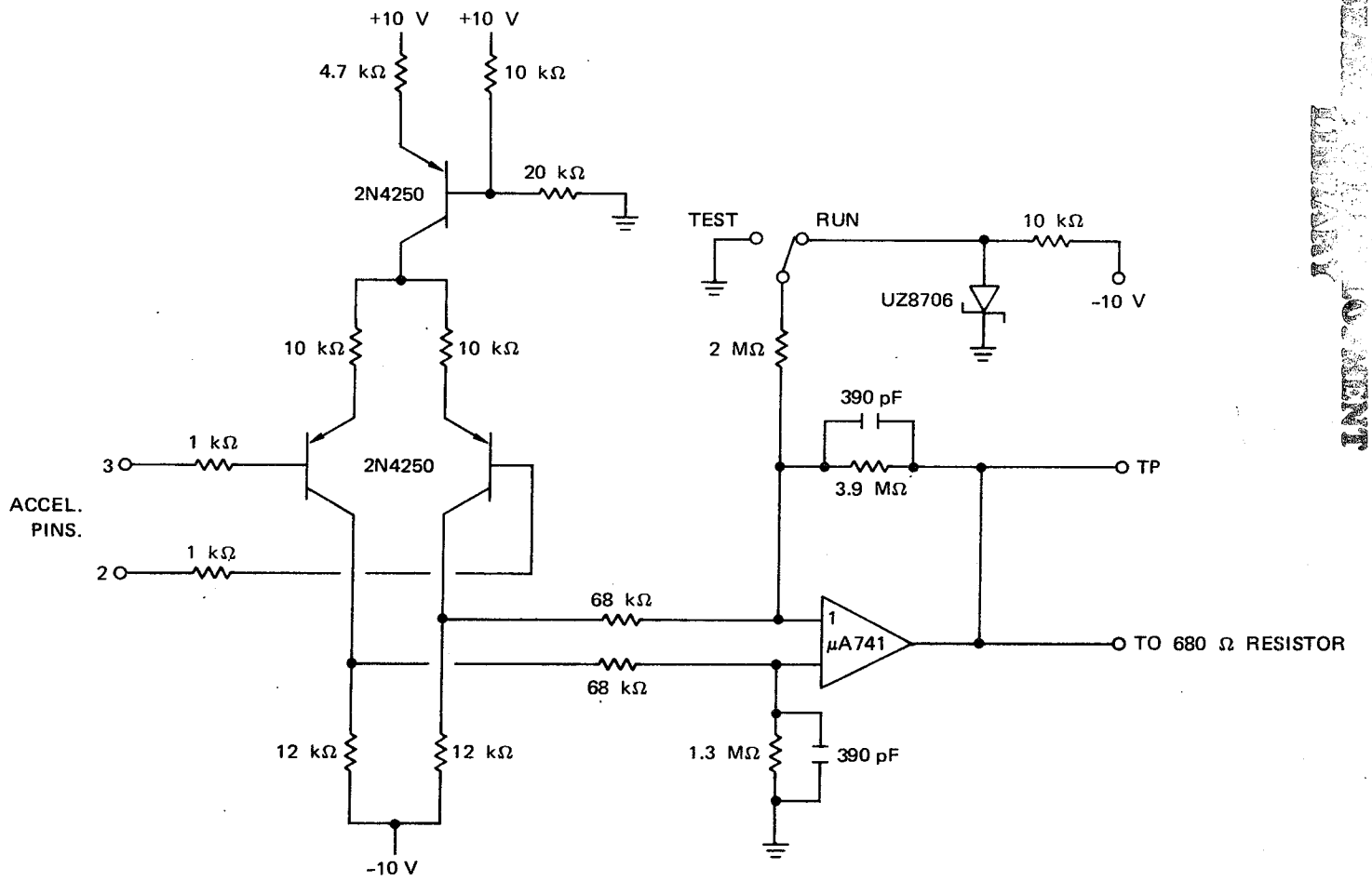

*Never tested. Proposed for future tests to eliminate low frequency instability due to ground loops and common mode input signals.

SA-1080-105

FIGURE B-3 PROPOSED DIFFERENTIAL PREAMPLIFIER